WL-TR-96-4109

MICROSTRUCTURE-DRIVEN DESIGN

HUGHES T.J.R., MULLER A.
Technical Management Concepts

MAY 1996

FINAL REPORT FOR MAY 1996

Approved for public release; distribution unlimited

MATERIALS DIRECTORATE
WRIGHT LABORATORY
AIR FORCE MATERIEL COMMAND
WRIGHT-PATTERSON AIR FORCE BASE, OH 45433-7734

NOTICE

When Government drawings, specifications, or other data are used for any purpose other than in connection with a definitely Government-related procurement, the United States Government incurs no responsibility or any obligation whatsoever. The fact that the Government may have formulated or in any way supplied the said drawings, specifications, or other data, is not to be regarded by implication, or otherwise in any manner construed, as licensing the holder, or any other person or corporation; or as conveying any rights or permission to manufacture, use, or sell any patented invention that may in any way be related thereto.

This report is releasable to the National Technical Information Service (NTIS). At NTIS, it will be available to the general public, including foreign nations.

This technical report has been reviewed and is approved for publication.

STEVEN R. LECLAIR, Chief
Materials Process Design
Integration & Operations Division
Materials Directorate

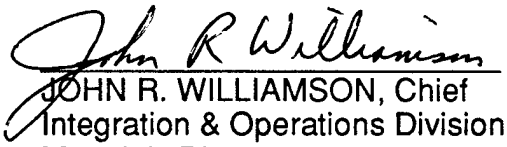

JOHN R. WILLIAMSON, Chief
Integration & Operations Division
Materials Directorate

If your address has changed, if you wish to be removed from our mailing list, or if the addressee is no longer employed by your organization please notify WL/MLIM, Wright Patterson AFB, OH 45433 to help maintain a current mailing list.

Copies of this report should not be returned unless return is required by security considerations, contractual obligations, or notice on a specific document.

REPORT DOCUMENTATION PAGE

FORM APPROVED
OMB NO. 0704-0188

1. AGENCY USE ONLY *(Leave Blank)*	2. REPORT DATE	3. REPORT TYPE AND DATES COVERED
	May 1996	Final May 1996

4. TITLE AND SUBTITLE

Microstructure-Driven Design

5. FUNDING NUMBERS

C: F33615-94-D-5801
PE: 62102F
PR: 2418
TA: 90
WU:01

6. AUTHOR(S)

Hughes T.J.R., Muller A.

7. PERFORMING ORGANIZATION NAME(S) AND ADDRESS(ES)

Materials Directorate
Wright Laboratory
Air Force Materiel Command
Wright Patterson AFB OH 45433-7734

8. PERFORMING ORGANIZATION REPORT NUMBER

9. SPONSORING MONITORING AGENCY NAME(S) AND ADDRESS(ES)

POC: James C. Malas, WL/MLIM, WPAFB OH; 937-255-8787
Materials Directorate
Wright Laboratory
Air Force Materiel Command
Wright Patterson AFB OH 45433-7734

10. SPONSORING/MONITORING AGENCY REP NUMBER

WL-TR-96-4109

11. SUPPLEMENTARY NOTES

12a. DISTRIBUTION/AVAILABILITY STATEMENT

Approved for public release: distribution is unlimited.

12b. DISTRIBUTION CODE

13. ABSTRACT

Microstructure-driven design, the application of optimal design and control methods to metal forming manufacturing processes can reduce part costs, improve part delivery schedules, and increase quality repeatability. Existing design methods are usually ad hoc and include inadequate evaluation of process parameters such as deformation rates, die and workpiece temperatures, and tooling system configuration. The systems approach used in this work is based on control theory and optimization concepts. A metal forming operation is viewed here as a combination of two interdependent systems: the microstructure development system and the process system. Inputs to the microstructure development system are field variables of the process, such as strain, strain rate, and deformation temperature. Microstructural system outputs are variables that characterize microstructure; in a dynamic recrystallization case, for example, grain size and volume fraction transformed are outputs of the microstructural system. The process system takes as inputs variables such as die profiles, preform shapes and temperature, and ram velocity profiles, and outputs field variables - strain , strain-rate and temperature - to which the different areas of the deforming workpiece are subjected during hot forming. Outputs of the process system are inputs to the microstructure development system. These presentations describe the microstructure development system and related issues as applied to process optimization.

14. SUBJECT TERMS

microstructure-driven design, strain, strain-rate, metal forming

15. NUMBER OF PAGES

49

16. PRICE CODE

17. SECURITY CLASSIFICATION OF REPORT	18. SECURITY CLASS OF THIS PAGE.	19. SECURITY CLASS OF ABSTRACT	20. LIMITATION ABSTRACT
UNCLASSIFIED	UNCLASSIFIED	UNCLASSIFIED	SAR

TABLE OF CONTENTS

RECENT ADVANCES IN MICROSTRUCTURAL MODELING DURING HOT DEFORMATION PROCESSES

James C Malas and Venugopal Srinivasan
Materials Process Design,
WPAFB

1. Introduction

Cold, warm and hot working techniques are being used to manufacture a variety of components ranging from tiny rivets to nuclear reactor vessels. The most common problems faced in cold forming operations are the formation of edge cracks, waviness and sliver defects, etc., and in hot working operations are formation of undesirable phases, surface imperfections, non uniform microstructure, wedge cracking, etc. These above defects decrease the yield and there by affect the profitability. This situation forces the manufacturing industries to optimize and control the process variable with in a restricted range in order to maintain the yield at higher level. Any scientific methodology, explored and employed to optimize the processing parameters with the view to achieving enhanced workability in order to produce defect free components is a significant research contribution to the area of manufacturing engineering. Numerous investigations have been oriented towards the optimization of processing parameters by various investigators either by physical or mathematical modeling [1-6]. These studies have lead to better understanding of the mechanisms of hot deformation. However, it is difficult to use them directly for the optimization of workability. In the recent past, significant advancement has been made in modeling the microstructural evolution during deformation. This paper is aimed to review the state of art in the area of microstructural modeling towards the optimization of workability and microstructural control during deformation processing.

2. Workability

The relative ease with which a metal can be shaped by deformation processes such as forging, extrusion, rolling, pressing and drawing is generally referred to as workability. it is also defined as the degree of deformation that can be achieved in a particular metal working process without causing cracking or fracture or poor mechanical properties. Generally, workability depends on the state-of-stress, strain, strain rate and temperature in combination with metallurgical factors such as resistance of the material

for ductile fracture. Therefore, the workability may be classified as (1) Intrinsic workability which depends on the previous history of the material, temperature, strain and strain rate of working (Fig. 1) and (2) state-of-stress related workability (Fig. 2) which depends on the die design and effects of friction and notches. A proper combination of these two will result in a sound product with good mechanical properties. The state-of-stress related workability can be optimized by proper die design and selection of lubricants. Where as the optimization of intrinsic workability requires the through understanding of the constitutive behavior of the material under processing condition.

In the current industrial practice the workability of the material is assessed by experimental methods. Commonly tension, torsion and compression tests are used to assess the workability. Special tests such as bend test, extrudability test, plane strain compression test, partial width indentation test, secondary tension test, ring compression test, wedge forging test, side pressing test, notched bar upset test and truncated cone indentation test have also been used to asses the workability. An important feature of these special tests is well defined state-of-strain. These techniques are trial and error in nature and the results based on these special tests are not amenable for process modeling and microstructural control.

3. Kinetics of Hot Deformation

The strength of pure metals and alloys increases with increasing strain rate at a fixed temperature, following the general kinetic equation for hot deformation (covering a wide range of stresses)[7]:

$$\dot{\varepsilon} = A(Sinh\alpha\sigma)^n \exp\left(-Q/RT\right) \qquad (1)$$

Where A, α and n are temperature-independent constants, $\dot{\varepsilon}$ is strain rate, σ, is true stress, T is the temperature in K, R is gas constant and Q is the activation energy. The apparent activation energy for hot deformation is determined using the above equation and the value corresponds to the rate controlling dynamic softening process. Eqn. (1) is rearranged to give a temperature compensated strain rate parameter Z, known as Zener-Hollomon parameter [7].

$$Z = \dot{\varepsilon} \exp\left(Q/RT\right) = A(Sinh\alpha\sigma)^n \qquad (2)$$

If the same value of activation energy is found for both creep and hot working, this parameter can be used to correlate data over many orders of magnitude of strain rate. But, if activation energy varies such a parameter can only be used in a limited range. The effect of Z on processes like static recrystallization (SRX), dynamic recrystallization (DRX) and dynamic recovery (DRY) has been studied [8]. It has been shown that as Z decreases,

- the nucleation of DRX requires less strain or lower stress,
- the difference between the critical strain (and stress) for SRX and that for DRX becomes progressively less, and
- deformation bands and shear bands decrease in frequency

There are more cycles of recrystallization present simultaneously at higher values of Z. Further, the subgrain size (d_g) formed during DRX and DRY is found to vary with Z according to the following relation [9,10]:

$$d_g^{-1} = a + b \log Z \qquad (3)$$

Empirical equations similar to Eqns. (2) and (3) have been generated for most of the common metals and alloys by numerous investigators. Though this kinetic approach lead to detailed understanding of the behavior of deforming metal, they are not directly useful for the design and optimization of deformation process.

4. Modeling of Hot Deformation

The optimization of hot workability requires an understanding of the constitutive behavior of the material under processing conditions. Earlier, attempts have been made by Ashby [11] and Raj [12] to understand the effects of strain, strain rate, temperature and microstructure on the flow behavior of metals during deformation processing. They developed maps which describe the deformation and fracture process that occur during processing.

4.1. Ashby Maps

In the Ashby maps [11] (Fig. 3) the normalized shear stress is plotted against absolute temperature. The maps are divided into regimes, within each of which a particular mechanism is dominant. The regime boundaries are the loci of the points at which two mechanisms contribute equally to the overall strain rate. The contours of constant strain rate are superimposed on the fields and they show the net strain rate that a given combination of stress and temperature will produce. These maps can be theoretically constructed for any poly crystalline material, showing the area of dominance of each flow mechanism.

4.3. Raj Maps

Raj maps [12] (Fig. 4) are developed considering the failure mechanism that can operate in a material over ranges of strain rate and temperature. These maps are useful for processing in the sense that they define the regions in which it is "safe" to process the workpiece material and avoid defect nucleation.

Both Ashby and Raj maps are deterministic since they use shear strain rate equations which are valid for steady state. The equations depend on a number of basic atomic processes such as dislocation motion, diffusion, grain boundary sliding , twinning and phase transformations. Both the maps are limited to simple systems and cannot be applied to complex commercial alloys since in these materials it is not always possible to identify the atomistic mechanisms unequivocally. As the maps are based on the atomistic theory, it is difficult to integrate them with continuum approaches. Also, process optimization is difficult to achieve, using these atomistic approaches.

A continuum approach has been therefore proposed by Gegel[13] and Prasad[14] and is briefly described below.

4.4. Dynamic Material Model

In this model, the work piece is considered to be a dissipator of power. The constitutive equations describes the manner in which the power is converted at any instant into two forms: thermal and microstructural, which were not recoverable by the system. The dissipater element can be considered to be non-linear, dynamic and

irreversible. At any instant, the total power dissipated consists of two complementary parts: G-content representing the temperature increase and J-co-content representing the dissipation occurring through microstructural processes. The power partitioning between G and J is decided by the strain rate sensitivity (m) of flow stress (σ). At a given temperature and strain rate J co-content is given by [14];

$$J = \frac{m}{m+1}\sigma\dot{\varepsilon} \tag{4}$$

The J co-content of the workpiece being a non-linear dissipator, is normalized with that of an ideal linear dissipator (m=1) to obtain a dimensions parameter η called the efficiency of power dissipation:

$$\eta = \frac{J}{J_{max}} = \frac{2m}{m+1} \tag{5}$$

The variation of η with temperature and strain rate constitutes a processing map (Fig. 5). The various domains in the map may be correlated with specific microstructural processes and applied for microstructural control. The dynamic materials model has its basis in the extremum principles of irreversible thermodynamics as applied to a large plastic flow described by Ziegler [15].

The power dissipation maps are continuum maps but the domains may be interpreted in terms of specific atomistic processes. This can be done with the help of Raj maps. In hot deformation there are "safe" and "damage" mechanisms that occur in different strain rate-temperature regimes. For example, the "safe" mechanisms involve DRY and DRX while the "damage" mechanisms are wedge cracking (dominant at lower strain rates and higher temperatures) and void formation at hard particles (dominant at high strain rates and lower temperatures). The damage processes are highly efficient in dissipating energy through production of new surfaces while the "safe" processes are relatively less efficient since power dissipation occurs by annihilation of dislocations or their groups. In the "safe" regime, dynamic recrystallization is more efficient than dynamic recovery.

The processing map is a more powerful tool for evaluating workability and controlling microstructure during thermomechanical processing than the other parameters

such as ductility, fracture strain/saturation stress. The optimization of the processing parameters may be done with the help of a processing map by identifying the peak in the efficiency of power dissipation in the "safe" regime of the map, e.g., DRX domain. As the approach is based on principles of continuum mechanics, the results may be integrated with simulation models. Also, the model is applicable even in the case of complex alloy systems since the input may be experimentally generated data unlike the atomistic models which require fundamental data.

4.5. Instability Maps

During deformation processing of materials under certain combinations of temperature and strain rate, the materials exhibit loss in ductility due to phenomena like dynamic strain aging, formation of new phases, adiabatic shear deformation, or regions of localized deformation, grain boundary and triple point cracks, void generation (cavitation) and hot shortness. The above phenomena may introduce inhomogeneous deformation and produce microstructures possessing defects like non-uniform microstructures, shear bands, and strain markings. In homogeneous deformation is detrimental to the mechanical properties of the product in particular the ductility, fracture toughness and fatigue crack growth rate. The phenomena which cause inhomogeneous deformation during forming can be termed as "Flow Instabilities" and the regimes of temperature and strain rate where deformation is not homogeneous can be termed as "Instability" regions. It is therefore necessary to avoid processing regimes where the instabilities are likely to occur. The regions of flow instability can be determined by a rigorous and detailed analysis on the values of flow stress, work hardening rate, saturation stress, strain rate sensitivity and activation parameters. The conventional analysis may not be a viable one for industrial applications because of the intricacy involved in performing the analysis. Moreover, this method is not suitable for the purpose of the process design and optimization. During the last decade several criteria have been developed for this purpose. These include: (1) Phenomenological criterion based on strain hardening and strain rate sensitivity suggested by Semiatin and co-workers [16], (2) Experimental techniques like distributed gage volume measurement which measures the volume of deformed material of the reduced gage section penetrating into the specimen ends and (3) Continuum criteria based on principle of maximum entropy production.

4.5.1. Phenomenological criterion:

According to Semiatin and co-workers [16], flow localization will occur if the parameter:

$$\alpha = \frac{1}{\dot{\varepsilon}} \frac{d\dot{\varepsilon}}{d\varepsilon} = -\frac{\gamma}{\sigma m} > 5 \qquad (6)$$

where, $\dot{\varepsilon}$ is the strain rate, ε the strain, γ the work hardening rate and m strain rate sensitivity. A critical value of 5 for a has been fixed on the basis of microstructural observations of the flow localization in titanium and its alloys.

4.5.2. Distributed Gage Volume Measurement

In this experimental method, cylindrical dumb-bell shaped specimens having a reduced gage section 12 mm in diameter (typical) and 12 mm height with head portion of 36 mm diameter and 12 mm height on both ends, are compressed to about 66% reduction in the gage height [17]. During deformation the deformed material penetrates into the head portions. The volume of the material penetrated into head portion is termed as distributed gage volume (DGV) and it is related to the susceptibility of the material to flow localization. The distributed gage volume is measured on the reduced gage section of the specimen deformed under compression and is given by,

$$DGV = \frac{V_o - V_f}{V_o} \times 100 \qquad (7)$$

where Vo = original gage volume between the head portions of the undeformed reduced gage section and V_f = final apparent gage volume between the head portions of the specimen ends after deformation. DGV is a measure of the material's propensity for localized flow during working or conversely its ability to distribute deformation. Low values of DGV are associated with localized plastic flow (Fig. 7). This technique is purely experimental and qualitative.

4.5.3. Continuum Criteria

These criteria are based on the extremum principles in the irreversible thermodynamics of large plastic flow proposed by Ziegler [15]. According to the principle of maximum rate of entropy production, a system undergoing large plastic deformation will be unstable if,

$$\frac{dD}{d\dot{\varepsilon}} < \frac{D(\dot{\varepsilon})}{\dot{\varepsilon}} \tag{8}$$

where $D(\dot{\varepsilon})$ is the dissipation function characteristic of the constitutive behavior of the workpiece. On the basis of the above equation, Gegel and co-workers[13] have derived an instability criterion given by:

$$\frac{\partial s}{\partial \ln \dot{\varepsilon}} > 0 \quad and \quad \frac{\partial \eta}{\partial \ln \dot{\varepsilon}} \tag{9}$$

where $s = (1/T)[\partial \ln \bar{\sigma} / \partial(1/T)]$, $\eta = 2m/(m+1)$, $\bar{\sigma}$ = effective flow stress and T = temperature of deformation. In physical terms, flow instabilities will occur when the applied rate of entropy input is higher than the rate of entropy generation by the workpiece. The parameters η and s are determined as functions of temperature and the effective strain rate and the inequalities in the above equation are calculated to determine the instability regimes. In deriving the Eqn. (9), Gegel *et al.* [13] have not separated the power dissipation function into those representing heat generation (G-content) and microstruvctural dissipation (J-Co-content). Kumar and Prasad [18] applied the principle of separability of the rate of entropy production into the conduction entropy (heat generation) and internal entropy (microstructural changes) and considered the dissipation function corresponding to the microstructural changes (J-co-content) for deriving a criterion for instability as:

$$\xi(\dot{\varepsilon}) = \frac{\partial \ln[m/(m+1)}{\partial \ln \dot{\varepsilon}} \tag{10}$$

The variation of $\xi(\dot{\varepsilon})$ with temperature and strain rate constitutes an instability map (Fig. 8). The instability map delineates instability regions where $\xi(\dot{\varepsilon})$ is negative and these could be avoided in processing. This instability criterion has been microstructurally validated in Al, Cu, Zr, Ni, Ti, brasses, iron, stainless steels, etc. The

advantages of the continuum criteria are that the approach is fundamental and instability maps may be directly superimposed on the processing maps for the purpose of optimization of workability.

5. Activation Energy Maps:

Deformation mechanisms can be identified by the amount of potential free energy required for their activation. Microstructural transformations require atomic mobility ; to activate this mobility, an increase in energy must be provided to transport the atoms from one site to another. During a thermomechanical process, a material system changes its state in accordance with the imposed conditions of temperature, strain ands strain rate for dissipating energy. In order for a system to achieve a more stable, lower energy state, it must first pass through an intermediate, less stable, higher energy state that acts as a barrier to the transformation unless the necessary activation can be provided. A material system can lower its free energy by transmitting through a series of dissipative energy states and microstructures. Typically, for a given free energy state of the material system, the potential exists for a number of possible dessipative paths. In this situation, the material response must be controlled such that the microstructure will transform in a stable and efficient way. Using the above concept Malas and Seetharaman [19] proposed a new method to identify the optimum processing domain.

The apparent activation energy (Q) associated with a prevailing deformation mechanism is computed and mapped over a given range of processing conditions. The DMM analysis provide a description of the desirable processing conditions under which the operative deformation mechanisms are stable and are thereby controllable. As shown schematically in Fig. 9, the processing window of a given metallic system is defined as the domain of processing conditions under which material behavior is stable and a desirable and relatively constant value of apparent activation energy exists. As a result, the optimal processing conditions for a particular softening mechanism can be identified and the corresponding microstructure development modeled for controlling deformation. The major advantage of this technique is that extensive microstructural investigations required to characterize the domains of a DMM processing map are not required because the activation energy values are well related to the deformation mechanisms.

This technique has been applied for the optimization of extrusion of Al + 20% SiO_2 composite material and the results are encouraging. Fig. 10(a) shows the products extruded at the optimal conditions predicted by Activation energy map and Fig. 10(b)

shows the product extruded at the "un safe" condition predicted by the activation energy map.

Summary:

A review has been made on the various methods proposed to optimize the workability of the materials have been reviewed. These methods are useful only to select the processing parameters such as strain, strain rate and temperature for processing of the materials based on intrinsic workability of the materials. In an industrial environment other important factors mentioned in Fig. 11 should be considered in process optimization. In the case of microstructural control during processing, models relating the microstructural state with strain, strain rate, temperature and state-of-stress are needed. The development towards this direction is primitive. Moreover, the conventional approach of establishing the relationship between the macroscopic variables with material behavior for controlling the microstructure is not yielding accurate results because of the complexities involved in the deformation behavior. Hence, in order to design a process and to control the microstructure during deformation processing advanced technique of electronicprototyping can be used for the best results.

Acknowledgments:

One of the authors (S.V) acknowledges National Research Council, USA for their support.

References:

1. Kurt Lange, Hand Book of Metal Forming, McGraw Hill, New York (1985).
2 J.J. Jonas, Mcta Metall., 17 (1969) 397.
3. C. Devadas, I.V. Samarasekara and E.B. Hawbolt, Metall. Trans. A, 22A (1991) 335-349.
4. J.M. Alexander, Modeling of Hot Deformation of Steel, ed. J.G. Lenard, Springer-Verlog, Berlin (1989) 101.
5. H.J. McQueen and J.J.Jonas, Treatise on Materials Science and Technology, (ed.) R.J. Arsenault, Academic Press, New York, 6(1975) 383.
6. M.J. Luton and C.m. Sellars, Acta Metall., 17 (1969) 1033.
7. J.J. Jonas, C.M. Sellars and W.J. McG Tegart, Met. Rev., 14 (1969) 1.

8. H.J. McQueen, Mater. Sci. Engg., A 101 (1988) 149.
9. H.J. McQueen, E.Evangelista and M.E. Kassner, Z. Metallkede., 82 (1991) 336.
10 D. Padmavarthani, Ph.D., Thesis, Indian Institute of Science, Bangalore, May 1993.
11. H.J. Frost and M.F. Ashby, Deformation Mechanism Maps, Pergamen Press, New York (1982).
12. R. Raj, Metall. Trans. A, 12A (1981) 1089.
13. H.L. Gegel, J.C. Malas, S.M. Doraivelu and V.A. Shende, Metals Hand Book, ASM International, Metals Park, Ohio, 9th Edition, 14 (1988) 417.
14. Y.V.R.K. Prasad, H.L. Gegel, S.M. Doraivelu, J.C. Malas, J.T. Morgan, K.A. Lark and D.R. Barker, Metall. Trans. A, 15A (1984) 417.
15. H. Ziegler, Progress in Solid Mechanics, John Wiley and Son, New York 4(1983)93.
16. S.L. Semiatin, and J.J. Jonas, Formability and Workability of Metals, ASM, Metals Park, Ohio, (1984) 13.
17. M.C. Mataya and G. Krauss, J. Appli. Metal Working, 2 (1981) 28.
18. Y.V.R.K. Prasad, Indian J Technol., 28 (1990) 435.
19. James C. Malas and V. Seetharaman, JOM, 44 (1992) 8-13.

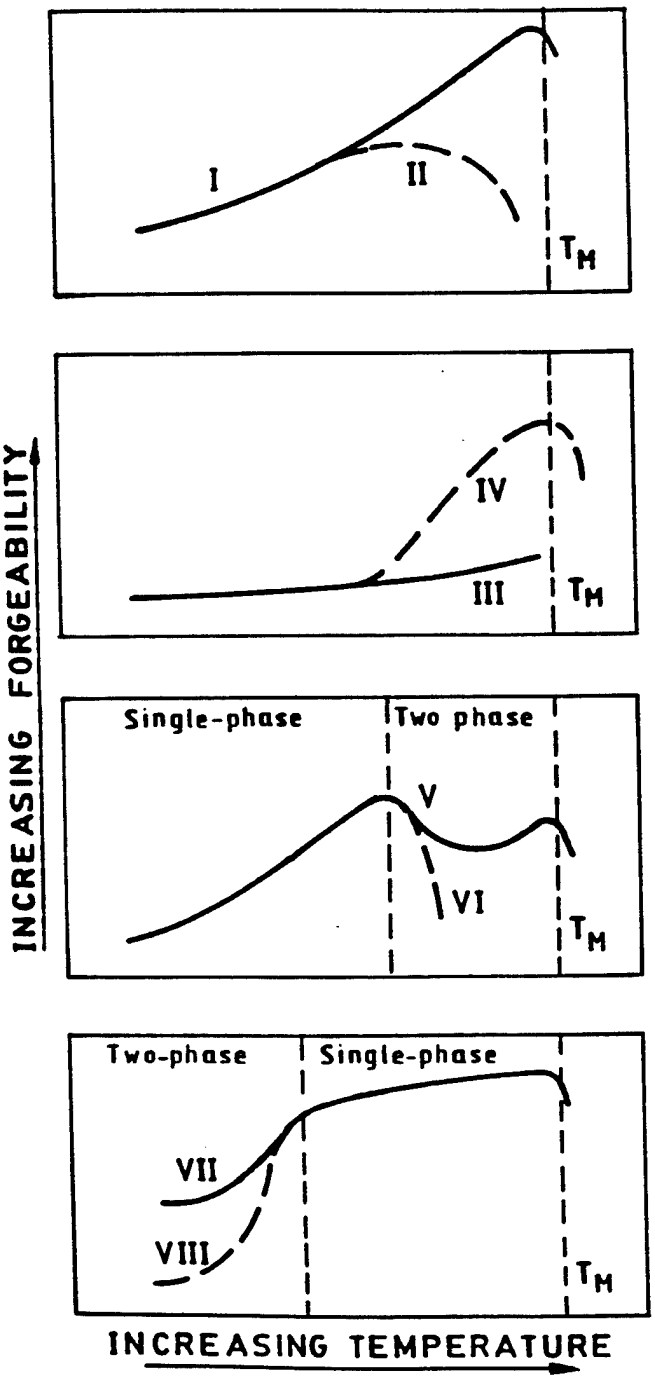

I Pure metals and single phase alloys
Al alloys
Ta alloys
Nb alloys

II Pure metals and single phase alloys exhibiting rapid grain growth
Be alloys
Mg alloys
W alloys
Alfa-beta Ti alloys

III Alloys containing elements that from insoluble compounds
Stainless steel containing Se
Resulfurized steel

IV Alloys containing elements that from soluble compounds
Mo alloys containing oxides
Stainless steel containing soluble carbides or nitrides

V Alloys forming ductile second phase on heating
High Cr stainless steels

VI Alloys forming low melting second phase on heating
Fe containing sulfur
Mg alloys containing zinc

VII Alloys forming ductile second phase on cooling
Carbon and low alloy steels
Alfa-beta and alfa titanium alloys

VIII Alloys forming brittle second phase on cooling
Super alloys
Precipitation hardenable stainless steels

Fig.1 Typical workability behaviour exhibited by different alloy systems; T_M is the absolute melting temperature.

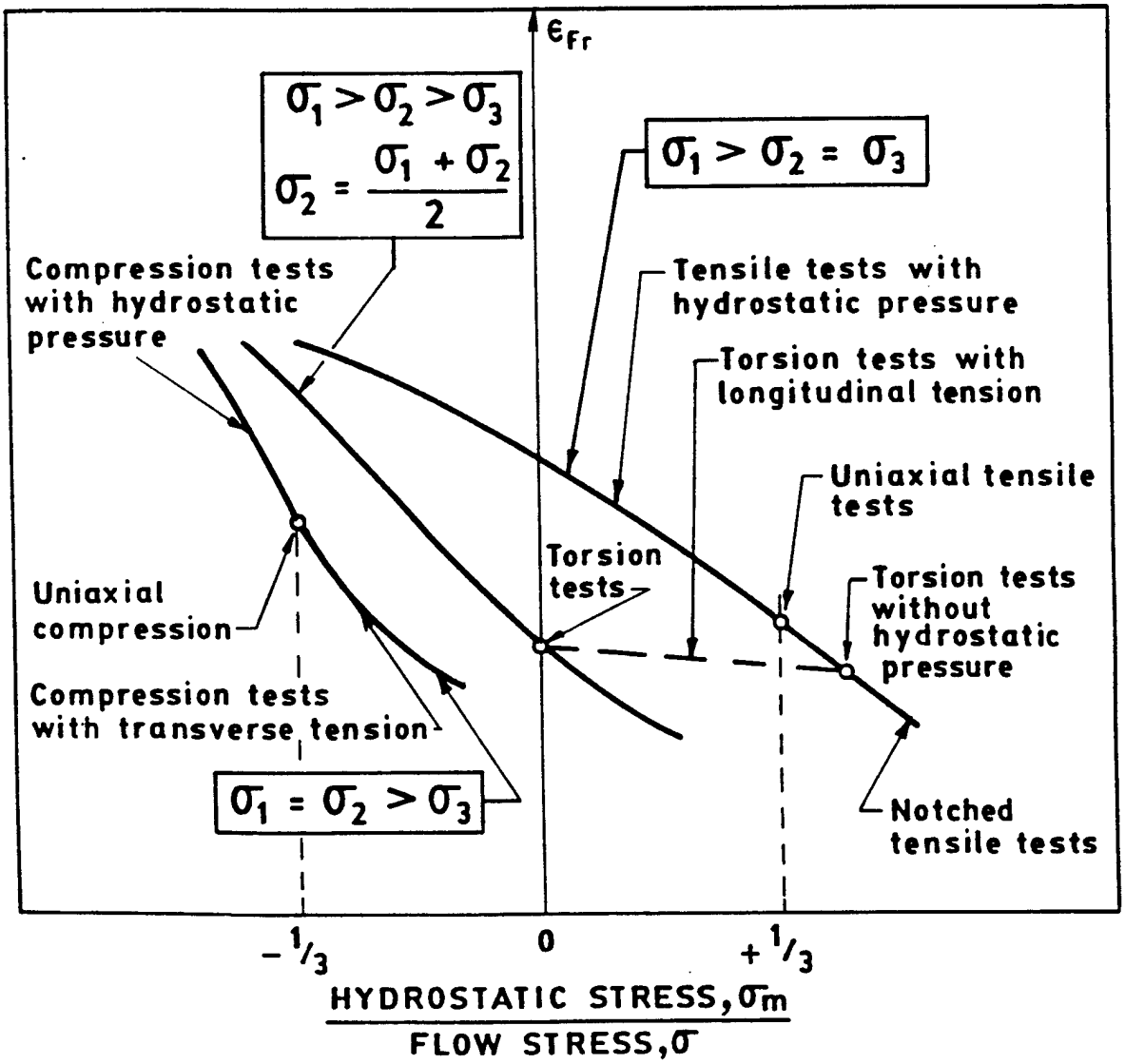

Fig. 2 Schematic sketch showing the effect of type of stressing on deformability. Fracture strain ϵ_{Fr} as a function of the relative mean stress σ_m / σ.

Fig. 3 Ashby's DEFORMATION-MECHANISM MAPS

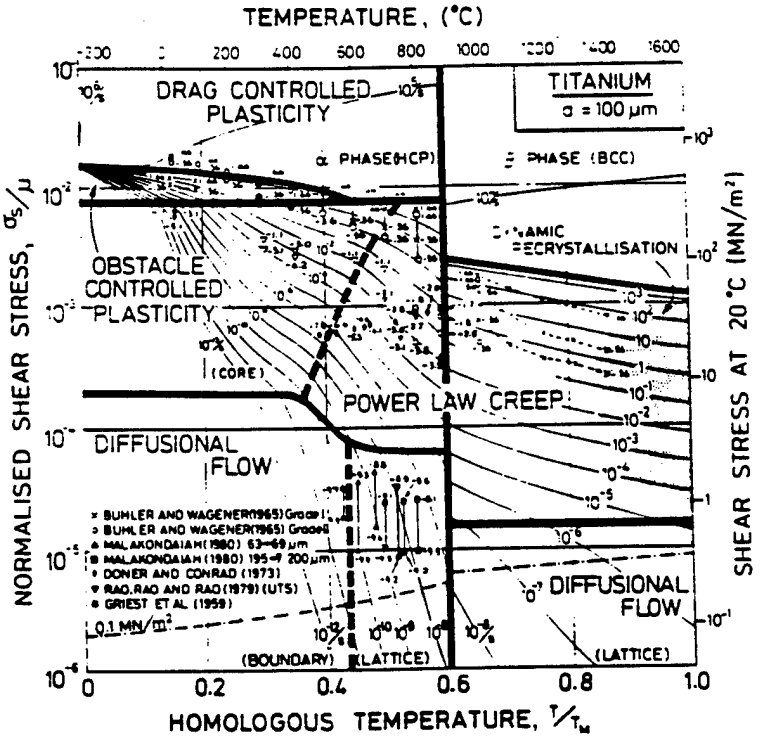

Fig. A stress/temperature map for commercially pure titanium with a grain size of 0·1 mm, showing data.

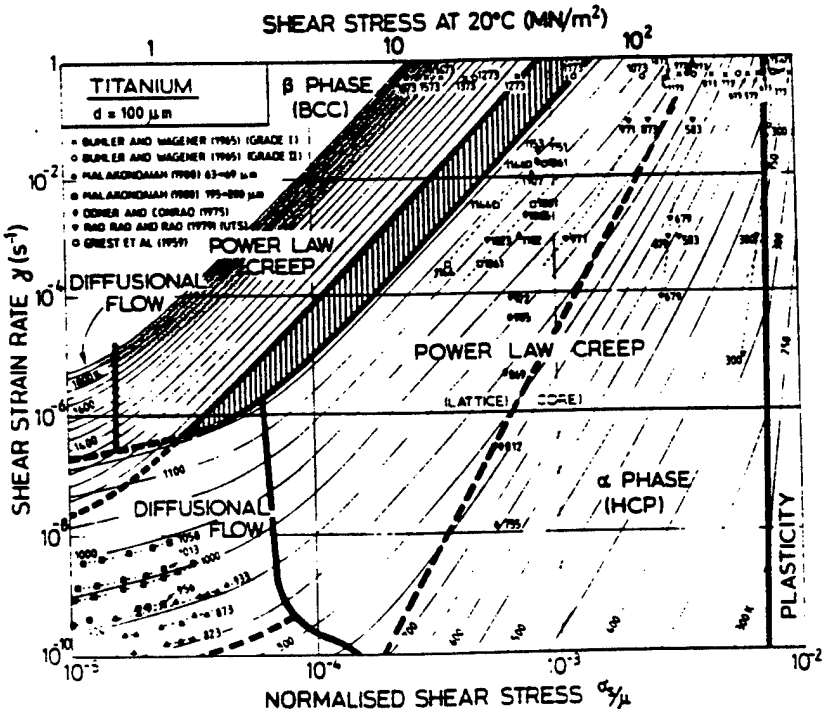

Fig. A strain-rate/stress map for commercially pure titanium with a grain size of 0·1 mm, showing data.

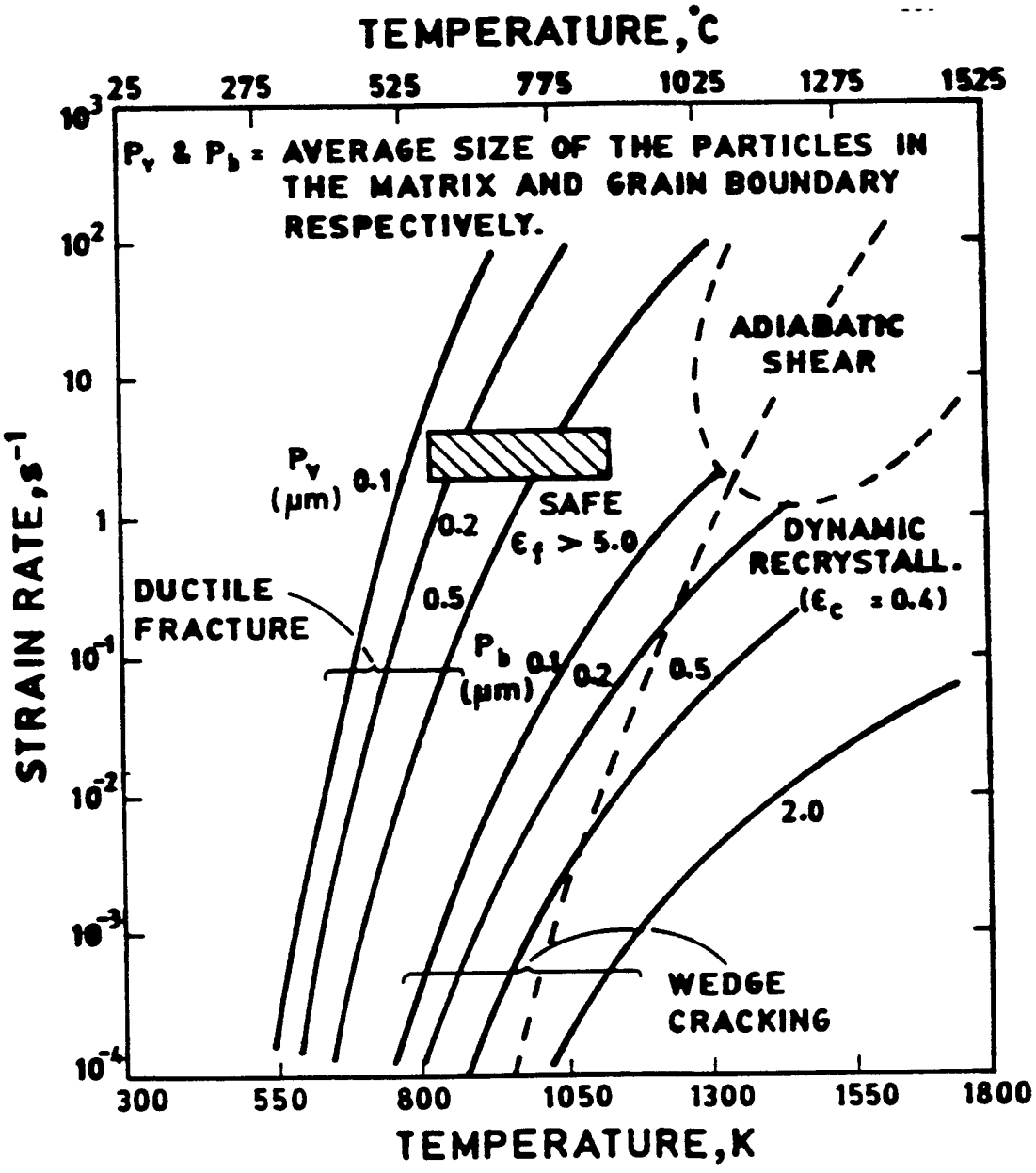

Fig. 4 Raj map for austenitic stainless steel

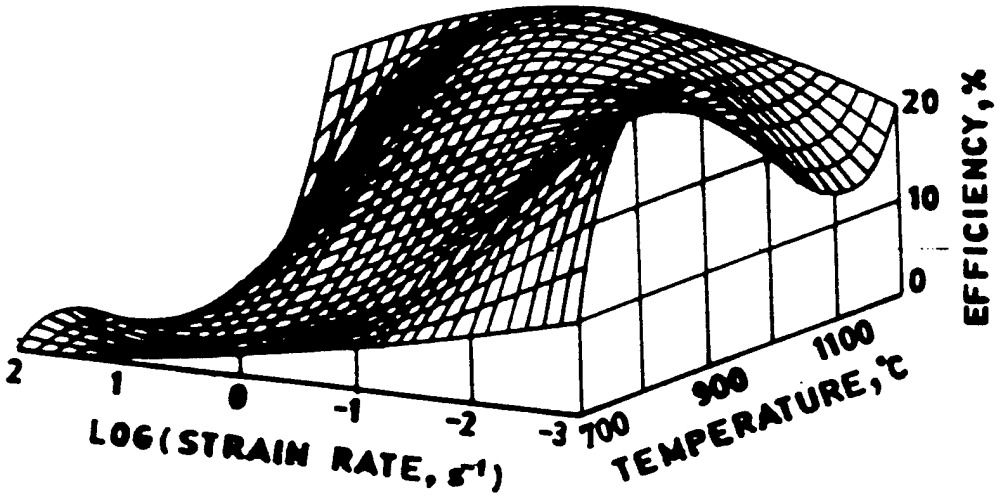

Fig. 5 (a) Three dimensional power dissipation map for 304L for a strain of 0.1.

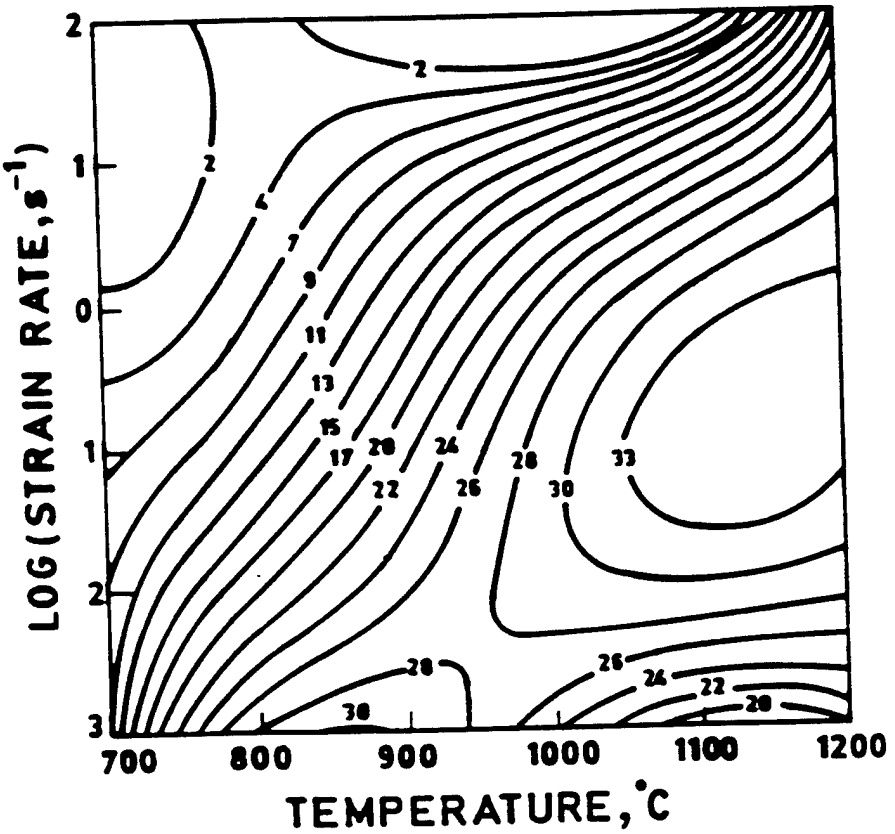

Fig. 5 (b) Contour map representing iso-efficiency contours [η = 2m/(m+1), marked as percent] for 304L at a strain of 0.1.

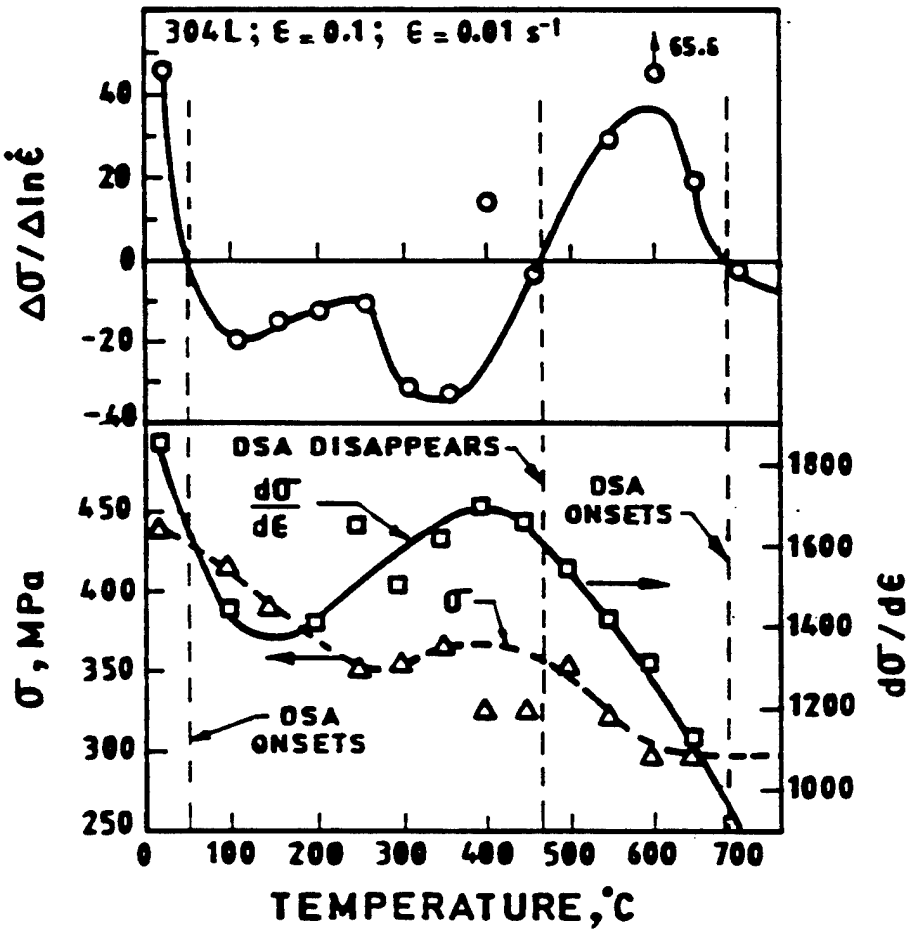

Fig.6 Variations of $(\Delta\sigma/\Delta \ln \dot{\varepsilon})$, (σ) and $(d\sigma/d\varepsilon)$ of 304L in the strain rate of 0.01 s^{-1} at a strain of 0.3.

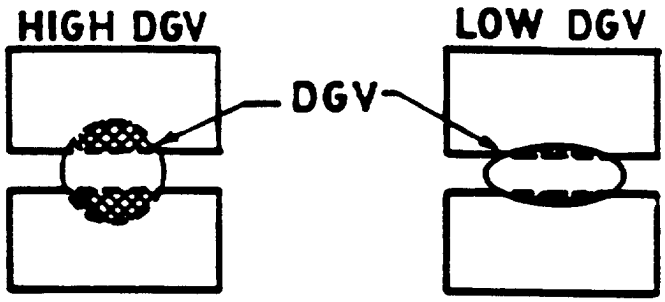

Fig. 7. **Schematic diagram of specimen cross-section showing relative amount of gauge volume penetration into specimen ends, equivalent to distributed gauge volume (DGV), for *a* distributed deformation and *b* concentrated deformation**

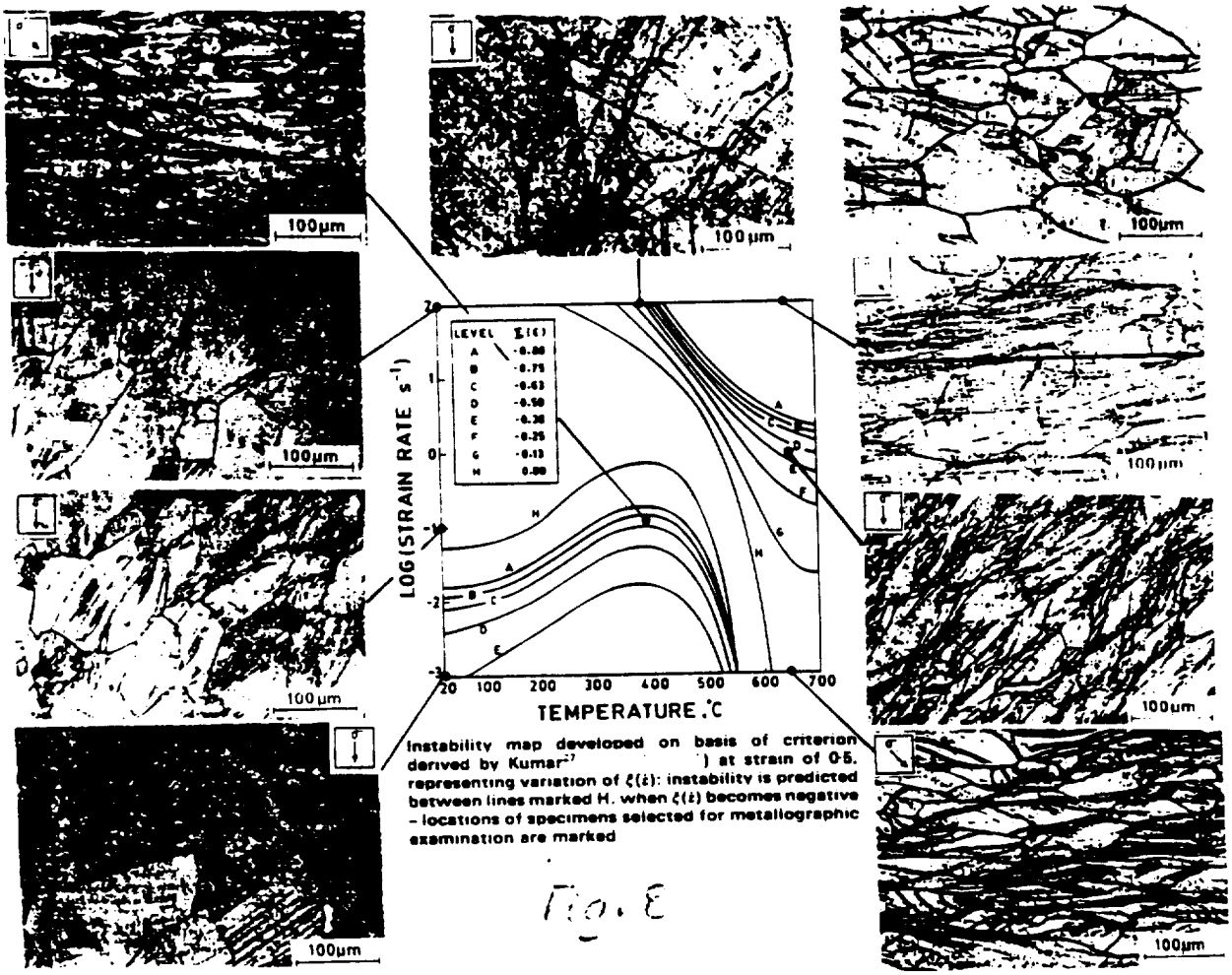

Instability map developed on basis of criterion derived by Kumar[7]) at strain of 0·5, representing variation of $\xi(\dot{\varepsilon})$: instability is predicted between lines marked H, when $\xi(\dot{\varepsilon})$ becomes negative – locations of specimens selected for metallographic examination are marked

Fig. 8

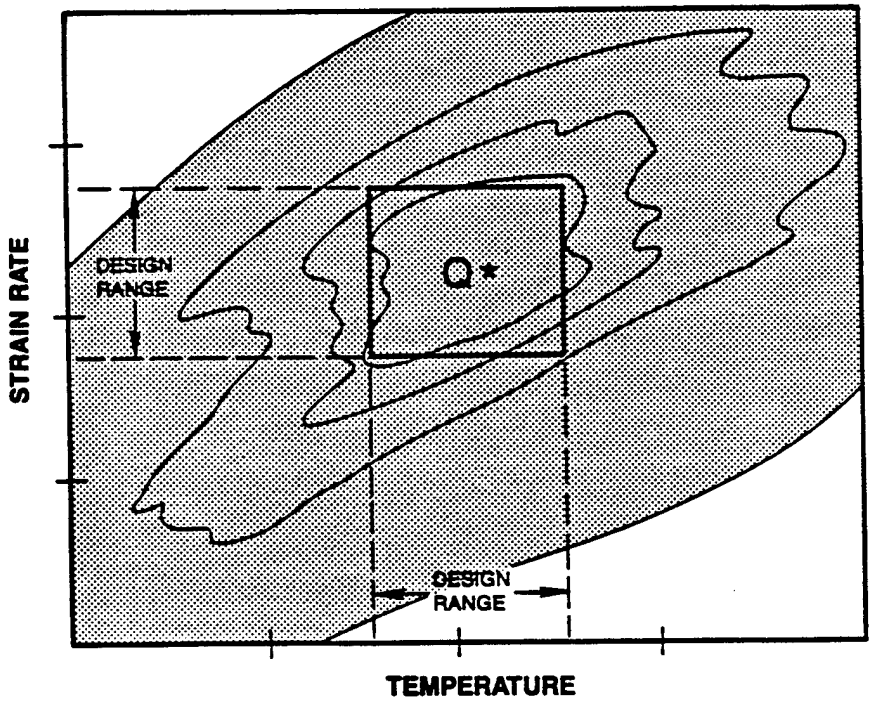

Fig. 9 A schematic diagram of system and design ranges for hot-working processes showing contours of activation energy with the desirable one identified as Q*. The shaded region satisfies all four DMM stability criteria.

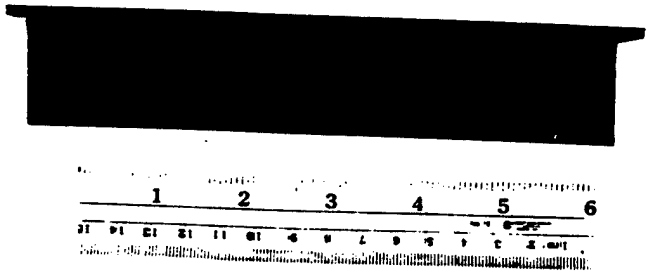

(a)

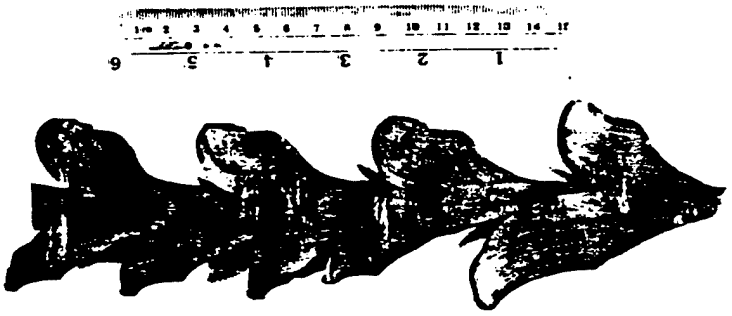

(b)

Fig. 10 Al 2024 + 20% (vol.) SiO_2 products extruded at (a) Optimal Condition (b) Unsafe Condition, predicted by Activation energy map and DMM

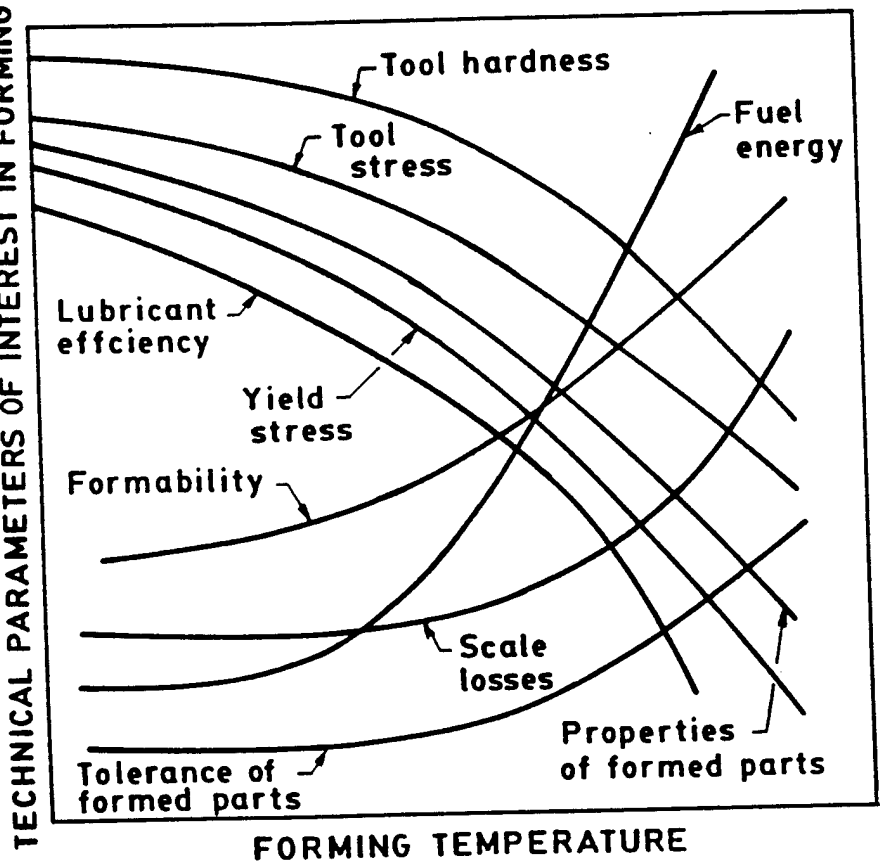

Fig.11 Consolidated concepts involved in selecting working temperature in metal forming.

Modeling and Simulation of Metalforming Equipment

W. Garth Frazier
Wright Laboratory

R. Dennis Irwin
Ohio University

Enrique A. Medina
Wright Laboratory

James C. Malas
Wright Laboratory

Abstract

This paper presents efforts to develop accurate models and computer simulations of metalforming equipment for the purpose of improving the design of metalforming processes. The emphasis is placed on modeling the dynamic behavior of a hydraulic, vertical forge press, although similar principles apply to other types of metalforming equipment. The application of these principles to a 1000 ton forge press in-service at Wright-Patterson Air Force Base, Ohio are presented along with experimental verification.

1.0 Motivation

The motivation for developing accurate models and computer simulations of metal forming equipment is three-fold. Firstly, the ability to develop improved control algorithms is greatly enhanced by the ability to perform repeated computer experiments without the need for costly and time-consuming experimental tests that can interfere with production. Secondly, as the use of finite-element modeling (FEM) techniques for the analysis and design of metalforming processes continues to increase and become more

analysis and design of metalforming processes continues to increase and become more sophisticated, the need to integrate accurate equipment models into the FEM-based simulations will increase. Thirdly, with the possibility of sensing workpiece conditions directly during forging operations (Mullins and Irwin, 1996) it is possible in the future that these measurements could be fed back to the metalforming equipment's control computer for direct control of the forming equipment. From a process control perspective, this approach should provide for the highest level of robustness and repeatability.

2.0 Subsystem Modeling

This section presents techniques for modeling the numerous components of a press system that play an important role in dynamic (transient and steady-state) performance. Those components of a press that are not directly related to dynamic performance, such as safety features and operator interface are not discussed.

2.1 Press System Description

A simplified block diagram of a typical hydraulic press system is given in Fig. 1, where the lines represent possible directions of fluid flow. The system is powered by an electric motor that drives a hydraulic pump. Transient demands for high ram speeds are met by an accumulator system. A counter-balance is employed to support and return the main ram to the top of its stroke after a forging operation is completed. The servo manifold controls the flow of fluid to the main ram cylinder and to the tank.

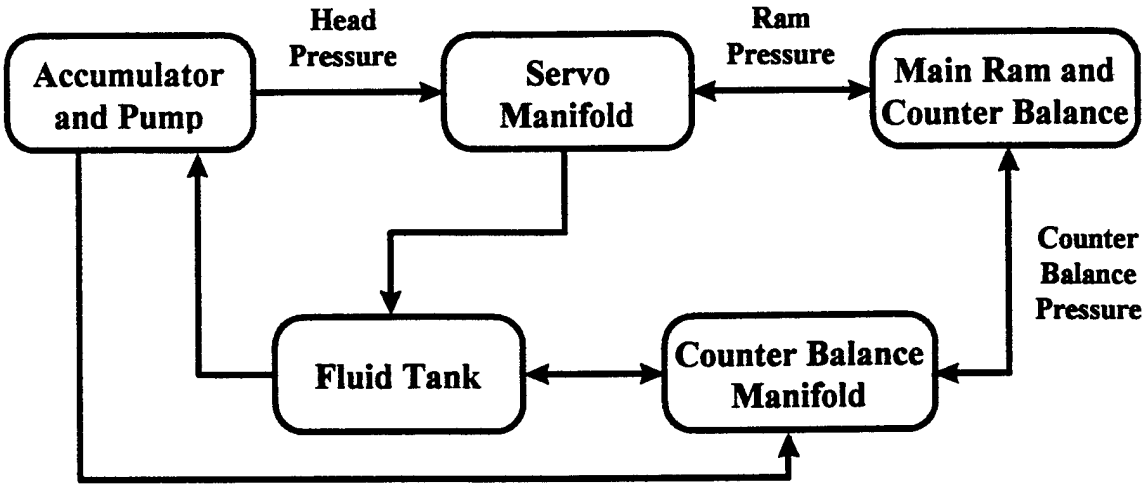

Figure 1: Simplified Block Diagram of a Typical Hydraulic Press

2.2 Hydraulics

The primary considerations involved in the modeling of hydraulics in a press system include the bulk modulus of the fluid, the flow rate of fluid from the pump, the head pressure, the flow rate through the servo manifold, and the main ram pressure. Other items that must be included are the hydraulic pressure on the counter-balance subsystem and pressure losses due to the flow of fluid through circular pipe. Each of these items is discussed in the sequel.

2.2.1 Pumps

Most often pumps are driven at a constant speed by an electric motor while the amount of fluid being delivered by the pump at any moment is usually governed by the position of an actuating spool of a servovalve[1]. The time response of this servovalve is the dominant factor in the dynamic performance of the pump. Therefore, from a *mechanical response*

perspective, the modeling of pump behavior can be viewed as being similar to the mechanical response of servovalves in general as will be discussed in section 2.3.

2.2.2 Head pressure

The head pressure of a pump-only system or a system using an accumulator in which the separator tank is completely full or empty is modeled from first principles of fluid mechanics[1] by the relationship

$$\dot{P}_{head}(t) = \frac{q_{pump}(t) - q_{sm}(t)}{C_{head}(t)}, \tag{1}$$

where q_{pump}, q_{sm} and C_{head} are the volumetric flow rate into the volume between the pump and the servo manifold, flow rate out, and hydraulic capacitance of that volume, respectively. The hydraulic capacitance is simply

$$C_{head}(t) = \frac{V_{head}(t)}{\beta}, \tag{2}$$

where V_{head} and β are the volume between the pump and the servo manifold and the bulk modulus of the fluid, respectively. The volume is shown to possess a time dependence to account for the fact that the volume can change if there is an accumulator in the pump circuit. In systems employing accumulators in which the separator tank is not full (the usual case), the head pressure is given by the differential equation

$$\dot{P}_{head}(t) = -\frac{P_0 V_0}{V_{nit}^2(t)} \dot{V}_{nit}(t), \tag{3}$$

where P_o, V_o, and V_{nit} are initial head pressure, initial volume of nitrogen, and instantaneous volume of nitrogen, respectively. Assuming the hydraulic fluid is

incompressible with respect to the nitrogen, the instantaneous volume of nitrogen is determined from the net flow of hydraulic fluid into the head volume, i.e.,

$$\dot{V}_{nit}(t) = q_{pump}(t) - q_{sm}(t). \tag{4}$$

2.2.3 Ram pressure

The most important hydraulic component affecting ram speed is the pressure on the ram piston. This pressure is modeled by the differential equation

$$\dot{P}_{ram}(t) = \frac{q_{sm}(t) - A_{ram} v_{ram}(t)}{C_{ram}(t)}, \tag{5}$$

where A_{ram}, v_{ram}, and C_{ram} are the cross-section of the ram piston, velocity of the ram and hydraulic capacitance of the fluid volume between the servo manifold and the ram piston, respectively. This capacitance is given by

$$C_{ram}(t) = \frac{V_{nom} + A_{ram} \Delta x_{ram}(t)}{\beta}, \tag{6}$$

where V_{nom} and Δx_{ram} are the nominal volume and the displacement of the ram from its nominal position, respectively. The term $A_{ram} v_{ram}(t)$ located in the numerator of Eq. (5) takes into account the effect of the rate of change of the volume as the ram descends. The force applied to the main ram due to the ram pressure is

$$F_{sm}(t) = P_{ram}(t) A_{ram}.$$

2.2.4 Counter-balance pressure

The counter-balance pressure in press systems is commonly maintained by a relief valve. The relief pressure of this valve is chosen so that the weight of the ram can be supported

entirely by the counter-balance cylinders. The weight that can be supported by such a system is given by

$$W_{sup} = A_{cb} P_{rv} , \tag{7}$$

where A_{cb} and P_{rv} are the cross sectional area of the counter-balance pistons and the relief valve pressure, respectively. When pressure is applied to the ram by fluid from the servo manifold, the load on the counter-balance exceeds W_{sup} and the relief valve opens allowing fluid to flow and the ram to descend. The force (no load) applied to the ram via the counter-balance is given by

$$F_{cb}(t) = A_{cb} P_{rv} + \gamma_{cb} A_{cb} \dot{x}_{ram}(t) , \tag{8}$$

where the term $\gamma_{cb} A_{cb} \dot{x}_{ram}$ represents the additional force applied to the ram due to the frictional effect of fluid flowing through pipe. The parameter γ_{cb} is a factor for determining the frictional force per unit of volumetric flow rate. It is determined from the Hagen-Poiseuille Law[2]:

$$\gamma_{cb} = \frac{128 \mu L}{\pi D^4} , \tag{9}$$

where D and L are the diameter and length of the pipe in inches, and μ is the viscosity of the fluid. This effect can add a significant amount of viscous damping to the overall system.

2.3 Servovalves

The primary factors determining the flow of fluid through the servo manifold are the current state of the servovalves and the differential pressure across the valves. Although

higher-order nonlinear analytical models of the mechanical behavior of servovalves can be developed from first principles, second-order linear models identified from experimental data have proven to be quite satisfactory for producing accurate simulations. A typical model in state-variable form [5] is given by

$$\begin{aligned} \dot{x}_1(t) &= x_2(t) \\ \dot{x}_2(t) &= A\omega_n^2 v(t) - 2\zeta\omega_n x_2(t) - \omega_n^2 x_1(t) \end{aligned} \tag{10}$$

where x_1, x_2, and v are the spool position, spool velocity, and applied voltage, respectively. A, ω_n, and ζ are the gain (e.g., in./volt), natural frequency and damping ratio of the valve. Equation (10) only describes the mechanical response of the power spool. The volumetric flow rate of fluid through a three-way servovalve into the main ram fluid volume can be modeled as a function of the position of the power spool and the differential pressure across the valve by a modified orifice flow equation[1]

$$q = \text{sgn}(x_1(t))\ \text{sgn}(\Delta P(t))\ f(|x_1(t)|)\ \sqrt{|\Delta P(t)|}\ , \tag{11}$$

where

$$\Delta P(t) = P_{head}(t) - P_{ram}(t), \tag{12}$$

and the function f is an experimentally determined relationship between spool position and flow rate. Experience reveals that a third degree polynomial is usually sufficient for the function f. Typical flow curves for a servovalve are shown in Fig. 2 for several values of differential pressure. The use of the signum function provides a means for modeling the flow direction switching capabilities of a three-way valve. The four flow possibilities are defined in Table I.

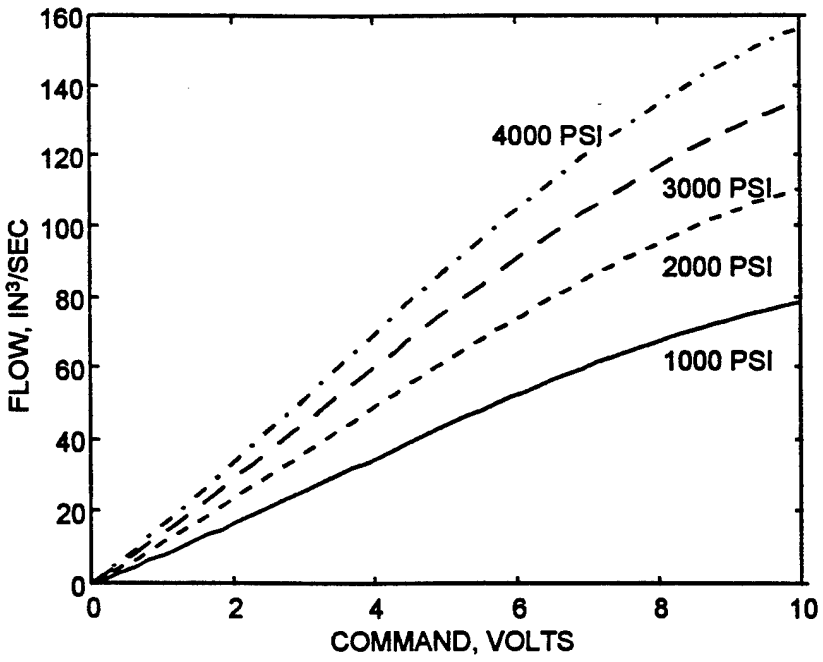

Figure 2: Typical Flow Curve for a Servovalve as a Function of Spool Position

Table I: Flow Possibilities for a Three-Way Servovalve

	$\Delta P > 0$	$\Delta P \geq 0$
$x_l \leq 0$	tank to ram	[illegible]
$x_l > 0$	ram to head	[illegible]

2.4 Ram Dynamics

The ram can be modeled as a rigid body with a mass M possessing a single degree of freedom. More complex bending and inertial effects can be included if increased precision is justified. The equation of motion for the ram is given by

$$a_{ram}(t) = [F_{sm}(t) - F_{cb}(t) + W_{ram} - F_{fric}(t) - F_{load}(t)] / M_{ram}, \qquad (13)$$

a_{ram} = acceleration of the ram

F_{sm} = forces due to hydraulic pressure from servo manifold

F_{cb} = forces due to hydraulic pressure from counter-balance

W_{ram} = weight of the ram

F_{fric} = frictional forces

F_{load} = forces due to workpiece loading

M_{ram} = mass of the ram.

The force of friction F_{fric} between the ram piston and the seals can be modeled as coulomb friction[7]. Values for the parameters associated with this difficult-to-measure effect are best determined by adjusting the simulation parameters to best match the experimental data. A model for this effect is given by

$$F_{fric}(t) = \text{sgn}(v(t)) * \left[c|v(t)| + b\right],$$

where $v(t)$ is ram velocity, c is similar to the effect of viscous friction and b is an offset that models the effect of sticking. Note that if b is zero then this model reduces to the standard model of viscous friction. The accurate modeling of the workpiece loading F_{load} is very difficult for situations involving the forming of complex shapes due to the

interaction of the workpiece and dies and the mechanical properties of the workpiece material. In most instances it is necessary to make simplifying assumptions in order to formulate a practical model.

2.5 Sensors

A modern press system can employ several types of sensors for safety, diagnostics, and feedback control. For the purpose of feedback control, measurement of pressure, linear displacement and linear velocity are most important. The pressure transducers[3] are employed to measure the head pressure and the pressure on the ram piston. Since the difference in these pressures provides for the differential pressure across the servo manifold, the control computer can use this difference for determining commands to the servovalves. This is the most common method employed for ram speed control. Used alone, it has the disadvantage of requiring very accurate models of the flow curves of the servovalves since the actual ram velocity is not actually used. Any error in the flow curve models will translate directly into errors in ram speed. The measurement from the head pressure transducer is also useful for actuating the main pump in order to maintain the appropriate head pressure. The response time of a pressure transducer is significantly shorter than that of a press and therefore these transducers and their associated electronics can safely be modeled as simple gains, i.e.,

$$\text{Voltage} = \text{Gain} * \text{Pressure}. \tag{14}$$

Linear displacement transducers[4] play a critical role in measurement of ram stroke. High accuracy and precision of these sensors is very important for ensuring repeated part

quality. Various types of linear displacement transducers are available that use a variety of technologies. Most of these have very rapid response times and can, like pressure transducers, be modeled as simple gains. Direct measurement of ram velocity is very difficult due to the lack of availability of reliable sensors for measuring translational velocity over a large dynamic range. A common method employed for obtaining translational velocity estimates is to numerically differentiate successive position measurements. This method is fraught with pitfalls and must be used with extreme caution due to the presence of electronic and analog-to-digital converter quantization noise[6] on the position measurements. The quantization noise problem is especially acute in situations where low velocities and high computer sampling rates are present. The simplest velocity estimate is calculated by

$$\hat{v}(t) = \frac{s(t) - s(t-T)}{T}\ , \tag{15}$$

where T is the sampling period and s is ram position. More complex schemes can be employed that are effectively digitally filtered estimates of velocity[6]. These techniques reduce the effect of noise problems at the expense of reducing response time. In many applications this trade-off is justified. Another method that can be employed is to numerically integrate accelerometer measurements. This technique considerably reduces the noise problem, but can introduce errors due to drift in the accelerometer output. The formula for the trapezoidal integrator is given by

$$\hat{v}(t) = \hat{v}(t-T) + \frac{T}{2}\left[a(t) + a(t-T)\right]\ , \tag{16}$$

where a is ram acceleration.

2.5 Control Processor

Press systems typically use two levels of processing for control. The highest level of control is usually called a supervisor and provides functions such as engaging safety locks, monitoring pressure switches for excessive pressures, etc. This level of control is usually provided by an industrial programmable logic controller (PLC). The lower level of control is usually called the servo loop and is responsible for having the main ram track the desired velocity or position profile. This level of control can be provided by a PLC with special servo control features or by a industrial PC-based system with custom software. Input to and output from the computer control system is usually provided by 12-bit analog-to-digital (A/D) and digital-to-analog (D/A) converters, respectively. Modern electronic computer control systems have the capability of providing very high sampling rates which provide in theory the capability of rapid response to changes in load conditions. However, the use of excessively high sampling rates can introduce problems as described previously.

3.0 Computer Simulation of Dynamic Systems

The use of a system model to predict the behavior of an actual system is desirable in many situations. In the case of design, the actual system may not yet exist and it may be desired to evaluate several possible configurations. In the case of analysis, an experiment on the actual system may take too much time or too little time, may be too expensive, or may even destroy the system - very likely an undesirable situation. Many complex, real-world systems cannot be accurately described by mathematical models that can be evaluated analytically to obtain responses to particular set of inputs or parameters. The

simulation alternative consists of evaluating the model numerically with the inputs and parameters in question to determine how the outputs of interest are affected[8].

Simulation has been a tool for analysis and design of engineering systems for many years now. In particular, simulation of continuous time and discrete time dynamic systems has been the subject of vast research for several decades. Simulation languages such as CSMP™ and ACSL™ have been specifically developed for building dynamic system simulation models.

3.1 Graphical Simulation Paradigm

The state of the art in simulation of dynamic systems includes software packages that not only aid the engineer in building simulation models, but facilitate the creation of models and interpretation of results by means of sophisticated graphical user interfaces. Simulink™, VisSim™, and Matrix$_X$™ are three of the several packages of this nature that are available.

In the sense used here, a simulation model is represented by a block diagram in which all relevant elements and relationships that model the system are included. For the case of the forging system under consideration, which includes the forge press, the workpiece loading, and the internal mechanisms by which the microstructure of the workpiece evolves, the top level block diagram of a Vissim™ simulation model is shown, for illustration purposes, in Fig. 3. Each block in such a simulation diagram models an element or group of elements in the actual system, a data input port, or an output port. Each line represents a path for the flow of information or energy. Note in Fig. 3 that the fundamental blocks in the forging process simulation are the forge press, the controller,

and the tooling package. Each of these blocks is comprised of several levels of subsystems, which can be observed with convenient editing tools in the graphical simulation environment.

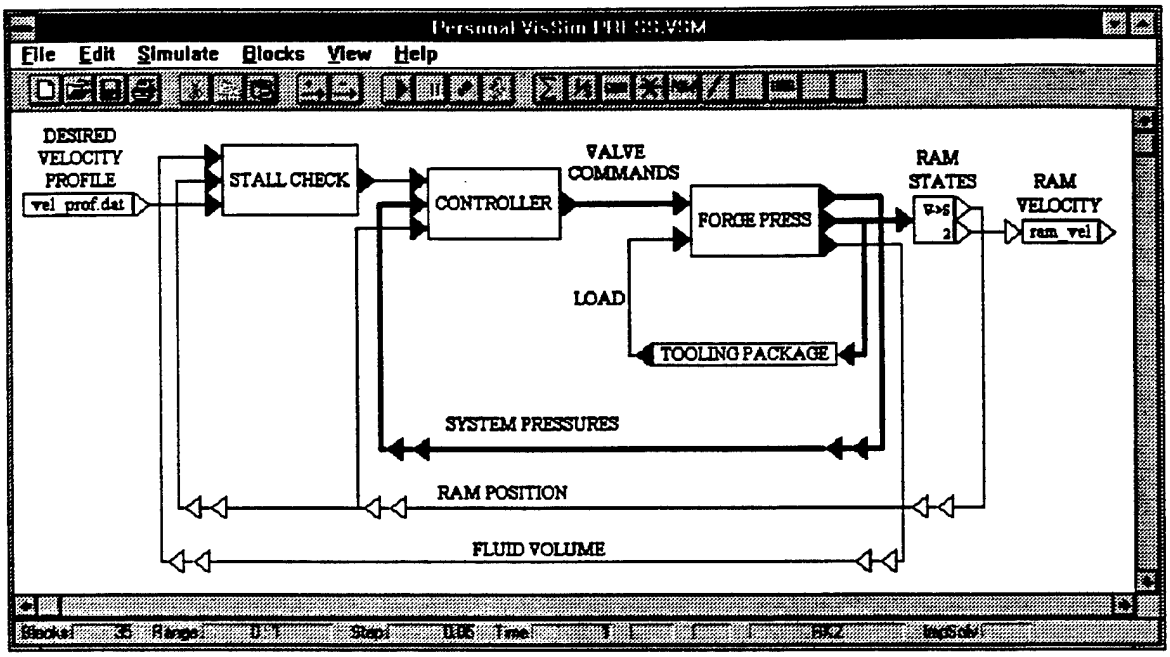

Figure 3: Vissim™ Window, Top Level Diagram of a Forging Process Simulation

3.2 Automatic Equipment Simulation Code Generation for the Metal Forming Industry

One objective underlying this work is to provide the metal forming industry with scientifically based tools that will expedite design by allowing the user to perform what-if studies that include all aspects of the manufacturing process. For that reason, it is desired to provide the user with a software module that will generate the response of the system to specific inputs without having to use a simulation package; i.e., a standalone program or a set of routines that will simulate the system without the need for a dedicated

simulation software package on the part of the end user. This can be achieved by using automatic code generation features that can be purchased for any of the state-of-the-art simulation packages mentioned above.

The idea here is to build the simulation model in one of the available simulation software packages and then generate high level language code that can be compiled to generate a program or library that will simulate the system. The original simulation model can be developed by a consulting firm that can deliver executable code or libraries for the simulation of the particular system. Such executable or library can then be used in conjunction with existing finite element analysis software for the simulation of the forging process by the engineer in charge of the design.

4.0 Application to the Erie 1000 ton Forge Press

In this section the application of the modeling principles and computer simulation tools presented in sections 2 and 3 to an in-service forge press are described. Comparison of experimental and computer simulation results are presented and discussed along with some lessons learned and suggestions for development of future press control systems.

4.1 Description of the Erie 1000 ton Forge Press

The Erie 1000 ton forge press located at Wright-Patterson Air Force Base (WPAFB) is a vertical hydraulic forge press possessing a programmable, computer-based ram velocity control system employing hydraulic pressure and ram position feedback. The press was manufactured by Erie Corporation, Erie, Pennsylvania, while the hydraulic control system

was designed and built by Oilgear Inc., Milwaukee, Wisconsin. The press has been in service since 199? for performing manufacturing and metallurgical research at WPAFB. The power plant consists of an axial piston pump with 82 gallons per minute (gpm) capacity driven at 1200 rpm by an 200 hp electric motor. Transient demands for higher flow rates are provided by a 16 gallon hydraulic separator tank and 195 gallon nitrogen bottle. Nominal head pressure is 3800 psi. The stroke of the ram is 15 inches and the maximum speed of the ram is approximately 300 in./min. This maximum speed cannot be maintained over the entire stroke due to the limited capacity of the pump and size of the separator tank. The cross sectional area of the main ram piston is 591 inches^2. The main ram is supported by two counter-balance pistons with cross sectional areas of 28.86 inches^2 each. The relief valve pressure on the counter-balance is 1000 psi. This implies that the counter-balance can support 28.86 tons. The nominal weight of the main ram is 21 tons.

The speed of the press is regulated by the use of two Oilgear three-way servovalves and one Parker proportional throttle valve. The gains of these valves are:

Oilgear 800 three-way servovalve	6 (gal/min)/volt @ 3000 psi
Oilgear 1600 three-way servovalve	36.7 (gal/min)/volt @ 3000 psi
Parker TDA 100 proportional throttle valve	330 (gal/min)/volt @ 3000 psi

The use of these three valves in parallel provides capability for wide dynamic range and precise control of ram velocity. The valves are controlled by an Intel 80368-based industrial computer that uses head pressure, ram pressure and ram displacement feedback for control of velocity. The details of the Oilgear-developed control law for the valves are proprietary and cannot be provided.

4.2 Erie Press Simulation

Using the principles described in section 2, a computer simulation was developed using the simulation software SIMULINK™. The block diagram for the overall press system is shown in Fig. 4. This diagram shows the interconnections between the forge press, the control computer, and the tooling package. Fig. 5 shows the model of the forge press, including the accumulator, pump, servo manifold, fluid dynamic effects, and the ram. Fig. 6 shows the block diagram for a three-way servovalve. Block diagrams for the rest of the press components and systems are similar.

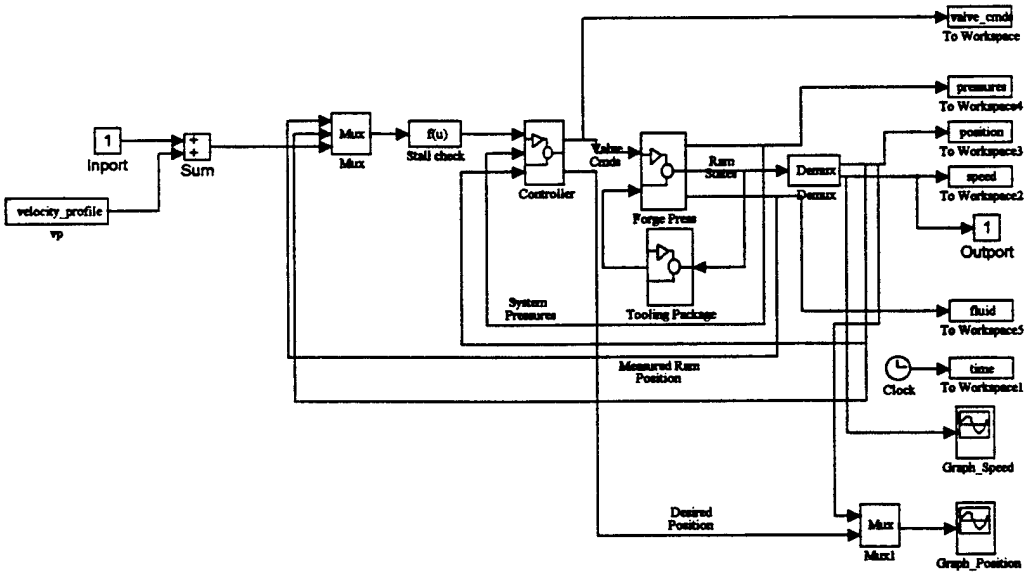

Figure 4: Press System Block Diagram

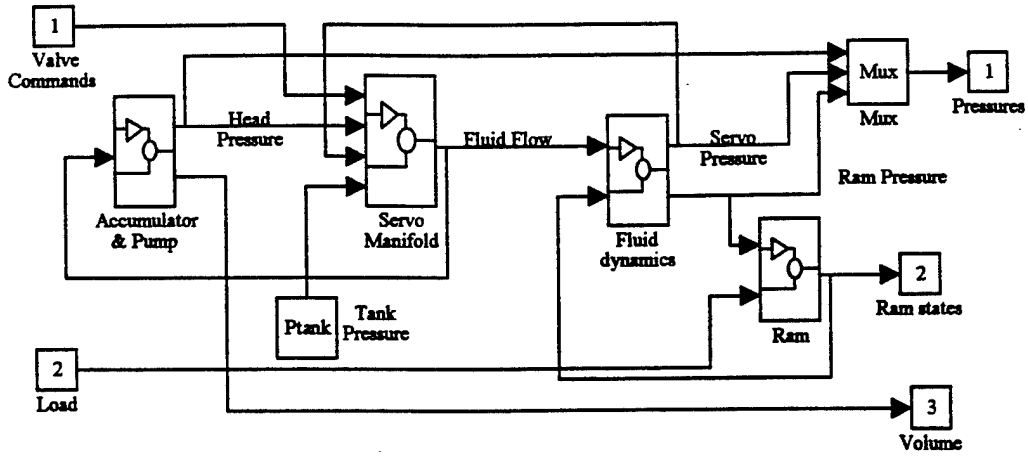

Figure 5: Forge Press Block Diagram

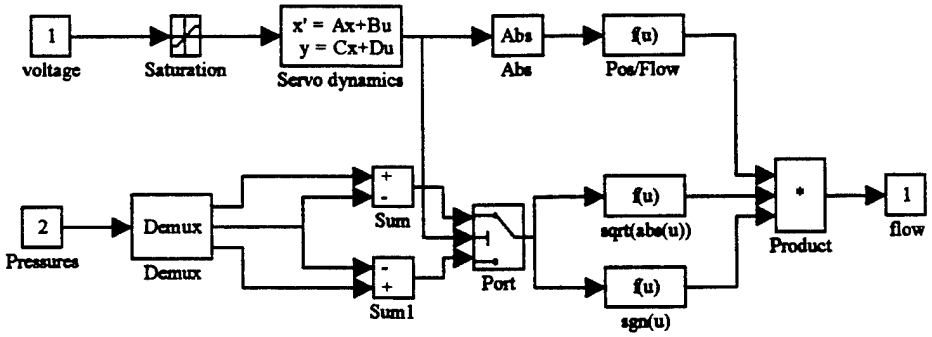

Figure 6: Three-way Servovalve Block Diagram

In order to verify that the computer model is accurate, experimental data from a simple forging was recorded and compared with the corresponding simulation data. The experimental forging was a cylindrical upsetting of steel. The press was programmed to forge at a constant velocity of 30 in/min. Plots of the experimental and simulated ram velocity and position are shown in Fig. 7 and Fig. 8, respectively. The irregularity in the experimental data of Fig. 7 is due to the method used by the press' computer to estimate the velocity. This behavior is not present in the actual press motion. Other than this effect, the simulation data is seen to closely resemble the experimental data. The data clearly reveals the ramping up and overshoot of the desired velocity. The brief change in velocity due to impact with the workpiece is clearly observed near 3.5 seconds.

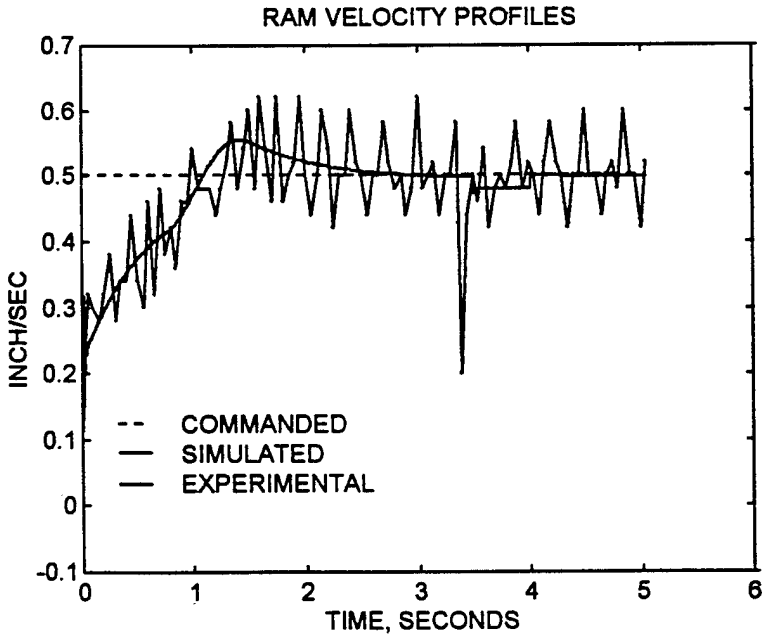

Figure 7: Plots of Experimental and Simulated Ram Velocities

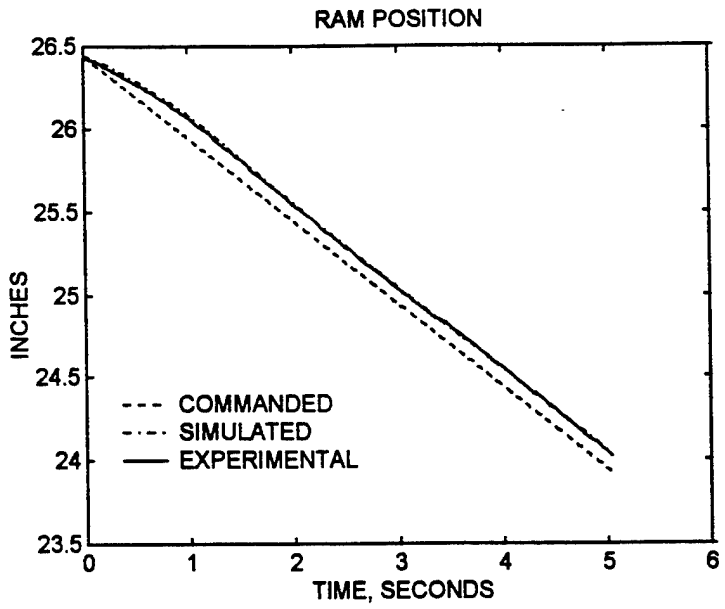

Figure 8: Plots of Experimental and Simulated Ram Position

Fig. 9 shows the experimental and simulated results for the ram load as derived from the ram pressure measurement. The plot reveals that approximately 10 tons are needed to overcome the counter-balance and frictional forces. The load increases rapidly beginning at approximately 3.5 seconds. This corresponds to impact with the workpiece. Beginning at approximately 4 seconds, elastic deformation of the workpiece and tooling ceases and plastic deformation of the workpiece begins. It is clear from the data that the press was able to maintain the desired velocity under load, as long as the load was not increasing too rapidly.

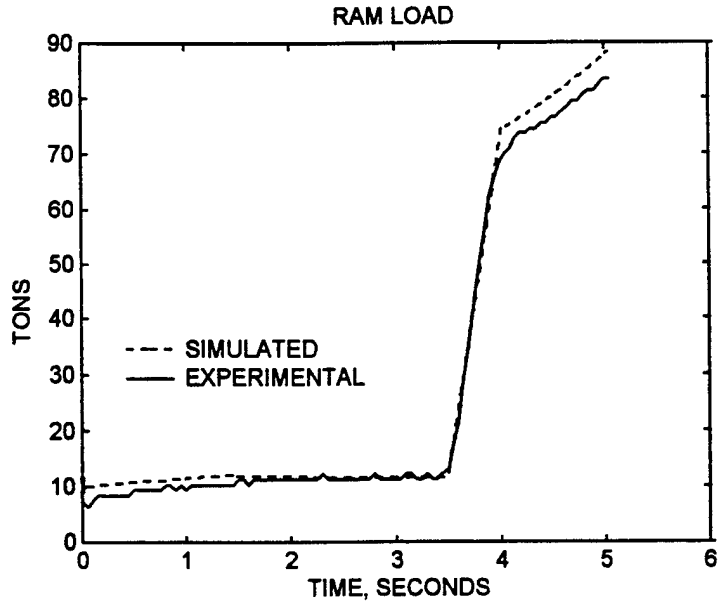

Figure 9: Plots of Experimental and Simulated Ram Load

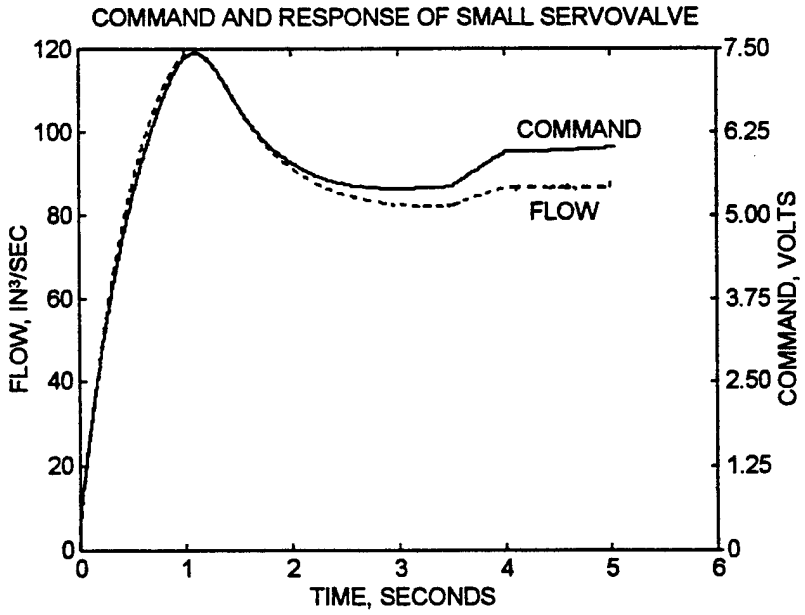

Figure 10: Simulation Results for Small Servovalve Command and Response

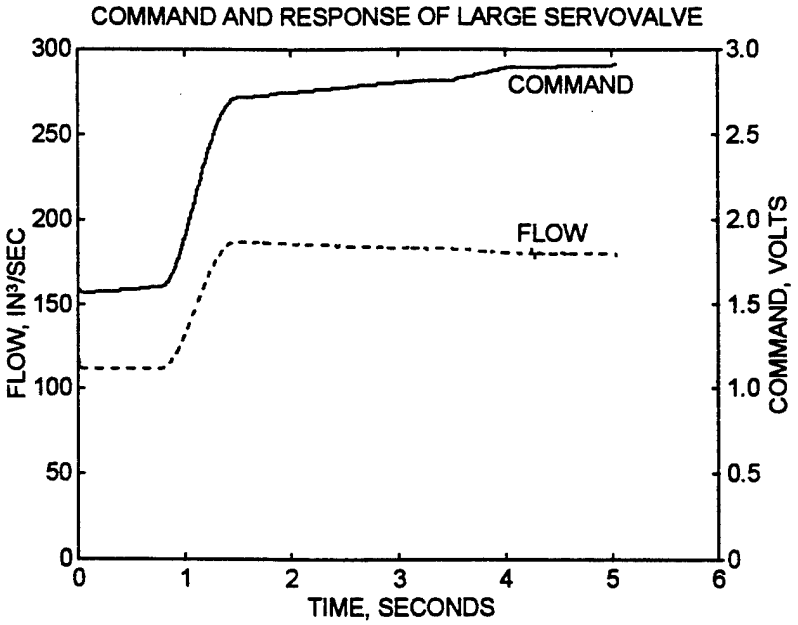

Figure 11: Simulation Results for Large Servovalve Command and Response

The press' computer does not record the commands to the hydraulic valves, but it is interesting to observe the plots of these commands and the corresponding valve flows from the simulation. These plots are shown in Figures 10 and 11. Notice that a particular valve command does not always result in the same flow rate. This is due to the changing pressure across the servo manifold. Fig. 11 clearly reveals that flow can decrease even as the command increases.

Conclusions

The use of graphics-based system modeling and simulation software greatly assists in making the modeling process systematic, self-documenting, accurate, and time efficient. The ability to quickly perform "what if" experiments with regards to different control strategies, sensors, actuators, and tooling aids the engineer in making informed decisions

regarding changes to existing metal-forming equipment and/or processing operations. For example, this approach will make it possible for the engineer to answer questions such as: would the addition of a sensor for direct measurement of ram velocity be justified for feedback control of the ram velocity? As the need for precise control of ram velocity, as well as position, increases, the need for direct measurement of velocity as a feedback control signal will become more acute. Current techniques for controlling velocity (inversion of servovalve flow models combined with pressure measurements and numerical differentiation of displacement measurements) are not adequate for high performance.

Experience has revealed the need for press operators to customize the press control law in order to achieve the desired velocity profile for different forming operations. Having a custom control law for equipment that repeatedly makes the same part for several weeks is satisfactory, but as the need to use the same equipment for several different parts in a day or custom small lots increases, customizing the control laws can waste a significant amount of time. Control laws need to be designed to be robust so that different loading conditions and velocity profiles can be handled successfully without the need for customization.

Acknowledgments

This work was performed under the sponsorship of the Material Process Design Branch, Wright-Patterson Air Force Base, Ohio. The authors are thankful to Mr. Douglas R. Barker, of UES, Inc., and his colleagues in the Materials Processing Laboratory at

WPAFB, for their assistance during the equipment modeling and experimental stages of the work.

References

1. Wayne Anderson (1988), Controlling Electrohydraulic Systems, Marcel Dekker, New York.

2. Ernest E. Lewis and Hansjoerg Stern (1962), Design of Hydraulic Control Systems, McGraw-Hill, New York

3. Duone Tandeske (1991), Pressure Sensors, Marcel Dekker, New York

4. Harry N. Norton (1969), Handbook of Transducers for Electronic Measuring Systems, Prentice-Hall, Englewood Cliffs, New Jersey

5. Paul M. DeRusso, Rob J. Roy, and Charles M. Close (1965), State-Variables for Engineers, John Wiley and Sons, New York

6. S. Bennet and D.A. Linkens (1982), Computer Control of Industrial Processes, Pter Peregrinus, LTD, New York

7. John G. Truxal (1955), Control System Synthesis, McGraw-Hill, New York

8. Law and W. D. Kelton (1991), Simulation Modeling and Analysis, McGraw-Hill, Inc., New York, 2nd Edition, pp. 1-6, 109-116.

PD-Vol. 75

ESDA 1996

PROCEEDINGS OF THE 1996 ENGINEERING SYSTEMS DESIGN AND ANALYSIS CONFERENCE

VOLUME 3
COMPOSITE MATERIALS
MANUFACTURING
FATIGUE/FRACTURE

presented at

THE THIRD BIENNIAL JOINT CONFERENCE ON
ENGINEERING SYSTEMS DESIGN AND ANALYSIS
JULY 1–4, 1996
MONTPELLIER, FRANCE

sponsored by

THE PETROLEUM DIVISION, ASME

edited by

F. VENIALI
ROMA UNIV. TOR VARGATA

D. GAMBY
ENSMA/LMPM, FRANCE

J. RASTY
TEXAS TECH UNIV.

M. BELLET
CEMEF, FRANCE

H. MASUDI
PRAIRIE VIEW A&M UNIV.

A. DRAGON
ENSMA, FRANCE

THE AMERICAN SOCIETY OF MECHANICAL ENGINEERS
UNITED ENGINEERING CENTER/ 345 E 47 47TH STREET/ NEW YORK, N.Y. 10017

PD-Vol. 75, Engineering Systems Design and Analysis
Volume 3
ASME 1996

OPTIMIZATION OF MICROSTRUCTURE DEVELOPMENT: APPLICATION TO HOT METAL EXTRUSION

James C. Malas, Anil Chaudhary, W. M. Mullins, Enrique A. Medina, S. Venugopal, and Steven Medeiros
Wright Laboratory, Wright-Patterson AFB, Ohio

R. Dennis Irwin
Ohio University
Athens, Ohio

W. Garth Frazier
Cedarville College
Cedarville, Ohio

Raghavan Srinivasan
Wright State University
Dayton, Ohio

ABSTRACT

A new process design method for controlling microstructure development during hot metal deformation processes is presented. This approach is based on modern control theory and involves state-space type models for describing the material behavior and the mechanics of the process. The challenge of effectively controlling the values and distribution of important microstructural features can now be systematically formulated and solved in terms of an optimal control problem. This method has been applied to the optimization of grain size and certain process parameters such as die geometry profile and ram velocity during extrusion of plain carbon steel. Various case studies are investigated and experimental results show good agreement with those predicted in the design stage.

NOMENCLATURE

$\beta_1,\ldots,\beta_5$	Weighting factors for terms of generic cost function
d	Average recrystallized grain size
$\hat{d}$	Desired final grain size
dl	Die length
ε	True, plastic strain
$\varepsilon_{0.5}$	Plastic strain for 50 vol% recrystallization
ε_c	Critical strain
$\dot{\varepsilon}$	Effective strain rate
$\dot{\varepsilon}_w$	Nominal strain rate value for acceptable workability
g	Cost function over entire trajectory
g_1	A penalty function
h	Terminal penalty function
J	Objective function
$npts$	Number of points in a data set
η	Fraction of work that transforms into heat
$\hat{p}$	Desired final volume fraction recrystallized
Q	Activation energy for dynamic recrystallization
Q_{gg}	Activation energy for static grain growth
R	Gas constant
r	Die radius
r_0	Die entrance radius
ρC_p	Heat capacity
σ	Flow stress
T	Temperature
t_f	Final time for complete deformation
T_w	Nominal T value for acceptable workability
T_{BILLET}	Initial billet temperature
u	Control variable
V_{RAM}	Ram velocity
y	Axial die coordinate
x_0	Initial state vector
x	State vector
χ	Volume fraction recrystallized

INTRODUCTION

Development of optimal design and control methods for manufacturing processes is needed for effectively reducing part cost, improving part delivery schedules and producing specified part quality on a repeatable basis. Existing design methods are generally ad hoc and lack adequate capabilities for evaluation of primary process parameters such as deformation rates, die and workpiece temperatures, and tooling system configuration. This situation presents major challenges to process engineers who are faced with ever increasing constraints on cost and quality which include growing production requirements for near net-shape

components with controlled microstructures and properties. It is important to develop new systematic methodologies for process design and control based upon scientific principles which sufficiently consider the behavior of workpiece material and the mechanics of manufacturing process.

A new strategy for systematically calculating near optimal control parameters for hot metal deformation processes is presented in this paper. This approach is based on modern control theory and involves developing state-space models from available material behavior and hot deformation process models. Two basic stages of analysis and optimization are established in this strategy for control system design. In the first stage, the kinetics of certain dynamic microstructural behavior and the intrinsic hot workability of the metal alloy system are used, together with an appropriately chosen optimality criterion, to calculate strain, strain-rate, and temperature trajectories. These trajectories are process independent in the sense that they are valid for different hot deformation processes such as forging, rolling, and extrusion and are thus independent of die geometry and flow pattern. A suitable process simulation model which could range from a simple slab type model to a high fidelity finite element simulation type model is then used in the second stage to calculate process control parameters such as ram velocity profiles and billet temperature which approximately achieve the strain, strain-rate, and temperature trajectories calculated in the first stage. The process control parameters are calculated by applying closed loop control principles to the process simulation model in order to maintain the strain, strain-rate, and temperature trajectories near those calculated in the first stage.

An application of the new process design approach to hot metal extrusion processes is investigated in this paper. An extrusion process was selected for study in this work for the following beneficial reasons: (1) extrusion typically involves large deformation with large variations in strain-rate; (2) relatively simple analytical models are available for describing the process; and (3) strain and strain-rate trajectories can be effectively controlled via optimized design of die geometry. In the following sections, a two-stage approach is utilized to design an extrusion process with case studies involving microstructure optimization and a validation experiment.

Description of Direct Extrusion

Extrusion is a process by which the cross section of a billet is reduced by forcing it to flow through a die. In a typical direct extrusion process, shown in Figure 1, a billet is placed in a chamber and the force exerted by the ram makes the metal flow through the die. The process is used to manufacture both finished and semi-finished products. As a primary processing operation, extrusion is used to refine the large grain cast structure. The extruded product is then in a condition more amenable to final shape making by other metal forming operations. The refinement of grains during extrusion is influenced by several factors including the initial temperature of the billet, the reduction in area, and the strain rate variation that the material experiences during deformation.

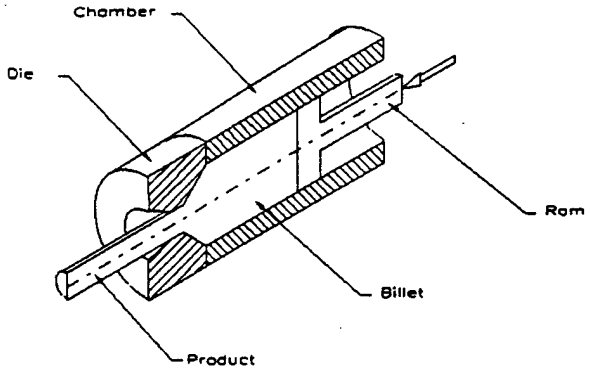

FIGURE 1 THE EXTRUSION PROCESS

Hot extrusion is usually carried out using converging dies, in which the cross section of the die orifice changes gradually from the initial billet shape to the final product shape over the length of the die. The strain and strain rate variation that the material experiences as it flows through the die depends on this die profile. Figure 2 shows three different die profiles that are used during hot extrusion: the conical die, cubic streamline die and the constant strain rate die. The various die shapes impose considerably different strain rate conditions on the deforming billet, as shown in Figure 3.

Microstructural Evolution During Hot Extrusion

Microstructural changes which occur during hot deformation are consequences of complex metallurgical phenomena such as recovery, recrystallization, grain growth, phase transformations, and precipitation/ dissolution reactions. These phenomena may occur dynamically during hot-deformation processing or statically during post-deformation cooling or heat treatment. The mechanisms and kinetics of these phenomena as well as the associated changes in size, morphology, distribution, volume fraction, and composition of the constituent phases are strongly dictated by the macroscopic heat-flow and material-flow processes. While the temperature distribution in the workpiece is controlled primarily by the interface heat transfer between the workpiece and the dies/rolls or platens, frictional-heating and deformation-heating effects also contribute significantly. At the same time, the distributions of strain, strain rate, effective stress, and hydrostatic stress within the deforming body are influenced by the material-flow behavior as well as the thermal history.

Dynamic recrystallization is commonly observed in hot extrusion processes which involve very large strains (typically $\varepsilon > 1.0$). Metals and alloys characterized by relatively low-stacking-fault energy (e.g., copper, nickel, austenitic steels) have a high propensity for undergoing restoration via dynamic recrystallization and recovery. Under practical hot-working conditions, these materials exhibit flow curves containing single maxima. A schematic representation of a typical microstructure evolution during dynamic recrystallization is shown in Figure 4. When the plastic strain exceeds a critical value, ε_c, dynamically recrystallized grains nucleate; principally through a mechanism involving strain-induced grain-boundary migration. Upon

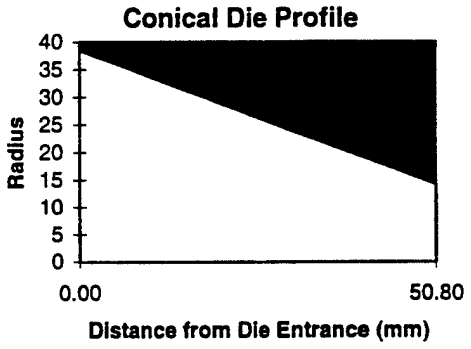

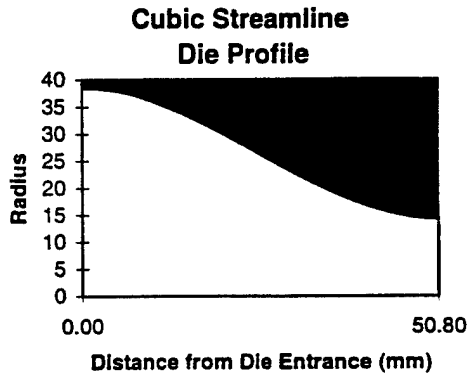

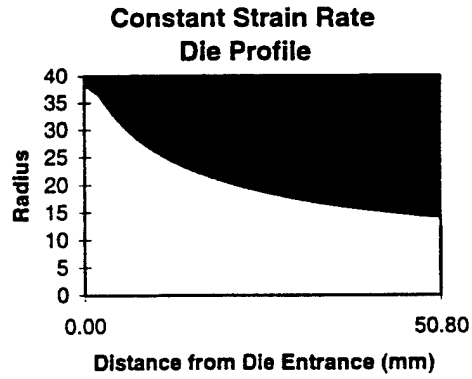

FIGURE 2 DIE PROFILES

continuation of deformation, additional nuclei form until all grain boundary/incoherent twin boundary sites are exhausted; thereafter, the reaction proceeds via nucleation at the boundary between recrystallized and unrecrystallized regions until the recrystallized grains impinge upon one another at the center of the original grains. Note that this transition from unrecrystallized

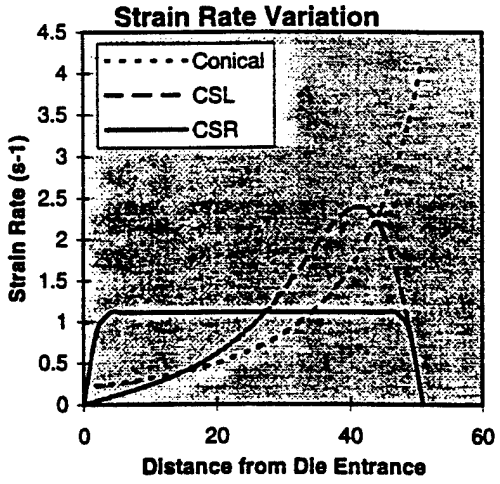

FIGURE 3 STRAIN RATE PROFILE

to recrystallized microstructure is strongly dependent on processing conditions and may correspond to a relatively small increment in deformation.

TWO-STAGE APPROACH TO OPTIMAL CONTROL OF DEFORMATION PROCESSES

A new process design and control strategy based on an optimization technique from modern control theory (Kirk, 1970) is used in this work to calculate near optimal control parameters for hot metal deformation. This design approach requires three basic characteristics for defining and setting up the optimization problem: (1) a dynamical system model, (2) physical constraints, and (3) an optimality criterion. In metalforming, the system models of interest are material behavior and deformation process models; constraints include the hot workability of the workpiece

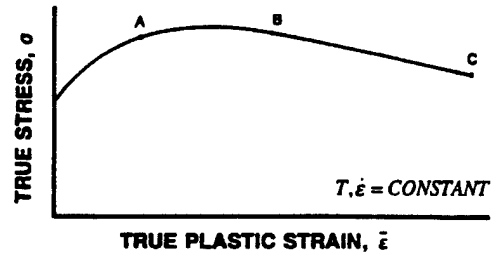

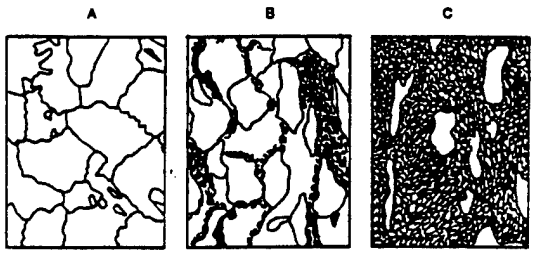

FIGURE 4 PROGRESSION OF DYNAMIC RECRYSTALLIZATION WITH STRAIN

and the limitations of the forming equipment. Optimality criteria could be related to achieving a particular final microstructure, regulating temperature, and/or maximizing deformation speeds.

The present two-stage approach decomposes the analysis and optimization into a workpiece material behavior control problem and a process mechanics control problem. As shown in Figure 5, the material behavior model has optimized outputs - $\varepsilon(t)$, $\dot{\varepsilon}(t)$, and $T(t)$ - which are used in determining the optimized outputs - $V_{RAM}(t)$, $T_{BILLET}(t)$ - of the process simulation model. Goals of the first stage are to achieve enhanced workability and prescribed microstructural parameters. In the second stage, a primary goal is to achieve the thermomechanical conditions obtained from stage one for predetermined regions of the deforming workpiece. It is recognized that this two-stage approach yields idealized process control solutions that could be further improved with advanced feedback methods.

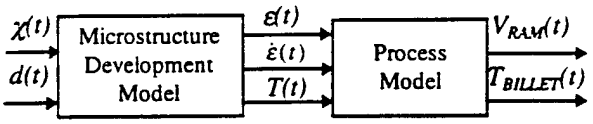

FIGURE 5 BLOCK DIAGRAM OF TWO-STAGE APPROACH

Material Behavior and Process Modeling Issues

The effectiveness of the two-stage approach presented in this article is largely dependent on the availability and reliability of the material behavior and process models to be used. In the first stage, material behavior models that describe the kinetics of primary metallurgical mechanisms such as dynamic recovery, dynamic recrystallization, and grain growth during hot working are required for analysis and optimization of material system dynamics. These mechanisms have been studied extensively for a wide range of metals and alloys (Jonas, et. al., 1969, Sellars, 1978, McQueen and Jonas, 1975, Roberts, 1984, 1986). The relationships for describing particular microstructural processes have been developed and reported for conventional materials such as aluminum, copper, nickel, and their dilute alloys, with steel receiving the most study. Elsewhere, it was claimed that, for certain ranges of temperature and strain rate, the operative deformation mechanisms of specialty alloys such as superalloys, intermetallics, ordered alloys, and metal matrix composites potentially become well defined and are amenable for modeling (Malas, 1991, Malas and Seetharaman 1992).

In several industries, process modeling has reached a high level of sophistication and acceptance as a process analysis tool (Jain, 1989, 1990). Current process models are capable of analyzing fairly complex material flow operations such as three-dimensional, nonisothermal deformation processes with a sufficiently high degree of accuracy. For example, in the forging industry, detailed numerical analyses of the phenomenon of the workpiece filling the forging die, the resulting die stresses, and the post-deformation heat treatment of the workpiece are being applied increasingly for verification of forging and heat treatment process designs.

Material Behavior Constraints and Optimality Criteria

In addition to dynamic system models, the formulation of an optimal control problem requires a statement of physical constraints and specification of an optimality criterion. The limiting process conditions for acceptable hot workability are important material behavior constraints in the first stage of the control strategy. Here, the acceptable strain rate and temperature variations for hot working metal alloys are based on material flow stability analysis (Malas and Seetharaman, 1991) and a desirable and relatively constant apparent activation energy. However, other definitions of safe processing conditions such as those based on Ashby-Frost deformation maps (Frost and Ashby, 1982) and Raj's damage nucleation maps (Raj, 1981) would also be valid in the optimal control formulation. So, within the acceptable processing variation, a particular thermomechanical trajectory is determined using the prescribed optimality criterion such as producing specified hot worked microstructural characteristics. As an illustration, consider a case of dynamic recrystallization for which the state-space model is given by

$$\begin{bmatrix} \dot{d} \\ \dot{\chi} \\ \dot{\varepsilon} \\ \dot{T} \end{bmatrix} = \begin{bmatrix} f_1(T, \dot{\varepsilon}, d) \\ f_2(T, \dot{\varepsilon}, d, \chi) \\ u \\ \eta\sigma\dot{\varepsilon} \,/\, (\rho C_p) \end{bmatrix}, \qquad (1)$$

where d is grain size, T is temperature, ε is strain, $\dot{\varepsilon}$ is strain rate, χ is percent recrystallized, f_1 and f_2 are pre-specified functions, η is a coefficient that determines how much work is converted into heat, σ is flow stress, and the product ρC_p is the heat capacity of the material. Note that the system input u is the strain rate.

General Formulation of Optimal Control Problem

Following the description above, the design problem is formulated here into an open-loop optimal control problem that can be stated as follows: Find u to minimize the cost functional

$$J = h(x(t_f)) + \int_0^{t_f} g(x(t), u(t))dt \qquad (2)$$

while satisfying the system state equation

$$\dot{x}(t) = f(x(t), u(t)) , \quad x(0) = x_0 . \qquad (3)$$

In the equations above, t is time, $x(t)$ is a vector of state variables, u is the system input, t_f is the length of time for the process, h is the cost associated with violating the desired final state, g is the integrand of the cost associated with the trajectories followed by the state variables and the input, f is a vector function that describes the process dynamics, and x_0 is the initial state vector.

This formulation relies on the following assumptions: (1) the system to be optimized can be modeled by a system of first-order, time-invariant ordinary differential equations (state equations),

(2) the final states are not specified explicitly. The restriction to free final states eliminates the need to solve a two-point boundary value problem, but implies that the final values are likely to vary from the desired values. The size of these variations can be regulated by a proper choice of weights on the different parts of the cost functional.

Optimality Criteria for Material Behavior Considerations

The cost function J, which is to be minimized to find ε, $\dot{\varepsilon}$ and T, can incorporate a number of physically realistic requirements, as is common in standard applications of linear quadratic optimal control. For example, suppose $\dot{\varepsilon}_w(t)$, and $T_w(t)$ are nominal trajectories required for material behavior considerations inferred from processing maps and $\dot{\varepsilon}(t)$ and $T(t)$ are the actual material trajectories to be determined. Suppose also that it is desired to maintain the material behavior parameters close to those determined from material processing maps and that because of microstructural considerations it is desired to achieve a final grain size $\hat{d}$, a final fraction recrystallized $\hat{p}$, and to maintain the instantaneous grain size below a desired value. Then, an appropriate optimality criterion would be

$$J = \beta_1 (d(t_f) - \hat{d})^2 + \beta_2 (\chi(t_f) - \hat{p})^2 + \int_0^{tf} \left(\beta_3(t)\left[\dot{\varepsilon}(t) - \dot{\varepsilon}_w(t)\right]^2 + \beta_4(t)\left[T(t) - T_w(t)\right]^2 + \beta_5(t) g_1\left[d(t)\right] \right) dt \quad (4)$$

which when below a certain value ensures that $\dot{\varepsilon}(t)$, and $T(t)$ lie within a family of ellipsoids parameterized by time and representing regions of acceptable hot workability properties, while final grain size and final percent recrystallized are close to their desired values and the grain size trajectory is kept under a prescribed maximum by means of the penalty function g_1. It is likely that some of the optimality requirements included in this function will conflict. As is common in control engineering, the weights $\beta_1, \ldots . \beta_5$ can be adjusted in order to obtain a satisfactory compromise solution.

The approach used in obtaining a solution to the optimization problem described above depends on two developments. First, a set of necessary conditions for optimality is obtained by applying variational calculus principles as given by Kirk (1970); this formulation transforms the optimization problem to a problem of solving a set of constraint equations. Next, a numerical algorithm is developed for the solution of these equations; this algorithm is guaranteed to converge. Details of the algorithm formulation are given by Frazier (1995). A software implementation that makes use of automatic differentiation was used to obtain the results presented in this work.

TWO STAGE OPTIMIZATION OF STEEL EXTRUSION

Results of the application of the two-stage approach to the optimization of a steel extrusion process are presented in this section. Before the optimization algorithm can be applied, a state space model of the microstructural response must be formulated.

Models for Dynamic Recrystallization of Steel

In the case of microstructural evolution during metal deformation, the required model must describe how the microstructure (e.g., grain size and volume fraction transformed) changes in time as a function of various process parameters (e.g. strain, strain-rate, and temperature. An experimentally identified model has been developed by Yada et.al. (1987) for the purpose of studying the effects of strain, strain-rate, and temperature on the microstructural evolution of steel during hot rolling. The equations that form this model are given in Table 1.

It is important to mention here that according to this model the percent recrystallized is zero until the strain reaches its critical value ε_c. From that point on, the material recrystallizes very rapidly until essentially 100% of the deformed material has transformed, in what could be called a step-function behavior. Because of this particular characteristic of the model, less than complete recrystallization is not likely to be achieved by any solution and in fact would not have much physical significance.

An issue of even greater importance is that although the expression for volume fraction recrystallized in Table 1 is a function of strain, strain-rate, and temperature, it is not an *instantaneous* function of all these variables because it assumes that the strain-rate is held constant during the entire deformation. Nevertheless, it is possible, by applying certain assumptions, to formulate a *dynamic* equation for recrystallization that is correct to first order. If it is assumed that the volume percent recrystallized is not a function of the rate of change of strain-rate or the rate of change of temperature, then the following dynamic equation for the time derivative of the percent recrystallized can be obtained by applying the chain rule of differentiation to the equation for χ in Table 1, which has been done in the first equation in Table 2.

Note also that because of the *instantaneous* nature of the recrystallization process, the equation for grain size given in Table 1 will have physical significance only when the deformation strain is greater than or equal to the critical strain. After dynamic recrystallization, it is assumed that grain size is stable, and does not change. It is also assumed, for steel, that a new cycle of recrystallization develops each time the strain reaches a value equal to an integer multiple of the critical strain ε_c.

Another important variable to track during deformation is temperature. The equation for the rate of change of temperature due to deformation given in Table 2 can be easily derived from basic mechanical principles. The expression for flow stress was obtained from Kumar, et al. (1987).

TABLE 1. YADA EQUATIONS FOR THE DYNAMIC RECRYSTALLIZATION OF STEEL

Volume fraction recrystallized	$\chi = 1 - \exp\left(\ln(2)\left((\varepsilon - \varepsilon_c)/\varepsilon_{0.5}\right)^2 \right)$
Critical strain	$\varepsilon_c = 4.76\times10^{-4}\, e^{8000/T}$
Plastic strain for 50% vol. recrystallization	$\varepsilon_{0.5} = 1.144\times10^{-5} d_0^{0.28}\, \dot{\varepsilon}^{0.05}\, e^{6420/T}$
Average recrystallized grain size	$d = 22600\dot{\varepsilon}^{-0.27}\, e^{-0.27\left(\frac{Q}{RT}\right)}$
Activation energy & gas constant	$Q = 267\, kJ/mol$, $R = 8.314x10^{-3}\, kJ/mol-K$

TABLE 2 EQUATIONS USED IN STATE-SPACE MODEL OF MICROSTRUCTURAL EVOLUTION

Time derivative of volume fraction recrystallized	$\dot{\chi} = \frac{\partial \chi}{\partial \varepsilon}\frac{\partial \varepsilon}{\partial t} = \frac{2\ln 2}{(\varepsilon_{0.5})^2}(\varepsilon - \varepsilon_c)(1-\chi)\dot{\varepsilon}$
Time derivative of temperature	$\dot{T} = \frac{\eta}{\rho\, C_p}\sigma(\varepsilon, \dot{\varepsilon}, T)\dot{\varepsilon}$
Flow stress (kPa)	$\sigma = \sinh^{-1}\left[\left(\dot{\varepsilon}/A\right)^{1/n} e^{Q/nRT} \right] / 0.0115\times10^{-3}$
	$\ln A(\varepsilon) = 13.92 + 9.023/\varepsilon^{0.502}$
	$n(\varepsilon) = -0.97 + 3.787/\varepsilon^{0.368}$
Activation energy & gas constant	$Q(\varepsilon) = 125 + 133.3/\varepsilon^{0.393}$, $R = 8.314\times10^{-3}$

In this work, the microstructural state of the material is given by the state vector $x = \left[\chi, T, \varepsilon\right]^T$, which transitions in time according to the equations given in Table 2 for time derivatives of χ and T and the obvious relationship between strain and strain rate. Grain size is treated here as an output of the dynamical system in the sense that it is not included as one of the state variables. As previously mentioned, strain rate is the system input, i.e., $u = \dot{\varepsilon}$.

First Stage: Formulation of a Cost Functional and Trajectory Optimization

Since microstructure directly influences mechanical properties, it can be a primary concern in deformation processing. Therefore, an appropriate cost functional should place a significant emphasis upon the final mechanical and microstructural state of the material. In most cases, however, it is also important that the intermediate state of the material remain within certain regions of the state space in order to avoid catastrophic failure as well as other less dramatic difficulties. For the case studied here, the cost function was chosen so as to attain a given final strain while assuring that the recrystallized grain size was kept at a desired value. The cost function was chosen as

$$J = 10(\varepsilon(t_f) - 2.0) + \int_0^{t_f} (d(t) - 26)^2 dt \quad , \qquad (5)$$

where a desired final strain of 2, with a weighting factor of 10, and a desired grain size of 26 μm have been specified. The trajectory optimization algorithm was successfully applied to this problem. The solid lines marked as "RUN 1" in Figures 6, 7, and 8 show the optimal strain-rate, temperature and strain trajectories as given by the optimization algorithm; the solid line labeled "RUN 1" in Figure 9 shows the corresponding grain size behavior, as predicted by the model. In Figure 9, the vertical line at the beginning of each average grain size trajectory corresponds to the first recrystallization that takes place. Each of these vertical lines starts at 180 μm, which is the average grain size in the workpiece before extrusion, but the vertical scale has been fixed to a maximum of 40 μm for presentation purposes. Each vertical line in the grain size trajectories corresponding to the use of a constant strain rate die and a conical die corresponds to a

new recrystallization. The fact that multiple recrystallizations occur also in the three optimization cases cannot be seen in the Figure 9 because the optimization algorithm maintains a constant average grain size throughout the deformation process. By keeping the grain size predicted by the model at a constant value, the optimization algorithm guarantees that whenever recrystallization occurs, the average size of the grains will be as desired. As can be observed in Figures 8 and 9, both the desired final strain and the desired grain size are achieved by the optimal solution.

The optimization was run successfully for a second and a third case. For the second case, the desired grain size was changed to 30 μm. Results of this run are shown by the dashed lines labeled as "RUN 2" in the figures. For the third case, the desired grain size was changed to 15 μm, and the initial billet temperature to 1223 K. Dashed-dotted lines labeled as "RUN 3" indicate the results of this run. For comparison purposes, two other lines appear in the plots: lines of short dashes correspond to the use of a constant strain-rate extrusion die: dotted lines correspond to the use of a conical die.

Stage Two: Process Mechanics Control and Optimal Die Design

It is not physically possible to ensure that all points in the deforming piece will undergo the strain, strain-rate, and temperature trajectories obtained in stage one. However, parameters of the deformation process such as die geometry, ram velocity, and billet temperature can be designed in order to ensure that selected areas of the material will experience trajectories that approximate those designed. It is feasible to formulate a second optimization problem that determines values for process parameters that will attempt to achieve the desired trajectories at pre-determined points in the material piece. In such an approach, each evaluation of the objective function for the optimization process usually requires a high fidelity finite element simulation of the deformation process.

In the case of extrusion, it is also possible to analytically calculate the die profile and ram velocity necessary for achieving the desired strain and strain rate profiles at the center line of the piece. It can be shown that if r_0 is the die entrance radius equal to the billet radius, *dl* is the die length, and the required strain trajectory is given as a sequence $\{\varepsilon(t), i = 1, \ldots, npts\}$, of *npts* data points then the ram velocity can be computed as

$$v_{ram} = dl \Big/ \int_0^{t_f} e^{\varepsilon(t)} dt \qquad (6),$$

and the die profile is given by the sequence of ordered pairs $\{(y(t), r(t)), i = 1, \ldots, npts\}$, where

$$r(t) = r_0 e^{-\varepsilon(t)/2}, \quad y(t) = v_{ram} \int_0^{t_f} e^{\varepsilon(t)} dt, \qquad (7)$$

y denotes axial distance and *r* is die radius.

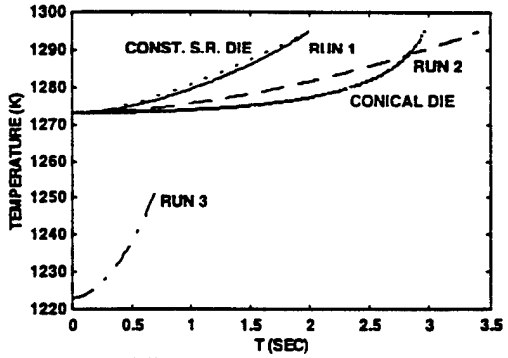

FIGURE 7 TEMPERATURE TRAJECTORIES

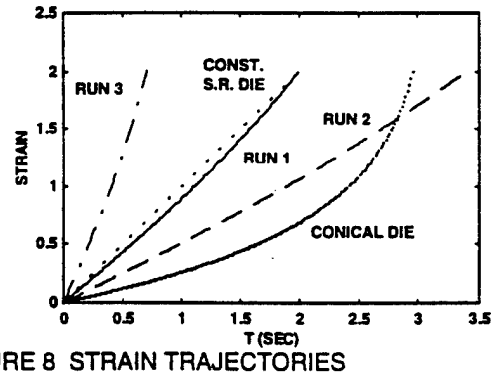

FIGURE 8 STRAIN TRAJECTORIES

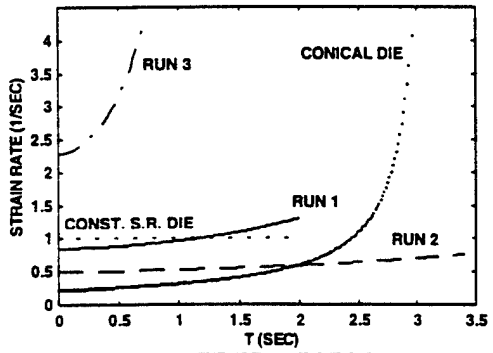

FIGURE 6 STRAIN RATE TRAJECTORIES

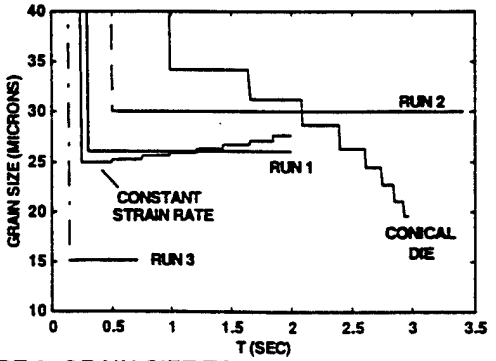

FIGURE 9 GRAIN SIZE TRAJECTORIES

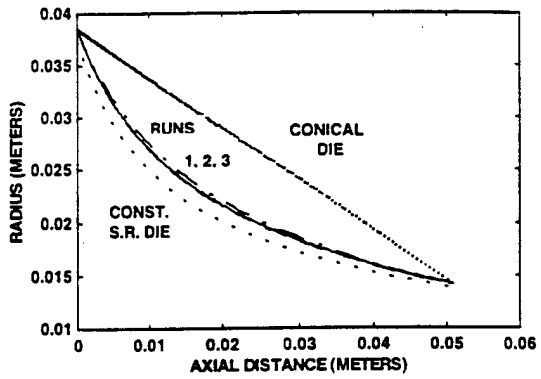

FIGURE 10 DIE PROFILES

The optimal die profiles shown in Figure 10 were obtained by using this approach. The dies used for the additional cases mentioned above are also included in this figure. Table 3 describes the lines in this figure and lists the ram velocity used for each case. Note that the die shape is almost the same for the three optimization cases. This means that the same die can be used to achieve the different recrystallized grain sizes by changing only the velocity of the extrusion ram. Note also that the shape of the constant strain rate die is somewhat similar to the optimal die shapes.

An extrusion experiment was performed using a die with the profile obtained from the first run of the trajectory optimization algorithm and the corresponding ram velocity (8.43 mm/sec). Grain size measurements of the extruded piece for this experiment showed a good degree of agreement with the grain size predicted by the optimization algorithm. Details of the experiment and results are given in the following sections.

TABLE 3 MICROSTRUCTURAL TRAJECTORY CASES

Case	Desired Grain Size (μm)	RamVel. (mm/s)	Line Type
RUN 1	26	8.43	Solid
RUN 2	30	5.0	Dashed
RUN 3	15	25.1	Dash-dot
Constant Strain Rate	Not applicable	8.0	Short dashed
Conical Die	Not applicable	8.43	Dots

VALIDATION OF THE TWO-STAGE APPROACH

The optimization methodology was validated by means of an extrusion experiment and a finite element simulation of the process. The extrusion test was performed on a 6000 kN Lombard horizontal extrusion press located at Wright-Patterson Air Force Base. The billet material was AISI 1030 steel and the extrusion die was fabricated with H13 tool steel. The die geometry, generated to yield 26 μm grain size, was utilized in this experiment with the ram velocity of 8.43 mm/sec. The ambient temperature for the die and the follower block was 533 K and soak temperature for the billet was 1273 K. The interface lubrication was representative of a shear friction coefficient of 0.30. The total ram stroke was 75 mm and it resulted in a partial extrusion of the billet. The billet was subsequently removed from the tooling and was water quenched. The transfer time from the end to extrusion to the beginning of quench was 39 seconds which corresponded to air cooling of the billet.

This extrusion experiment was simulated using the 'Antares' process simulation software (UES, 1995). The billet and die domains were discretized to an average mesh size of 3 mm square. The finite element simulation was performed using an individual step increment approximately equal to 1/100 of the total ram stroke. The process was simulated for the nonlinear coupled response of the billet and the thermal response of the die. After the partial extrusion, the temperature at the billet centerline increased to 1313 K due to deformation heat-up. Accumulated strain at the billet centerline was 2.0 while the strain at the billet surface was 2.27 (see Figure 11). The difference is attributed to the chilling on the billet surface which increases the billet material flow stress. Since variations in friction can further change the surface region deformation path, all calculations for the billet microstructural predictions were performed using the centerline strain information. The extrusion load was observed to be 2800 kN. The partially extruded billet was considered for the subsequent air cool thermal behavior for a period of 39 seconds. Figure 12 shows the resultant transient behavior at the billet centerline. This evolution of temperature was utilized for correlation of the grain size increase due to grain growth .

Grain size measurements were carried on the partially extruded sample. The extruded piece was cut along its longitudinal axis and polished for microstructural investigations. 2% Nital was

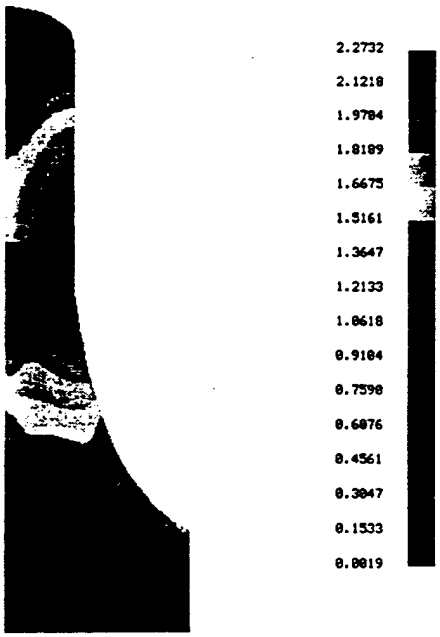

FIGURE 11 STRAIN DISTRIBUTION AFTER EXTRUSION

used as etchant to reveal grain boundaries for grain size measurements. Grain size measurements were done using Heyn intercept method (Vander Voort, 1994). Histograms were made to find the grain size distribution and the average grain diameter. Grain size measurements were carried out at various locations in the deformation zone and the variation of grain size along the axis, as a function of die throat height was recorded. Both dynamic recrystallization during extrusion and grain growth during the air cool period were considered to correlate experimental results with Yada's model for microstructural evolution (Yada, 1987).

The average grain diameter, measured at various locations in the deformation zone of the partially extruded sample is presented in Figure 13 as a function of the die *throat* length. Microstructural studies on the extruded sample revealed features such as equiaxed grains and straight twin boundaries. The partially extruded piece was water quenched 39 seconds after the completion of deformation. Due to this elapsed time period, it is anticipated that the Austenitic microstructure will experience static recrystallization. This phenomenon is modeled by Yada as

$$d^2 = d_0^2 + At\exp\left(\frac{-Q_{gg}}{RT}\right), \qquad (8)$$

where d_0 and d are the recrystallized grain size upon extrusion and the statically grown grain size, respectively, t is the time elapsed, in seconds, between the end of extrusion and the quenching operation. In addition, A equals 1.44×10^{12} and Q_{gg}/RT is 32100 at the extrusion temperature of 1273 K.

The temperature distribution in the partially extruded piece during the period of 39 seconds as a function of time was modeled using FEA and the results are given in Figure 12. In order to evaluate dynamic responses of the material, the observed grain size from the microstructural study was corrected using the above mentioned equation to account for static grain growth to yield the dynamically recrystallized grain size at the end of deformation as 27.5 μm. This grain size is in good agreement with the 26 μm grain size for which the extrusion process was designed.

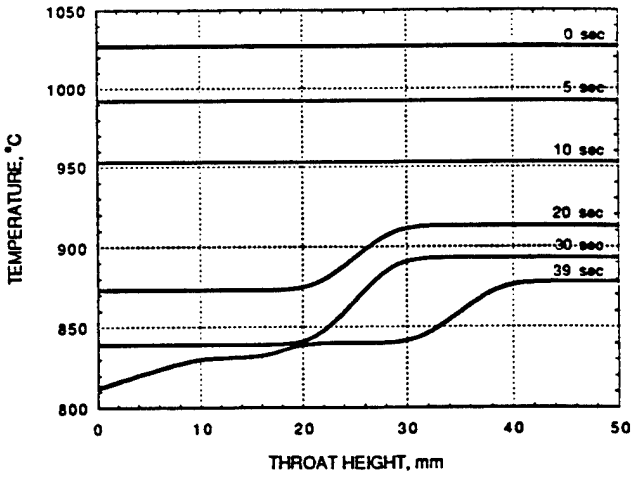

FIGURE 12 TEMPERATURE DISTRIBUTION ALONG CENTERLINE OF PARTIALLY EXTRUDED PIECE DURING THE AIR COOL PERIOD

CONCLUSIONS AND FUTURE WORK

A two stage approach was utilized for optimal design of hot extrusion process. In the first stage, Yada's equations for dynamic recrystallization of plain carbon steel were utilized to obtain an optimal material deformation path such that the terminal grain size would be 26 μm. This trajectory determination was performed via minimization of a cost function. In the second stage, the geometric mapping was utilized to develop an extrusion die profile such that the strain rate profile during extrusion matches with the optimal trajectory computed in the first stage. This die design was verified using a finite element based process simulation software.

A validation experiment was performed by utilizing the extrusion die geometry obtained in the second stage. A process simulation was performed to correlate the temperature evolution with time for the extruded material for the time duration elapsed between end of extrusion to quench. This temperature evolution profile was substituted in Yada's equations for static grain growth to obtain the correction to the as-quenched grain size which would give the as-extruded grain size. A microstructural study was performed on the extruded sample and the grain size measurements were correlated with the desired grain size. The as-extruded grain size was observed to be in a close agreement with the optimal design performed in the first stage.

Future work will be directed toward investigating the true dynamical response of microstructural mechanisms, optimizing 2 or more series of thermomechanical processes, and validating the two-stage approach using other metallic systems and deformation processes. A longer term goal is to develop an integrated software environment for calculating process design parameters and to enhance the control system design technique using advanced feedback methods.

ACKNOWLEDGEMENTS

Support for this research was provided by the Materials Process Design Branch, Materials Directorate, Wright Laboratory, WPAFB. UES, Inc. and Austral Engineering and Software, Inc. participated in this effort as part of a Small Business Innovative Research Program. S. Venugopal is thankful to the National Research Council, U.S.A., for their support.

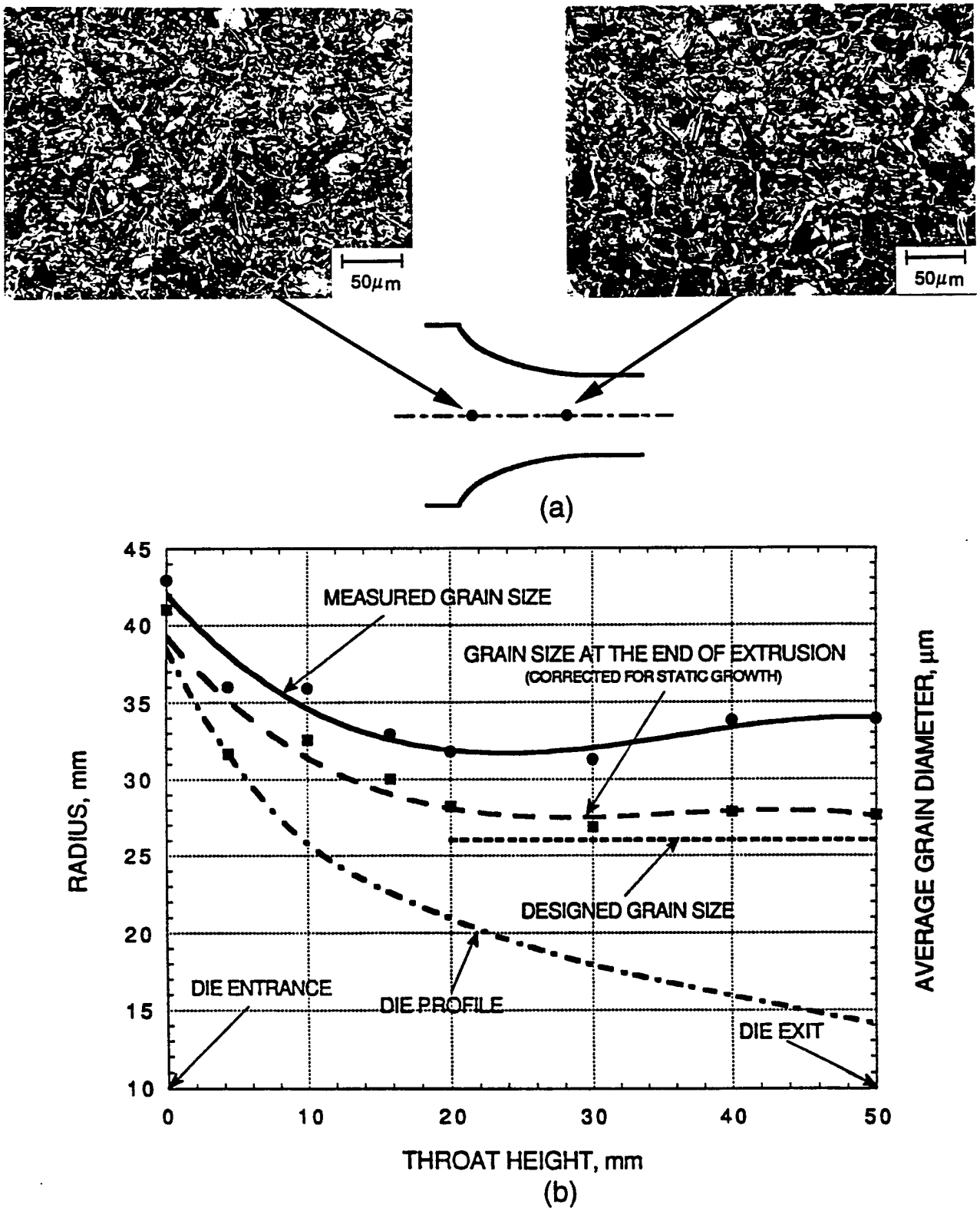

FIGURE 13 (a.) MICROSTRUCTURES AT LOCATION OF (FIRST) CRITICAL STRAIN AND DIE EXIT, (b.) MEASURED AND CORRECTED PRIOR-AUSTENITIC GRAIN SIZE VS. POSITION ALONG DIE THROAT CENTERLINE.

REFERENCES

Beyon, J.H., Brown, P.R., Mizban, S.I., Ponter, A.R.S., and Sellars, C.M., 1986, Proc. of NUMIFORM Conf., Gothenburg, Sweden, Aug. 25-29, K. Mattiasson, A. Samuelsson, R.D. Wood, and O.C. Zienkiewicz, eds., A.A. Balkema, Rotterdam, Holland, pp. 213-18.

Derby, B. and Ashby, M.F.:, 1987, *Scripta Metall.*, Vol. 21, p. 879.

Derby, B., 1991, *Acta. metall. Mater.*, pp. 955-62.

Devadas, C., Samarasekera, I.V., and Hawbolt, E.B., 1991, *Metall. Trans. A*, Vol. 22A,, pp. 335-349.

Frazier, W. G., 1995, "Robust Control Techniques for Hot Deformation Processes,", Contributive Research and Development, Volume 228, SYSTRAN Corp. Final Report, Task 178, Contract F33615-90-C-5944, March.

Frost, H.J., and Ashby, M.F., 1982, *Deformation Maps*, Pergamon Press.

Hansen, S.S., Jensen, D.J., Lefjers, T., and Ralph, B., eds., Riso National Laboratory, Roshilde, Denmark, pp. 547-52.

Jain, S.C., 1989, Process Modeling and Manufacture: Where We Stand, *JOM*, Vol. 41 (No. 2).

Jain, S.C., 1990, Emerging Trends in Process Modeling and Manufacture, *JOM*, Vol. 42 (No. 2), p. 15.

Jonas, J.J., Sellars, C.M., and McG, Tegart, 1969, Strength and Structure under Hot Working, *Metall. Rev.*, Vol. 14 (No. 1).

Kumar, A., Rao, K.P., Hawbolt, E.B., and Samarasekera. I.V., 1987, The Application of Constitutive Equations for Use in the Finite Element Analysis of Hot Rolling Steel, Unpublished Research.

Kirk, D. E., 1970, *Optimal Control Theory: An Introduction*, Prentice-Hall.

Malas, J.C., Irwin, R.D., and Grandhi, R.V., 1993, *J. Mater. Engg. Perf.*, Vol. 2, pp. 703-13.

Malas, J.C. and Seetharaman, V., 1992, Use of Material Behavior Models in the Development of Process Control Strategies, *JOM*, Vol. 44 (No. 6).

Malas, J.C., 1991, "Methodology for Design and Control of Thermomechanical Processes," Ph.D. dissertation. Ohio University.

McQueen, H.J. and Jonas, J.J., 1975, Recovery and Recrystallization During High Temperature Deformation, in *Treatise on Materials Science and Technology*, Vol. 6, *Plastic Deformation of Materials*, Academic Press, pp.393-493.

Raj, R., 1981, Development of a Processing Map for Use in Warm-Forming and Hot-Forming Process, *Metall. Trans. A*, Vol. 12, p. 1089.

Roberts, W., 1984, Dynamic Changes That Occur During Hot Working and Thjeir Significance Regarding Microstructural Development and Hot Workability, in *Deformation, Processing, and Structure*, G. Krauss, Ed., ASM International, pp.109-184.

Saito, Y., Enami, T., and Tanka, T., 1985, *Trans. Iron Steel Inst. Jpn.*, Vol. 25, pp. 1146-55.

Saito, Y., Saeki, M., Nishida, M., Ito, Y., Tanaka, T., and Takizawa, S., 1980, *Proc. Int. Conf. on Steel Rolling, Iron Steel Inst., Japan*, Tokyo, Sept. 29-Oct. 4, pp. 1309-20.

Sellars, C.M., 1985, *Mater. Sci. Technol.*, Vol. 1, pp. 352-32.

Sellars, C.M. and Whiteman, J.A., 1979, *Met. Sci.*, Mar-Apr., pp. 187-94.

Sellars, C.M., 1980, Proc. Int. Conf. on Hot Working and Forming Processes, July 17-20, C.M. Sellars and C.J. Davies, eds., The Metals Society of London, London, pp. 3-5.

Sellars, C.M., 1988, Int. Conf. on Physical Metallurgy of Thermomechanical Processing of Steels and Other Metals, THERMEC 88, Tokyo, June 6-10, I. Tamura, ed., Iron and Steel Inst. Japan. Tokyo, pp. 448-57.

Sellars, C.M., 1978, Recrystallization of Metals During Hot Deformation, *Philos. Trans. Roy. Soc.*, Vol. 288 (No. 147).

Senuma, T. and Yada, H., 1986, Annealing Processes, Recovery, Recrystallization and Grain Growth, Proc. 7th Riso Int. Symp. on Metallurgy and Materials science, Sept. 8-12. Suehiro, M., Sato, K., Tsukano, Y., Yada, H., Senuma, T. and Matsumura, Y., 1987, *Trans. Iron Steel Inst. Japan*, Vol. 27, pp. 439-45.

Srinivasan. R., Gunasekera, J.S., Gegel, H.L, and Doraivelu, S.M., 1990. Extrusion Through Controlled Strain Rate Dies, *J. Mater.ial Shaping Technology*, Vol. 8, No. 2, pp. 133-141.

UES, Inc., 1995, *Antares Software User Manual.*

Yada, H., 1987 *Proc. Int. Symp. Accelerated Cooling of Rolled Steels*, Conf. of Metallurgists, CIM, Winnipeg, MB, Canada, Aug. 24-26, G.E. Ruddle and A.F. Crawley, Eds., Pergamon Press, Canada, pp. 105-20.

Vander Voort, 1994, in *Metallography, Principles and Practice*, McGraw Hill Book Co., New York, p. 410.

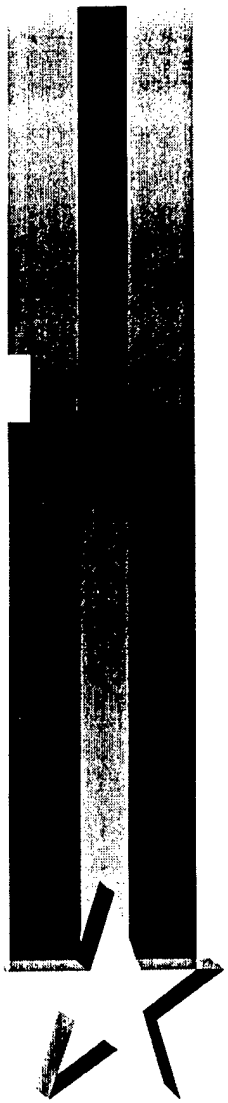

Optimal Material Trajectories

Enrique A. Medina and W. Garth Frazier
Materials Process Design Branch
Wright Laboratory

R. Dennis Irwin
Ohio University

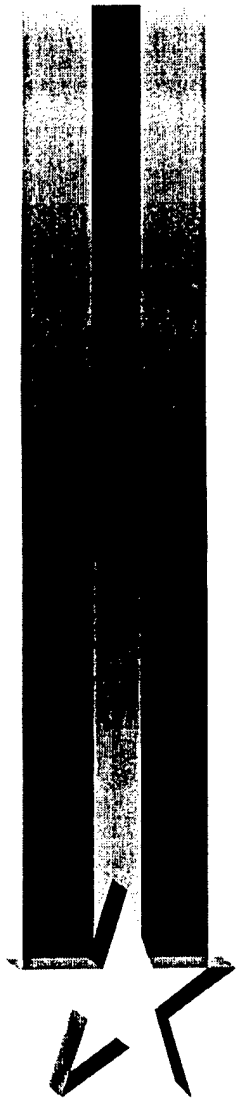

Outline

- ★ Motivation
- ★ Systems and Control Approach
- ★ The Microstructure Development Problem
- ★ Modeling and System Identification Issues
- ★ Optimal Control Problem Formulation
- ★ Optimal Control Problem Solution
- ★ Example: Application to Steel Extrusion
- ★ Conclusions and Research Opportunities

Motivation

★ Design of metal forming processes is often based on costly trial and error procedures

★ Insufficient evaluation of process parameters such as
- deformation rates
- die and workpiece temperatures
- tooling system configuration

★ Optimal design and control methods can help
- reduce part costs
- improve part delivery schedules
- produce specified part quality on a repeatable basis
- meet growing production requirements
- satisfy near net-shape component requirements
- achieve controlled microstructure and properties

Systems Approach

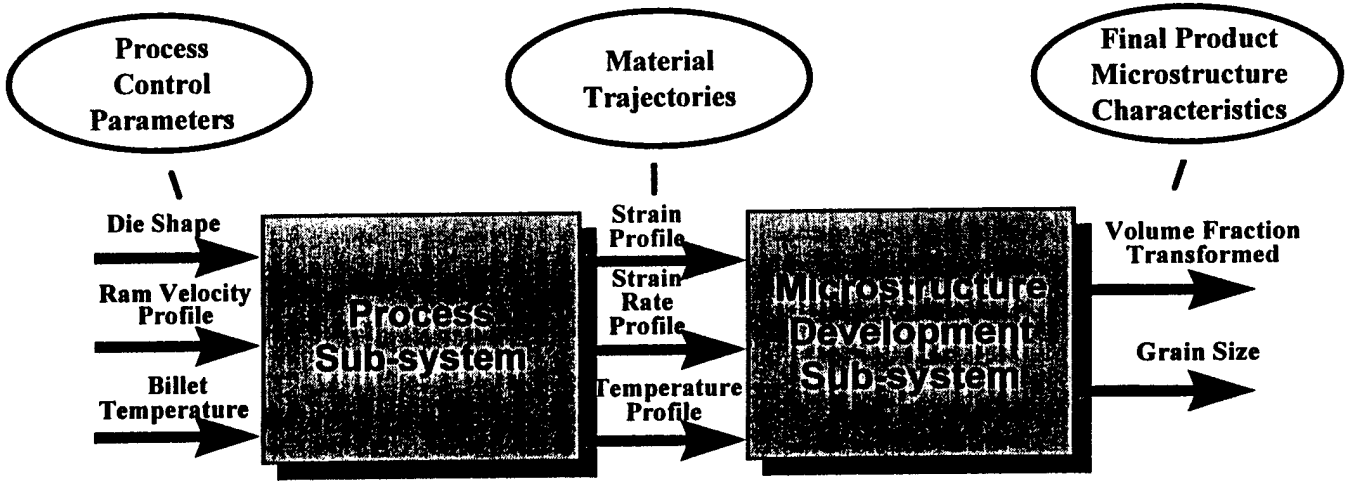

- This is one model that represents part of the problem
- Other configurations could give better or worse results
- The limiting factors are complexity and *computability*
- Additional issues that can be considered are
  - Forming press
  - Lubrication
  - Controllers (speed, ...)
  - Transfer equipment
  - Heating equipment (furnace, ...)
  - PART SHAPE

The Ideal Control Situation

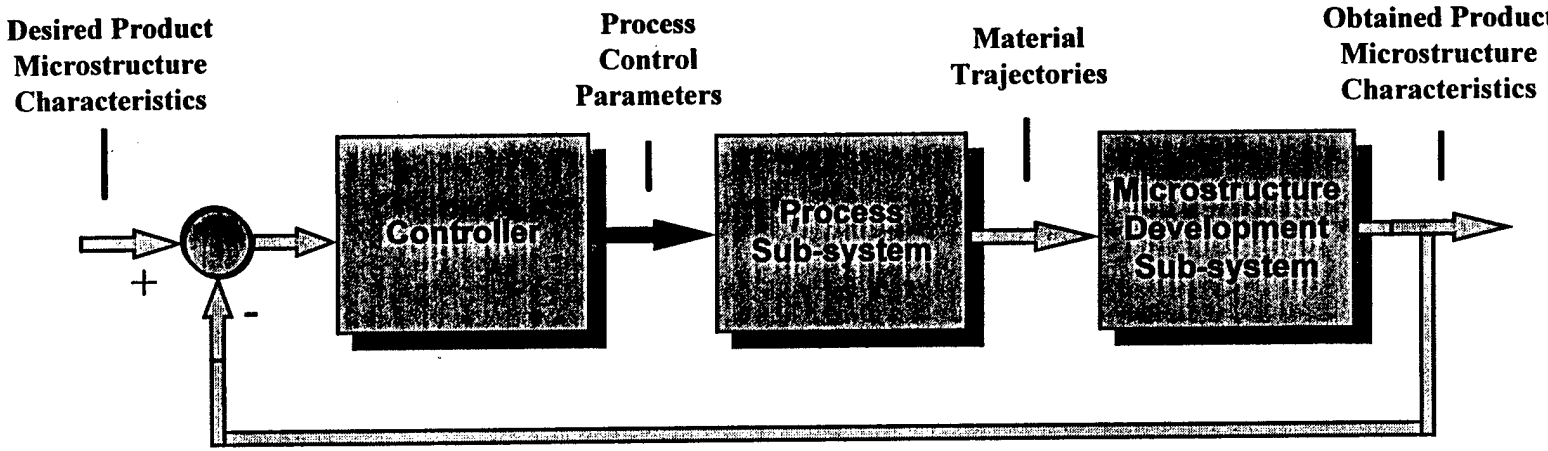

- Feedback could improve accuracy and robustness
- On-line measurement of microstructure is not possible
- On-line change of control parameters not always easy
- **Open-loop control is the best current alternative**

The Microstructure Development Problem

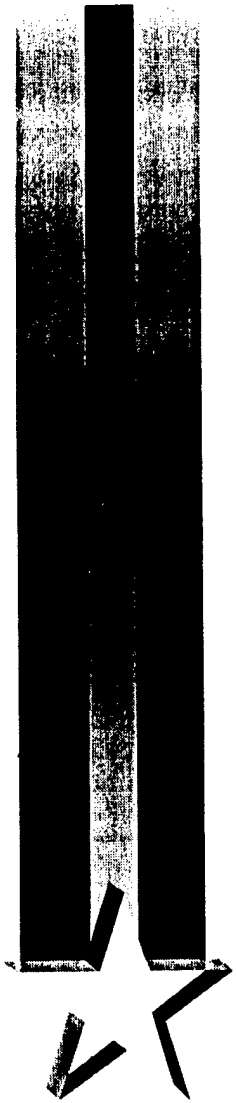

- ★ During hot deformation, microstructure evolves due to metallurgical phenomena such as
  - recovery
  - recrystallization
  - grain growth
  - phase transformations
  - precipitation reactions
  - dissolution reactions
- ★ These phenomena can occur
  - dynamically, during hot-deformation processing
  - statically, during post-deformation cooling or heat treatment
- ★ Mechanisms are dictated by heat and material flow behavior, and depend on deformation and thermal history
- ★ A system model of microstructure development will likely be *nonlinear*

Modeling and System ID Issues

★ A state-space model that describes the dynamics of microstructure evolution is necessary

$$\begin{bmatrix} \dot{\chi} \\ \dot{\varepsilon} \\ \dot{T} \end{bmatrix} = \begin{bmatrix} f_1(\chi, \varepsilon, T, u) \\ u \\ f_2(\varepsilon, T, u) \end{bmatrix}$$

← volume fraction transformed evolution

← strain evolution

← temperature evolution

$$d = f_3(T, u)$$

← grain size evolution

★ Inputs, states, and outputs vary from material to material

★ This type of model is not widely available

- system theory has not been the preferred approach
- nonlinear behavior is difficult to identify accurately

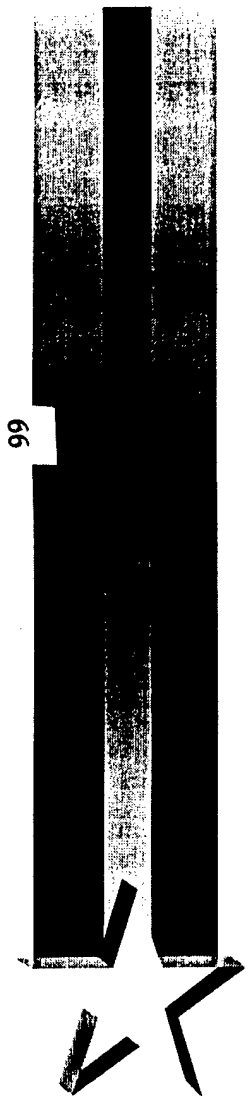

Example: Yada Models for Steel

★ Original equations are for dynamic recrystallization of steel during hot rolling

- Volume fraction transformed

$$\chi = 1 - \exp\left(\ln(2)\left((\varepsilon - \varepsilon_c)/\varepsilon_{0.5}\right)^2\right)$$

$\varepsilon_c = 4.76 \times 10^{-4} e^{8000/T}$ — Critical strain

$\varepsilon_{0.5} = 1.144 \times 10^{-5} d_0^{0.28} (\dot{\varepsilon})^{0.05} e^{6240/T}$ — Strain for 50% volume recrystallization

- Average recrystallized grain size (μm)

$$d = 22600(\dot{\varepsilon})^{-0.27} e^{-0.27\left(Q/RT\right)}$$

$Q = 267\ kJ/mol$ — Activation energy

$R = 8.314 \times 10^{-3}\ kJ/mol - K$ — Gas constant

Reference: Yada, H., 1987, *Proc. Int. Symp. Accelerated Cooling of Rolled Steels, ...*

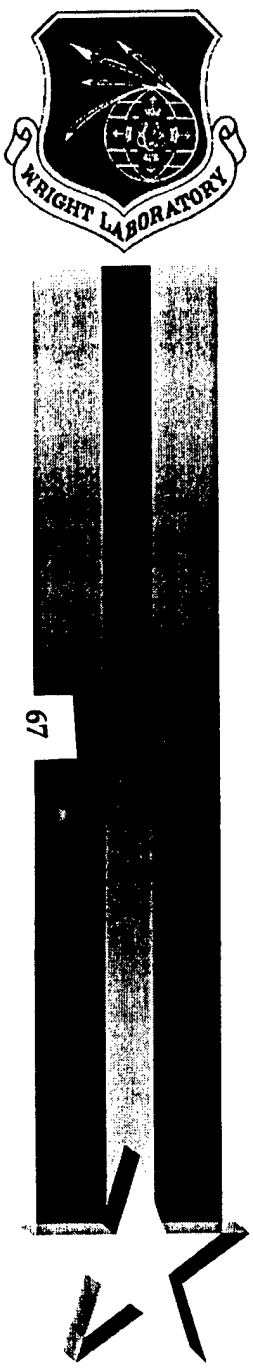

Yada Model for Steel

★ State-Space Model derivation

$$\dot{\chi} = \frac{\partial \chi}{\partial \varepsilon}\frac{\partial \varepsilon}{\partial t} + \frac{\partial \chi}{\partial (\dot{\varepsilon})}\frac{\partial (\dot{\varepsilon})}{\partial t} + \frac{\partial \chi}{\partial T}\frac{\partial T}{\partial t} = \frac{\partial \chi}{\partial \varepsilon}\dot{\varepsilon} = \frac{2\ln 2}{\varepsilon_{0.5}^{\,2}}(\varepsilon - \varepsilon_c)(1-\chi)\dot{\varepsilon}$$

(the $\frac{\partial \chi}{\partial (\dot{\varepsilon})}$ term: 0; the $\frac{\partial T}{\partial t}$ term: small)

$\dot{\varepsilon} = u$ ⟵ Strain rate is the system input

$$\dot{T} = \frac{\eta}{\rho C_p}\sigma(\varepsilon, \dot{\varepsilon}, T)$$

ρ — density; C_p — specific heat

$$\begin{cases} \sigma = \sinh^{-1}\left[(\dot{\varepsilon}/A)^{1/n} e^{Q/nRT}\right] / 1.15\times 10^{-5} & \text{— Flow stress, kPa} \\ \ln A(\varepsilon) = 13.92 + 9.023/\varepsilon^{0.502} & \\ n(\varepsilon) = -0.97 + 3.787/\varepsilon^{0.368} & \\ Q(\varepsilon) = 125 + 133.3/\varepsilon^{0.393}\ kJ/mol & \text{— Activation energy} \\ R = 8.314\times 10^{-3}\ kJ/mol - K & \text{— Gas constant} \end{cases}$$

State Space Model

$$\begin{bmatrix} \dot{\chi} \\ \dot{\varepsilon} \\ \dot{T} \end{bmatrix} = \begin{bmatrix} \frac{2\ln 2}{\varepsilon_{0.5}^{\,2}}(\varepsilon - \varepsilon_c)(1-\chi)\dot{\varepsilon} \\ u \\ \frac{\eta}{\rho C_p}\sigma(\varepsilon, \dot{\varepsilon}, T) \end{bmatrix}$$

$$d = 22600\dot{\varepsilon}^{-0.27} e^{-0.27 Q/RT}$$

Optimal Control Approach

Optimal Control Problem

Find $u(t)$ to minimize the optimality criterion

$$J(u(t)) = h(x(t_f)) + \int_0^{t_f} g(x(t),u(t),t)dt,$$

while satisfying the system state equation

$$\dot{x}(t) = f(x(t),u(t),t), \qquad x(0) = x_0.$$

A Typical Hot Metal Forming Case

Control inputs, $u(t)$: strain, strain rate, temperature

System states, $x(t)$: grain size, vol. fraction transformed

System model, $f(x,u,t)$:
- microstructural model, deformation model,
- heat transfer model

Trajectory criteria, $g(x,u,t)$:
- regulate microstructure development
- minimize deformation heating
- stay within workability ranges
- integrate equipment characteristics

Final state criteria, $h(x(t_f))$:
- achieve final microstructure
- achieve final strain

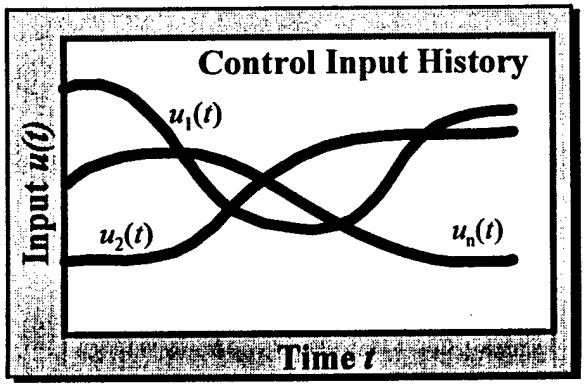

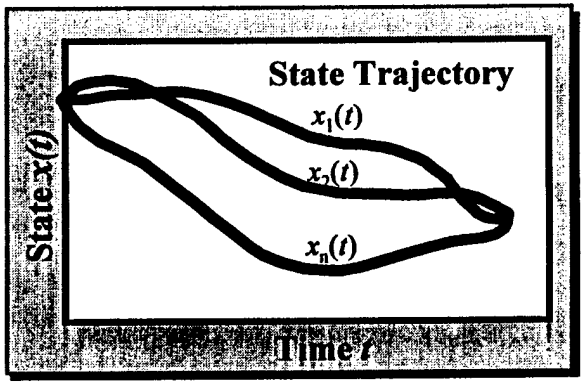

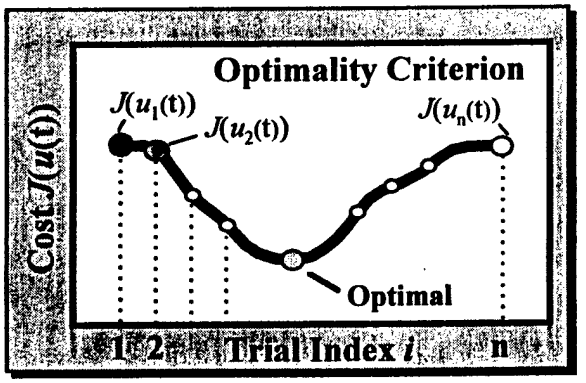

Optimal Control Problem
Building an Objective Function

★ Costs related to final values, $h(x(t_f))$

- Weighting of individual terms is almost always necessary to balance scales and perform trade offs
- Terms are usually quadratic.

$$J_{fd} = w\left(f_d\left(x(t_f)\right) - d_1\right)^2$$

weight — w

$f_d(x(t_f))$ — a function of the states

d_1 — desired value

★ Costs related to trajectories, $g(x(t),u(t))$

- Trajectories followed by inputs, states, and/or outputs may be important
  - Minimize control energy
  - Keep material within workability ranges
  - Keep processing conditions within material model and equipment limits
- Inequality constraints are incorporated into optimality criterion by using penalty functions

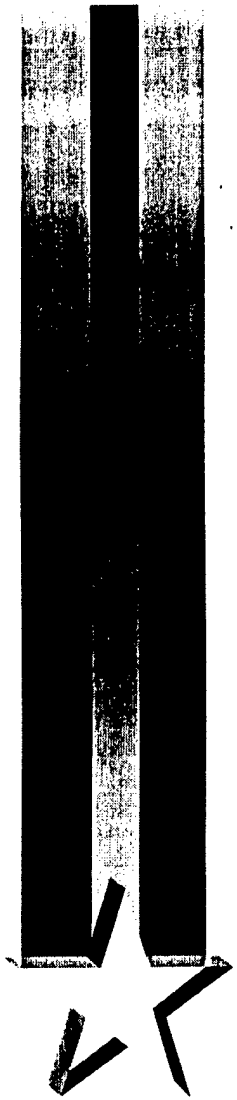

A Penalty Function

$$p(z) = 1000\left[1 - 0.5\tanh\left(\frac{40\,(z-0.01)}{0.01}\right) + 0.5\tanh\left(\frac{50(z-0.02)}{0.02}\right)\right]$$

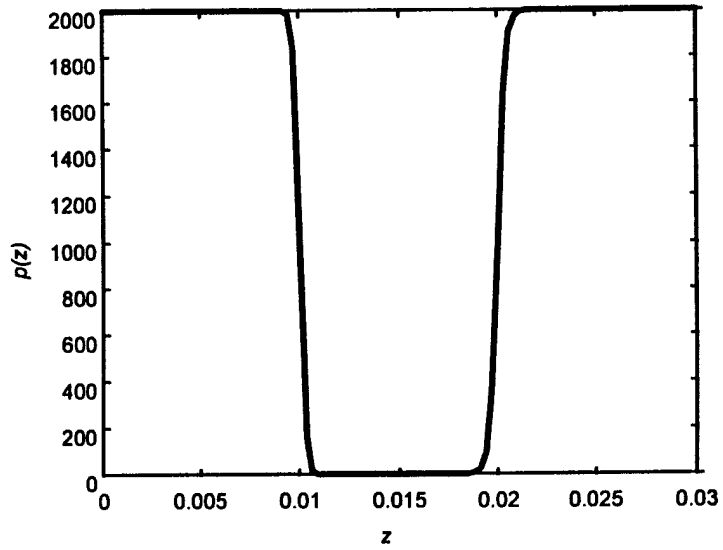

Optimal Control Problem: Solution

Employs iterative numerical algorithm

Quasi-Newton method used for determining "search" direction

Employs automatic differentiation software for calculation of necessary partial derivatives

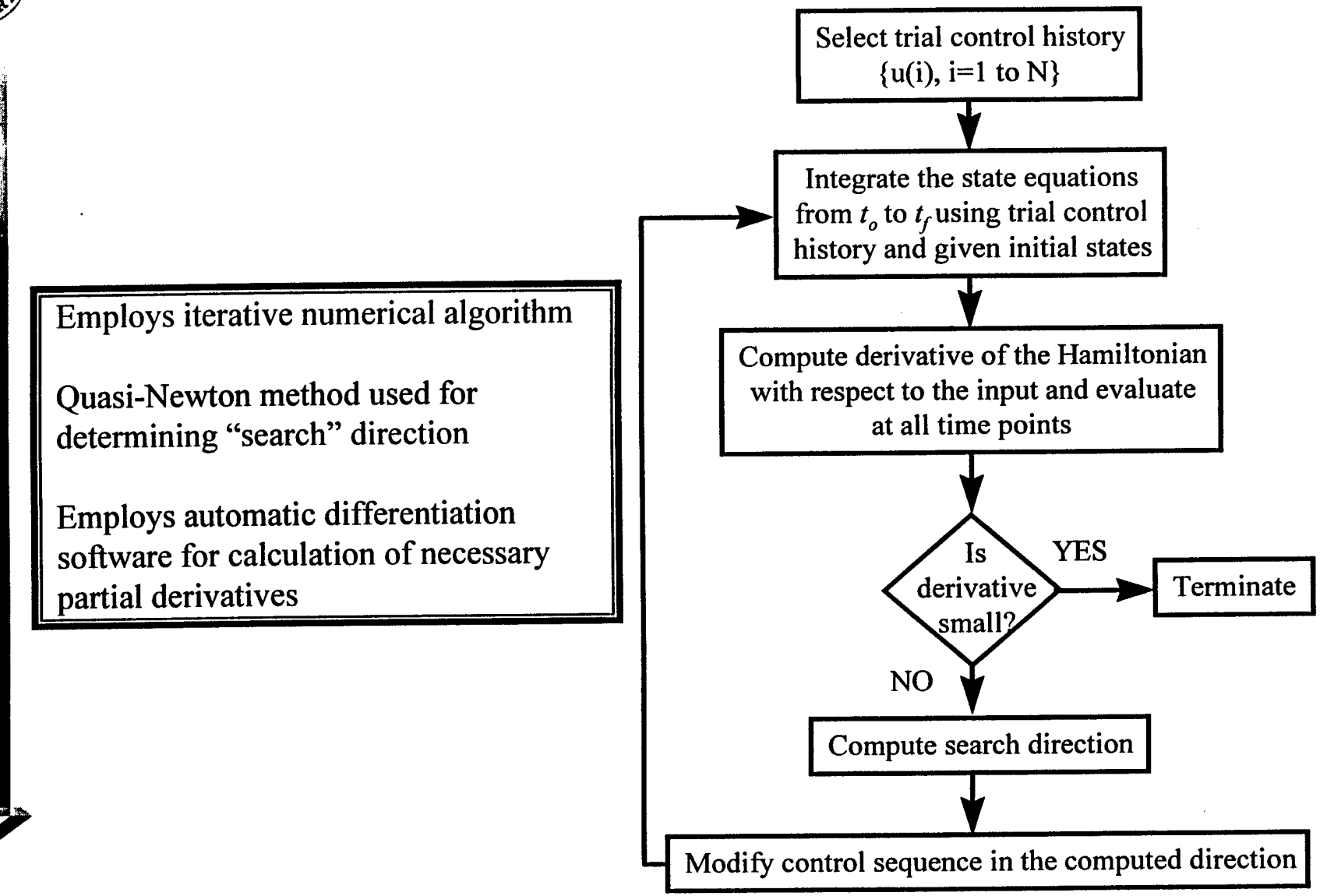

Software Package

- ★ Implement optimal control approach to microstructure development design
- ★ Necessary derivatives by automatic differentiation
  - Jakef
- ★ The user provides only
  - State space model of microstructure development
  - Objective function terms
- ★ Materials and processing conditions changed by simply changing model and objective function
- ★ User friendly GUI

Software Package

★ Graphical User Interface

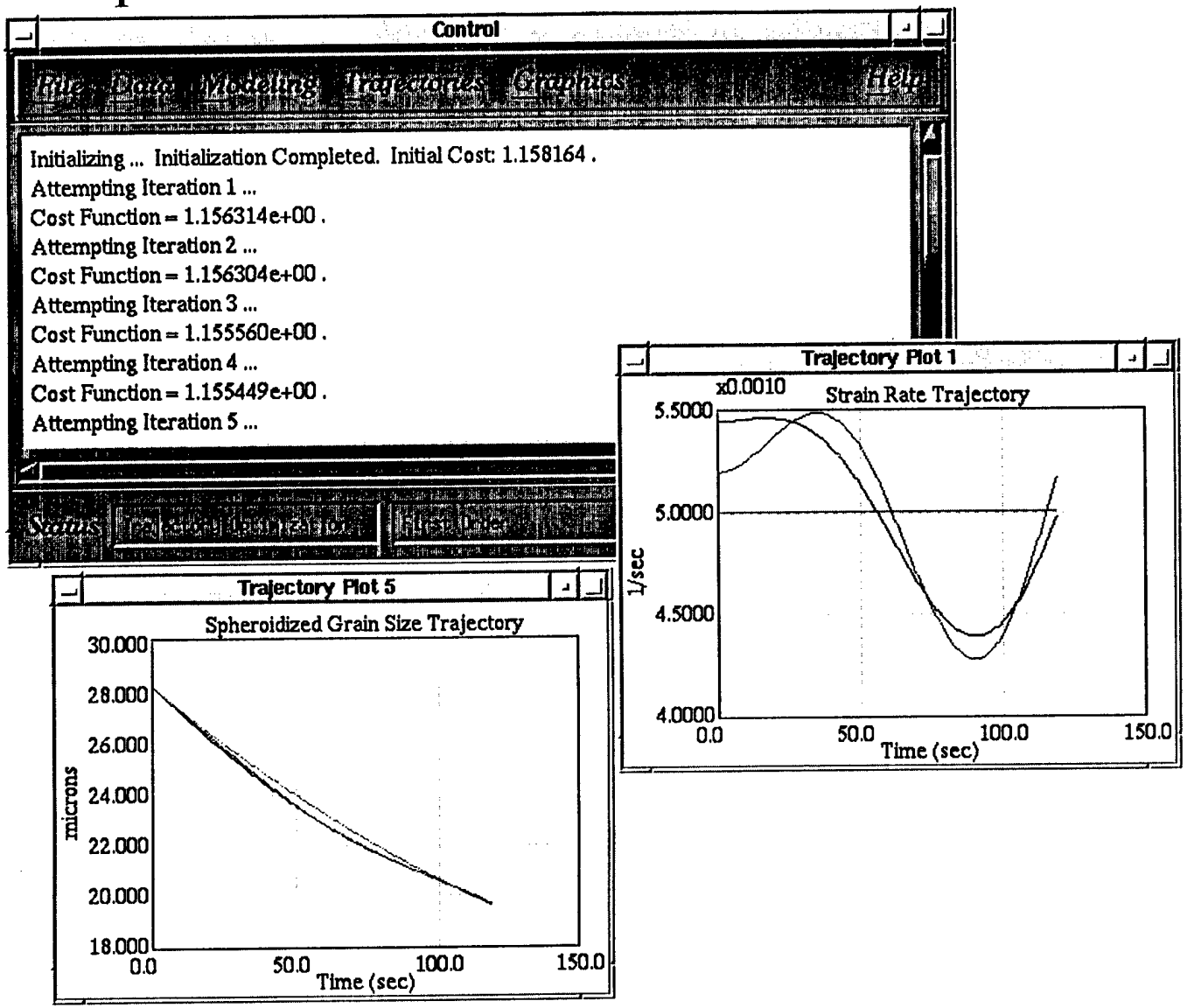

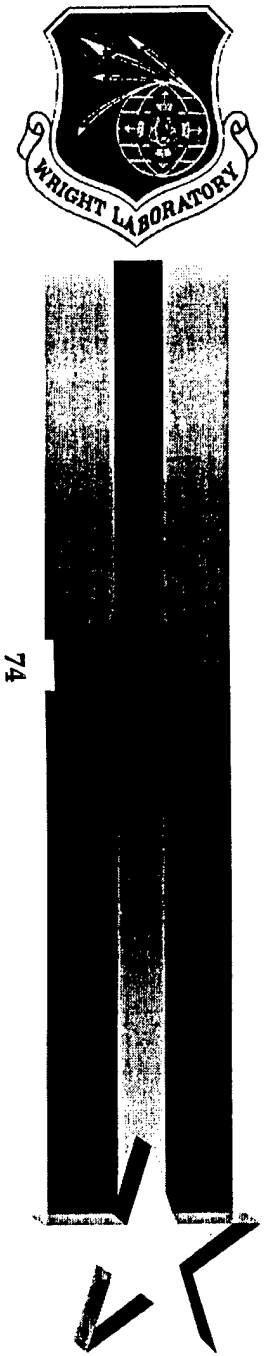

74

Example 1

Application to Steel Extrusion

PROCESS DESIGN: Approach

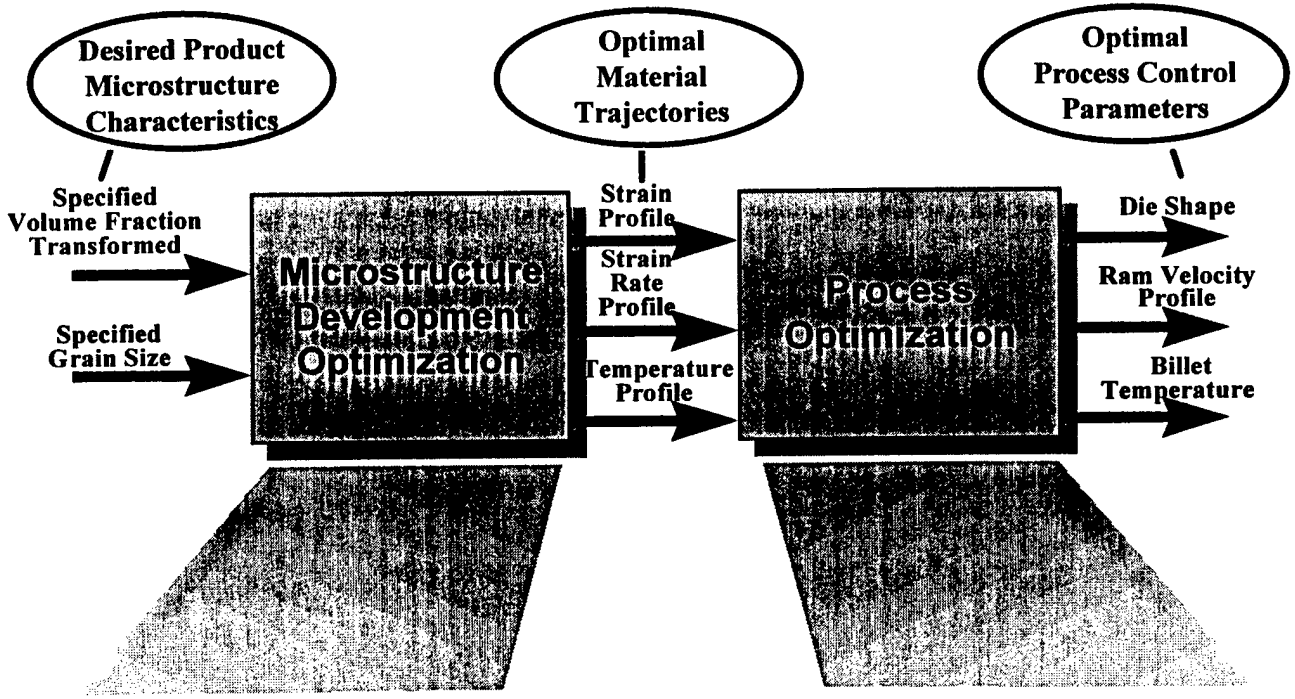

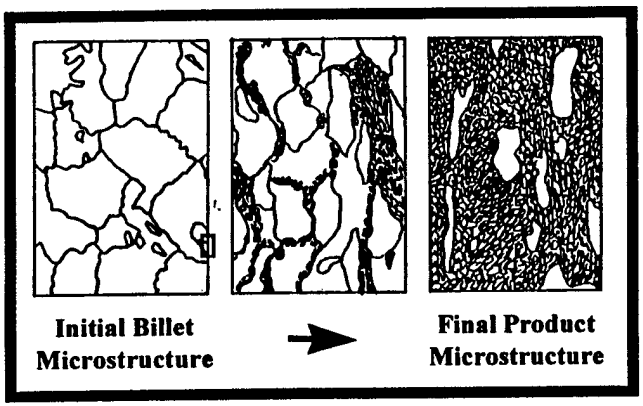

Dynamic Recrystallization

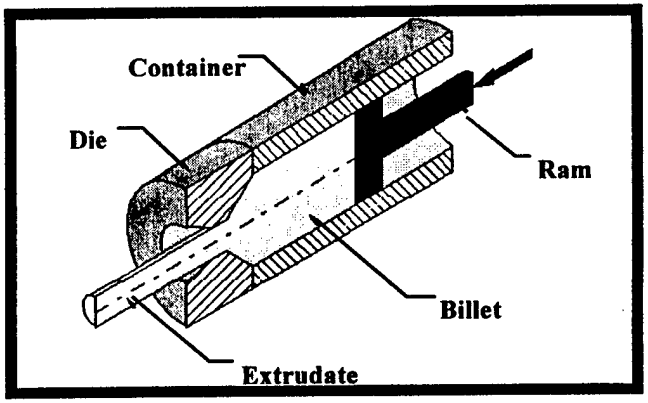

The Extrusion Process

PROCESS DESIGN: Case Studies

Optimality Criterion

$$J(\dot{\varepsilon}(t)) = 10\left(\varepsilon(t_f) - 2.0\right)^2 + \int_0^{t_f} \left(d(t) - d_{desired}\right)^2 dt$$

- Strain Rate Trajectory
- Desired Final Strain
- Desired Grain Size

System State Equation

$$\begin{bmatrix} \dot{\chi} \\ \dot{\varepsilon} \\ \dot{T} \end{bmatrix} = \begin{bmatrix} f_1(\chi, \varepsilon, T, u) \\ u \\ f_2(\varepsilon, T, u) \end{bmatrix}$$

$$d = f_3(T, u)$$

EXTRUSION OF PLAIN CARBON STEEL RODS

CASE	DESIRED GRAIN SIZE (μm)	RAM VELOCITY (mm/s)
OPTIMAL SOLUTION 1	26	8.43
OPTIMAL SOLUTION 2	30	5.0
OPTIMAL SOLUTION 3	15	25.1
CONSTANT STRAIN RATE	-	8.0
CONICAL DIE	-	8.43

1 Define Optimality Criteria

PROCESS DESIGN: Case Studies

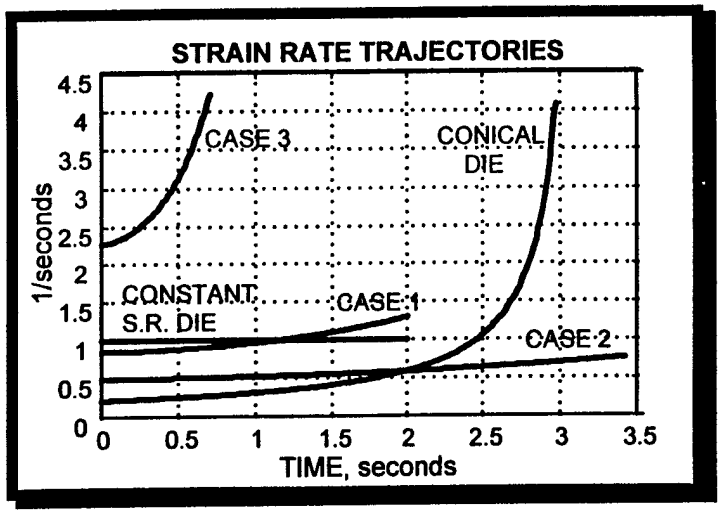

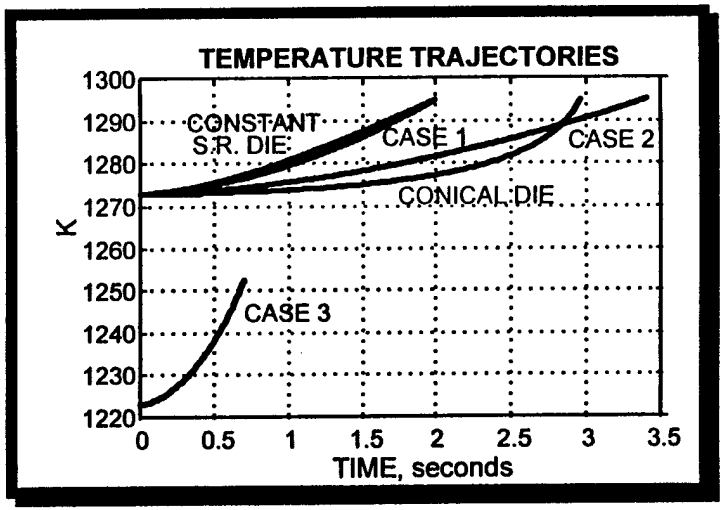

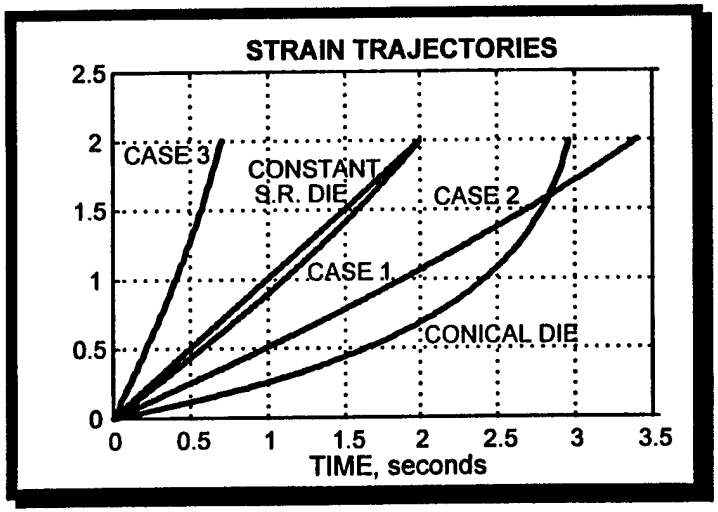

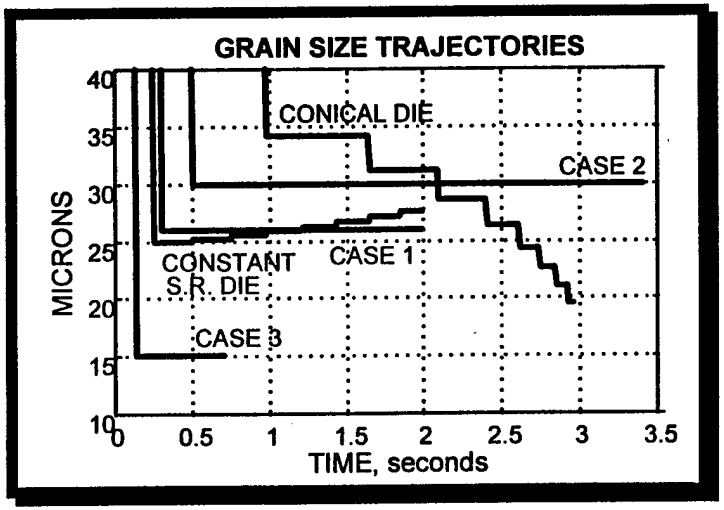

2 Compute Material Trajectories

PROCESS DESIGN: Case Studies

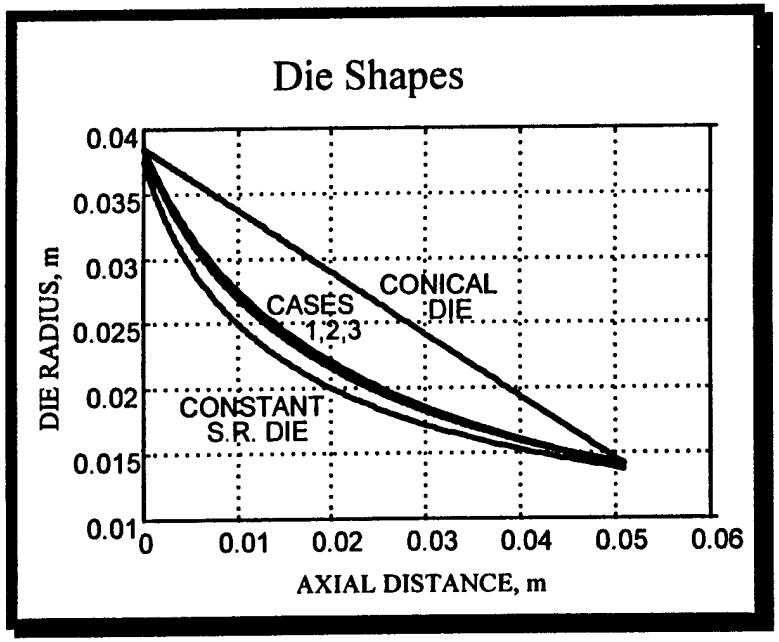

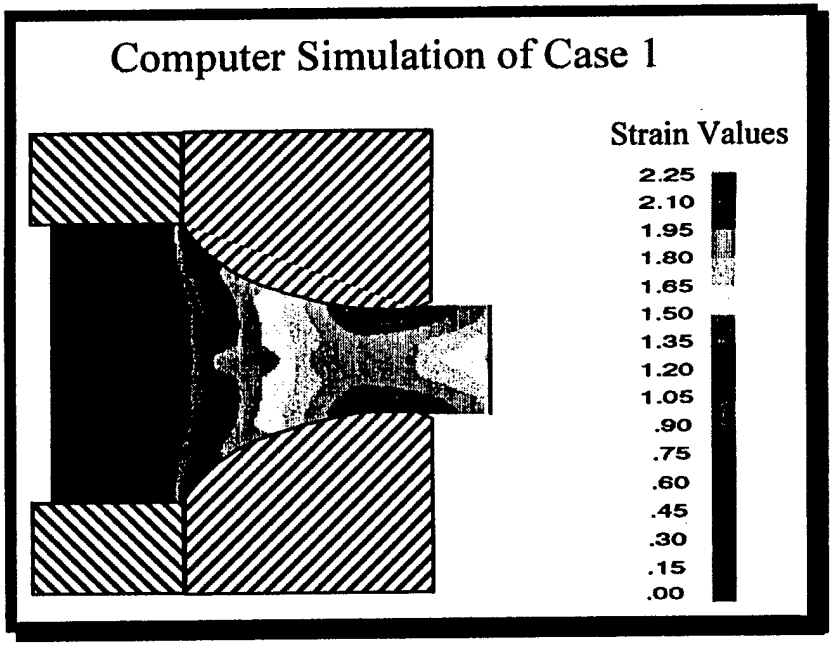

3 Compute Process Control Parameters

Determination of Process Parameters

★ For round to round extrusion
- compute die shape and ram velocity profile
- should obtain required strain rate trajectory at billet centerline

★ If required strain trajectory is given as a sequence

$$\{\varepsilon(t_i), i = 1,\ldots,npts\}$$

★ then the ram velocity can be computed as

$$v_{ram} = l_{die} \Big/ \int_0^{t_f} e^{\varepsilon(t)}\, dt$$

★ and the die profile is given by the sequence of ordered pairs

$$\{(y(t_i), r(t_i)), i = 1,\ldots.npts\}$$

★ where

$$r(t) = r_0 e^{-\varepsilon(t)/2}, \quad y(t) = v_{ram} \int_0^t e^{\varepsilon(\tau)} d\tau$$

$r(t)$: die radius; $y(t)$: axial distance measured from die entrance

PROCESS DESIGN: Validation

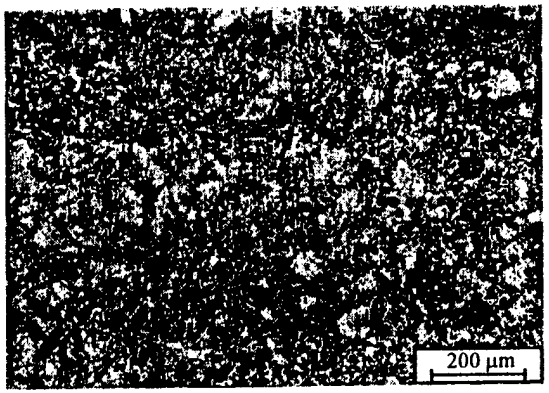

MICROSTRUCTURE OF BILLET

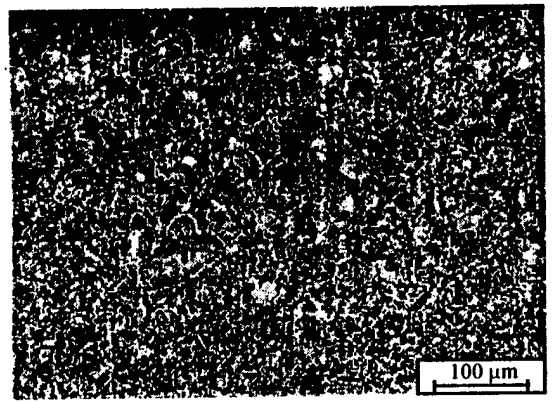

MICROSTRUCTURE OF EXTRUDATE FOR CASE 1

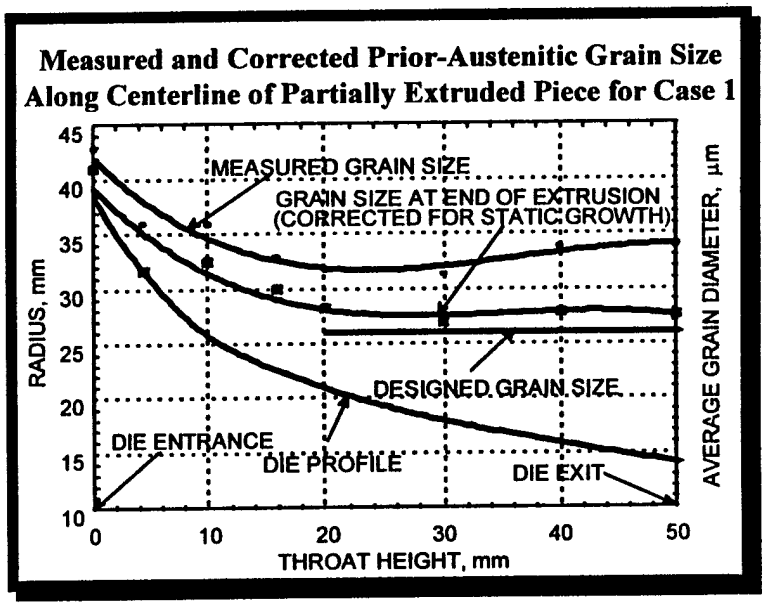

Conclusions and Research Opportunities

- ★ A system approach can be benefitially used in microstructure development design
  - Results of example cases are promising

- ★ Research Challenges
  - Investigation of microstructure modeling issues
    - Is it necessary to do more system ID?
    - How much dynamics are in these systems?
    - Are the necessary models affordable?

  - Inclusion of additional effects
    - Could optimize sequences of material processes
    - Cooling and heating periods must be modeled
    - Optimize robustness to changes in material properties
    - Generalization to include shape, equipment, and other process issues

Materials Models for Discrete Event Optimization

W. M. Mullins
Visiting Scientist
Wright Laboratory
Wright-Patterson AFB, Ohio

Outline

- Background & Motivation
- Physical Metallurgy of Ti-Al alloys
- Constitutive Behavior and Microstructure Evolution Models
- Implementation Issues for Discrete Event Optimization
- Equipment and Process Model Examples
- Objective Function Development Issues
- Future Work

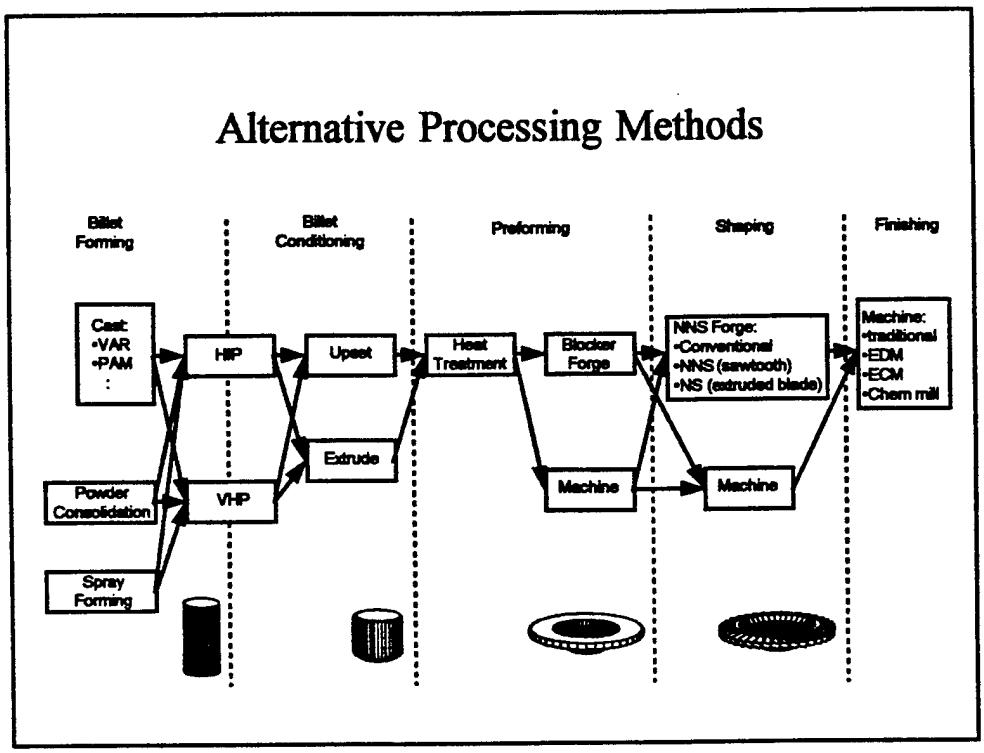

Different Processing Alternatives

Each alternative can be evaluated with respect to cost of the entire process to produce a global optimum path for achieving product shape and microstructure.

- Sequence Design based on Experience
  - –very expensive to obtain
  - –conservative in approach
- Most process optimization focuses on tweeking of individual processing operations.
- Detailed modelling effort is enormous.
- Metallurgical considerations often ill-suited to optimization analysis.

Physical Metallurgy of Ti-Al Alloys

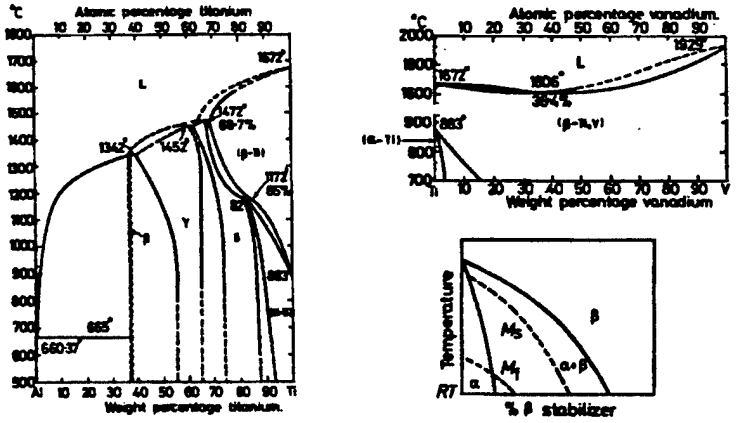

Figures from Porter & Easterling, Van Nostrand Reinhold (1981).

Phase equilibria *et al.*

•high temperature phase is BCC, β

•low temperature phase is HCP, α... stabilized by addition of Al

•increased Al (FCC) additions lead to formation of ordered intermetallic structures δ and γ

•the β–>α possible through a shear transformation, related to Martensite in steels

•results in Martensitic transformations at high cooling rates and Widmanstatten at lower cooling rates

•both result in semi-coherent interfaces, Burgers relations (0001)||(110) and [11-20]||[111]

•V (BCC) stabilizes the β phase and suppresses Martensite formation and Widmanstatten

Ti 6Al 4V, common alloy of interest here

•currently used in 777 fan stages, related to Ti6242

4

Typical Microstructures for Ti-64

Annealed Widmanstatten structure:
- high temperature strength
- high cycle fatigue life
- fracture toughness

α+β processed structure:
- low temperature ductility
- low temperature strength

Figures from Titanium Alloys Handbook, Battelle Labs (1972).

β Microstructure:

Advantages:

•has some advantageous mechanical properties

•lower loads for tooling

Disadvantages:

•greater reactivity -> lower die life

•oxygen pick-up from atmosphere -> severe microstructure effects and lower fracture toughness

•the β microstructure can be obtained from a beta-anneal process of uniform α+β structure

duplex structure:

Advantages:

•easier to achieve with consistency

•superior low temperature strength

Disadvantages:

•higher tooling stresses

Constitutive Behavior

- Dependent on Initial Microstructure.
- Flow softening exhibited due to dynamic globularization process.
- Macroscopic properties essentially identical at strains larger than 0.4 though globularization process is not complete.
- Steady state flow properties developed from microscopic mechanisms.

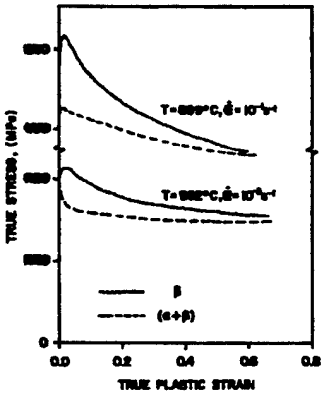

Figure from Semiatin *et al.* unknown source.

DMM for CP Ti, d=100μm

- Power Law Creep Model:

$$\dot{\varepsilon} = A\frac{b\mu}{kT} D_o e^{\frac{-Q}{RT}} \left(\frac{\sigma}{\mu}\right)^{n}$$

for steady-state flow stress

- Related to microscopic creep mechanisms
- All parameters related to physical constants for material

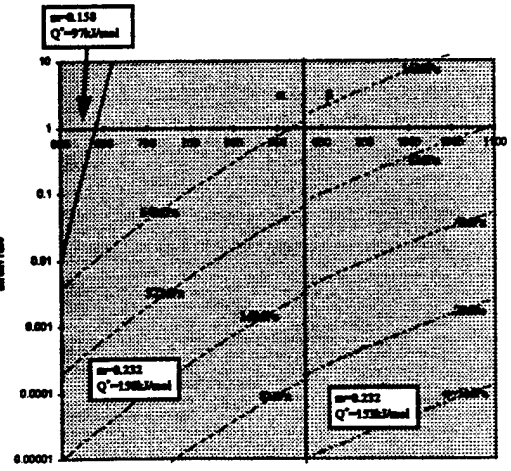

•Taken from Frost & Ashby, Fig 17.4.

•Discontinuous behavior at α–β boundary only.

•HCP phase flow stress much greater than for BCC

•Both regions typical of dynamic recovery, deformation dominated by mobility of dislocation cells by vacancy diffusion mediated climb mechanism (dislocation core diffusion mechanism at low T high strain-rate)

•DRX appears only above 1370C.

•GB "wedge cracking" at transition to Coble or Nabarro/Herring Creep, only at strain-rates below 10^{-6} at this temperature range.

"Ideal" DMM for Ti-64

- Power Law Creep Model:

$$\sigma_i = k_i \dot{\varepsilon}_i^{n_i} e^{\frac{nQ}{RT}}$$

for steady-state flow stress

- fraction a given by:

$$f_\alpha = 0.925\left(1 - e^{-0.0055(T-T_t)}\right)$$

- Taylor model for flow stress (after Briottet *et al.*)

$$\sigma = f_\alpha \sigma_\alpha + (1 - f_\alpha)\sigma_\beta$$

- anomalous apparent activation energy at T>850°C

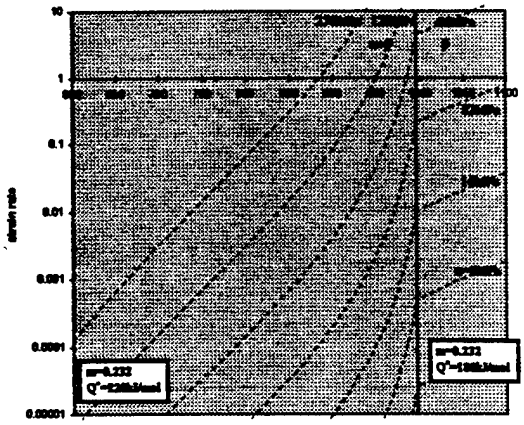

•data from Briottet *et al*, Acta Met. 44(1996) 1665.

•alloy strengthening apparent

•only accounts for dislocation flow mechanisms

•anomalous high activation energy at T>880C due to change in phase equilibrium with temperature

•m constant for system... no indication of instabilities in this model

Globularization of Lamellar Microstructures

- Reaction initiates at prior β grain boundaries and proceeds inward to consume grain.
- Fraction transformed given by :

$$\chi = 1 - \left(\frac{d_o}{2R(\varepsilon - \varepsilon_c) + d_o} \right)^{3/2}$$

d_o = prior β grain size
$R(\dot{\varepsilon},T)$ = reaction rate
ε_c = critical strain

- Strain path dependency implicit in physics.
- Flow softening not directly related to transformation.

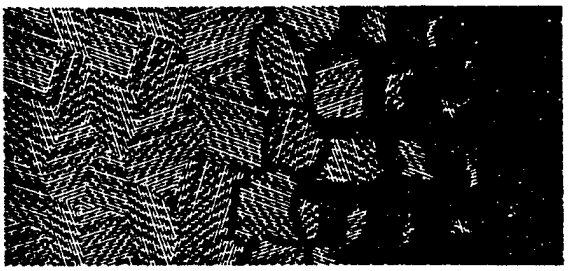

increasing strain →

Cartoon represents γ-TiAl reaction very well, for Ti64 *et al.* the trends are similar, but complicated by lamellar kinking and static recrystallization.

The kinetic equation presented here has been used to fit the initial data of Semiatin *et al.* with good success, the model will be further tested and published as soon as applicable.

Confusion exists over the exact definition of transformed and globularized. That used here is the most severe, the structure is dynamically broken up. Weaker definitions allow for simple static recrystallization of the lamella, which can be accomplished with low strains followed by heat-treatment. More of the "ghost" lamella structure is often visible but the tensile properties are similar. This definition was allowed in the cost function initially posted to VPI, but later changed to restrict.

Stress Induced Porosity

- Appearance of "wedge-cracks" at prior β grain triple junctions.
- 1->50 μm sized pores in material
- Occurs in β-microstructure only.
- Links to prior β grain size and/or grain boundary α .
- Can be closed by subsequent rolling or HIPing operations (in theory).
- Macroscopically observable as:

$$\left(\frac{\partial m}{\partial \ln \dot{\varepsilon}}\right)_{\varepsilon} > 0$$

on "ideal" DMM.

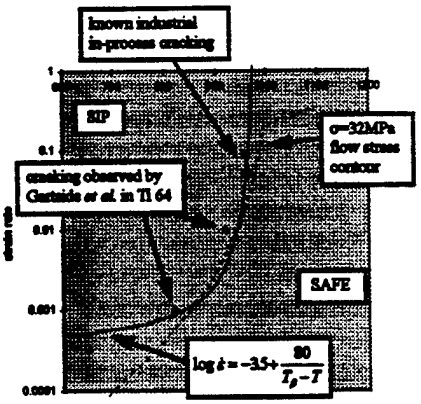

•appearance of "wedge-cracks" at prior β grain triple junctions

•1->50 μm sized pores in material - below reliable ultrasonic detection range and difficult for radiography in thick sections

•nearly all are sub-critical to UTS, but can serve as fatigue nuclei!!!

•occurs in β-microstructure only... prior to globularization... during deformation processing

•possible linked to tensile stresses... laboratory observations mostly in uniaxial and bi-axial tensile testing (some shear cracking possible in compression!)

•possibly linked to prior β grain size and/or grain boundary α , no consistent models available

•can be closed by subsequent rolling or HIPing operations (in theory)

•macroscopically observable as:

$$\left(\frac{\partial m}{\partial \ln \dot{\varepsilon}}\right) > 0$$

since m=constant for ideal system!

Dwell-time Fatigue

- Sub-critical crack propagation by modified Paris eqn. or

$$\frac{da}{dt} = A(K)^n \frac{-(1-R)K_o + K}{(1-R)K_c - K}$$

- Critical stress intensity related to microstructural feature size by

$$K_c = A + B\sqrt{d}$$

- Large regions of textured α behave as a single microstructural feature and lead to low fracture toughness and subcritical crack growth to failure.
- Linked to globularization reaction, apparently alleviated by processing at high T and lower strain-rates to large strains.

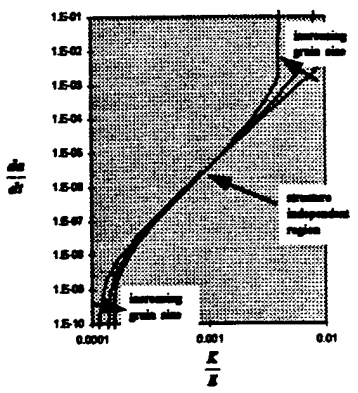

In some forgings, though apparently fully globularized, unexpected failure occurred due to rapid growth of sub-critical flaws.

Linked to regions of micro-texture in the globularized α, which were on the order of the prior β grain size (huge).

Sub-critical crack growth rates determined to be related to the sized of these features at high(er) applied K.

Much work has been done by GE CRD and RR in initial characterization, more work is being initiated to better characterize.

Current thoughs... large strains required at high T and low strain-rates to ensure adequate recrystallization of the globularized α and random orientation.

Implementation Issues for Discrete Event Optimization

- Microstructure Evolution Model Structure:
  - Derived in dynamical form, but presented as static models.
  - Experimental validation not often available.
  - For poly-phase materials, often completely empirical so that no dynamical form available.
- Material State Variables:
  - Selection of appropriate state variables for material system.
  - State variable storage for workpiece.
  - Up-date of state variables during evaluations of sequence.
- Recommendation:
  - *A Priori* Feature-based approach ... object-oriented implementation.

Machine Parameters and Tool Life Predictions

- typical machining analysis:

$$F = Cf^{\alpha}d^{\beta} \qquad t_{tool} = \frac{K}{f^{\alpha}d^{\beta}f}$$

- Inappropriate for Ti machining operations due to:
  - high chip temperature
  - high reactivity with tool
- Chip temperature determined by heat transfer through tool by

$$T_c \approx \frac{\kappa\sigma\varepsilon}{C_p} e^{-C_p\rho_{tool}hv^2/fs} + T_{RT}$$

- wear rate on tool face is given by the solution model

$$\dot{x} \approx \frac{c^o}{\rho} D_o e^{\frac{-Q}{RT_c}}$$

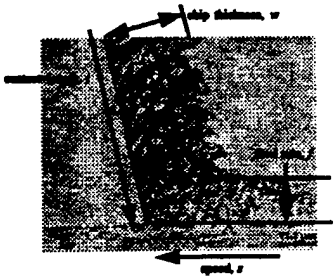

Typical chip for Ti-alloy

Figure from N. Suh, Tribophysics.

•Adiabatic heating leads to flow localization and semi-discontinuous chip formation. The leads to severe chatter in the system.

•High chip temperature --> very hot tool

- •decreased tool life
- •increased reaction kinetics

•Thermal conduction through tool only gives:

$$T_c \approx \frac{\kappa\sigma\varepsilon}{C_p} e^{-C_p\rho_{tool}hv^2/fs} + T_{RT}$$

•recession rate by dissolution only of tool material gives

$$\dot{x} \approx \frac{c^o}{\rho} D_o e^{\frac{-Q}{RT_c}}$$

tool life determined by integration to maximum allowable tool recession.

•high chemical reactivity, no built-up edge but a reaction layer that can/will spall off... leads to uneven wear and apparent chipping of tool.

•For forging die life predictions... essentially the same physics.

Objective Function Development Issues

- Actual cost of unit operations
  - tool and die costs are fairly standard
  - labor rates are estimable
  - effective capital equipments usage usabe rates are not easily attainable without special arrangements with the industries involved (particualrly true for casting and forging)
- Assigning costs to microstructure objectives
  - Simple Taguchi-type function method used
  - Cost to correct by heat-treatment and/or scrap
  - Cost to scrap if detectable "damage" occurs
  - no Taguchi Safety Design done for potential fatigue-life damage due to lack of quantitative models at this time.

•tool and die costs for VPI cost function are simple estimates... likely to be close

•labor rates are close for all operations, though the labor overhead rates were rather low for the VPI cost function

•machining cycle times are generous ans should cover most of the non-special machine tool costs (they are assumed low compared to labor)

•forge-press costs are not good estimates... these are considered trade secrets within the industry!!!

Taguchi Safety Design

•worst-case, total liability cost of failure used in analysis

•for aerospace... loss of vehicle and crew (~$5B for an airliner) and loss of mission.

Future Work

- state variable approach to materials behavior
- traditional machining and forge-die life modelling
- heat treatment
- solidification
- ECM